Physics – Uspekhi **40** (8) 773 – 806 (1997)

REVIEWS OF TOPICAL PROBLEMS PACS numbers: 14.60.Pq, 12.15.Ff

The nature of neutrino mass and the phenomenon of neutrino oscillations

S S Gershteĭn, E P Kuznetsov, V A Ryabov

Contents

Abstract. Various aspects of the neutrino mass problem are discussed in the light of existing model predictions and extensive experimental data. Generation mechanisms are considered and possible gauge-theory neutrino mass hierarchies, in particular the most popular 'flipped see-saw' models, are discussed. Based on the currently available astrophysical data on the integral density of matter in the Universe and on the spectral anisotropy of the relic cosmic radiation, the cosmological implications of a non-zero neutrino mass are described in detail. Results from various mass-measuring methods are presented. Considerable attention is given to heavy neutrino oscillations. Oscillation mechanisms both in vacuum and in matter are considered in detail. Experiments on oscillations at low and high energies and new generation large-flight-base facilities are described. The present state of research into oscillations of solar and atmospheric neutrinos is reviewed.

S S Gershteiŷn State Research Center 'Institute for High Energy Physics' 142284 Protvino, Moscow Region, Russia
Tel. (7-277) 1-38 33
E P Kuznetsov, V A Ryabov P N Lebedev Institute of Physics, Russian Academy of Sciences
Leninskiĭ prosp. 53, 117924 Moscow, Russia
Tel. (7-095) 132-64 39, 132-64 88
Fax (7-095) 135-78 80
E-mail: ryabov@sgi.lpi.msk.su

Received 26 December 1996 1997
Uspekhi Fizicheskikh Nauk **167** (8) 811 – 848 (1997)
Translated by Yu V Morozov; edited by A I Yaremchuk

1. Introduction

Neutrinos came to be known to physicists after Pauli, in his letter to the Physical Society of Tubingen [1], postulated the existence of a particle with semi-integer spin and almost zero mass, in order to ensure the conservation of energy, momentum, and angular momentum in nuclear beta-decay. A few years later, Fermi called this particle the neutrino [2]. Since then over six decades have passed, but the neutrino remains the most enigmatic of all known elementary particles. Unlike quarks and leptons, the neutrino has neither electrical nor color charge and interacts with matter only in weak processes through the exchange of charged and neutral intermediate bosons. As the sole neutral fermion the neutrino can be massless. There is no convincing *a priori* reason to require that the neutrino be exactly massless. Therefore, in current theoretical models based on the standard electroweak theory which implies quark-lepton universality a small but non-zero mass is taken for the neutrino [3].

Until now, the main questions concerning the nature of neutrino remaining unanswered are:

1. Do neutrinos carry masses and, if so, what are they?

2. What are the mechanisms of neutrino mass generation?

3. Are weak interaction states identical to the eigenstates of neutrino mass operator or does neutrino mixing occur?

4. Are neutrinos analogous to their antiparticles? Are they actually neutral (Majorana) particles or not (Dirac particles)?

5. Is the neutrino stable?

Answers to these questions are of primary importance for particle physics since they determine the applicability of Grand Unification Theories (GUT). In a standard model with a normal set of quarks and leptons, it is impossible to introduce a renormalized interaction which could violate lepton number conservation and give mass to the neutrino. The discovery of neutrino mass would mean the development of a new physics lying far beyond the standard model, very probably at GUT scales in the range 10^{15} GeV.

The problem of neutrino mass is equally important for astrophysics and cosmology since its solution could affect current concepts of the structure and evolution of the Universe. The role of a massive neutrino as main candidate for 'dark' matter stirs up imagination of theorists and experimenters. If relic neutrinos actually make the greatest contribution to the mean density of matter in the Universe, they must have been involved in the development of gravitational instability during formation of its large-scale structure. The non-linear stage in the evolution of inhomogeneities in a gas of massive neutrinos leads to the creation of superclusters of galaxies with massive neutrino halos at the periphery of elongated 'pancakes', i.e. condensates of baryonic matter and neutrinos. Also, neutrinos could be responsible for the appearance of supernovae carrying away the major part of the energy, equivalent to the mass deficit of a neutrino star or black hole during gravitational collapse.

The idea of detecting of the free neutrinos from reactors using radiochemical methods (and, in particular, chlorine–argon) was first suggested by Pontecorvo at 1946 [4]. Neutrino experiments date back to the pioneering studies of Cowen and Reines who were the first to observe the interaction of anti-neutrinos with matter through the reaction $\bar{\nu}_e + p \rightarrow n + e^+$ at Henford [5]. With the advent of accelerators, it became possible to generate relativistic pion and muon beams, giving rise to high energy physics. The hypothesis of longitudinal neutrino polarization related to parity non-conservation [6] was most definitively confirmed in the experimental reactions $\pi^+ \rightarrow \mu^+ + \nu$ and $\mu^+ \rightarrow e^+ + 2\nu$ [7]. The next important step in the development of the two-component neutrino theory was the discovery of the absence of the decay $\mu \rightarrow e + \gamma$ which was impossible to explain without assuming the existence of two types of neutrinos. An experiment independently designed by Pontecorvo [8] and Feinberg, Lee, and Yang consisted in the comparison of the numbers of muons and electrons formed in the interaction between the detector's matter and muon neutrinos generated in an accelerator. This experiment was carried out by Lederman, Shwartz and Steinberger with the AGS accelerator at Brookhaven. It was concluded, based on the predominance of muon events, that $\nu_e \neq \nu_\mu$; thus, the existence of two types of neutrinos was confirmed experimentally [9]. Many years later, Lederman told in his Nobel lecture that "the discovery of two types of neutrinos was a crucial step in the 'assembly' of the up-to-date world picture which we call standard model in elementary particle physics" [10].

Glashow [11], Weinberg [12], and Salam [13] developed the universal gauge theory of electroweak interactions which was first experimentally confirmed in 1973 when the muonless reactions $\nu_\mu(\bar{\nu}_\mu) + N \rightarrow \nu_\mu(\bar{\nu}_\mu) + \text{hadrons}$ via the neutral current channel were observed using the Gargamell bubble chamber at CERN [14], and neutrino scattering by electrons, $\nu_\mu + e^- \rightarrow \nu_\mu + e^-$, of the same nature was discovered [15]. The ratio of cross-sections of neutrino interactions via neutral to charged current channels was used to estimate the Weinberg angle ($\sin^2 \theta_W$) — the parameter of the standard model.

The double structure of the quark weak current introduced by Glashow, Illiopoulos, and Maini [16] and the quark-like nucleon structure were confirmed by an FNAL experiment which demonstrated events involving two muons with opposite charge in the final state, one of which arises from the charmed quark decay [17]. The discovery of the τ-lepton using the e^+e^--collider at Stanford [18] and the occurrence of a dimuonic resonance at 9.5 GeV in proton-nucleus collisions at 400 GeV at FNAL (interpreted as b-quark binding to its antiparticle $\bar{b}$ [19]) added particles of the third generation to the standard model. Direct observation of $W^{\pm}$- and Z^0-bosons with the SPS collider at CERN [20] was a triumph of the standard model and allowed it to be finally formulated as the unified theory of electroweak interactions. Neutrino experiments played a key role in the development of this theory, but further studies of the fundamental properties of the neutrino, primarily of its mass, may be expected to bring even more exciting results.

The determination of neutrino mass appears to be most feasible by means of experimental investigation of neutrino oscillations, whose existence was first predicted by Pontecorvo [21, 22]. He considered transitions of maximum amplitude between one known type of neutrino and its sterile antiparticle $\nu \leftrightarrow \bar{\nu}_{ster}$. The oscillation hypothesis for the case of two neutrino generations ($\nu_e \leftrightarrow \nu_\mu$) was generalized by Maki et al. [23] and Pontecorvo [24]. The latter work also concerned the methodology of experimental studies on neutrino oscillations in reactors, accelerators, cosmic rays, and in the field of solar neutrino astronomy. The oscillation technique was shown to be a highly sensitive tool for detecting small neutrino masses.

Pontecorvo and Gribov [25] presented the most consistent consideration of the oscillation problem for the case of two-component neutrino states with the mass term in the Lagrangian taking into account real and virtual transitions violating lepton number conservation. This work 'had a decisive influence on all subsequent basic and experimental studies in the physics of neutrino oscillations' [26]. The mixing of neutrino states for the case of three neutrino generations was reviewed in line with the current understanding of the problem in [27].

In fact, the number of theoretical and experimental publications on massive neutrino oscillations amounts to a few thousand. Oscillation studies are becoming a main line of research in elementary particle physics. Theoretical models are being developed in which Dirac and Majorana neutrino masses are generated by high-dimensional operators and related to other fermions' masses m_f in the range from electron to t-quark masses by the dependence $m_\nu \sim m_f(m_f/M_x)^n$, where M_x is the high-energy limiting interval of new physics from a few TeV to Plank masses at which unification of interactions may be expected. Such 'see-saw' models (e.g. [28]) lead to three light left-handed Majorana neutrinos (ν_e, ν_μ, ν_τ) with mass matrix eigenstates $m_\nu = m_f M_x^{-1} m_f$ and three superheavy non-observable Majorana particles. The smallness of the neutrino mass is ensured by a high M_x value in both the quadratic 'see-saw'

model with $m_\nu = m_f^2/M_x$ and hierarchy $m_{\nu_e} : m_{\nu_\mu} : m_{\nu_\tau} = m_u^2 : m_c^2 : m_t^2$, and the linear model with $m_\nu = m_f/M_x$ and hierarchy $m_{\nu_e} : m_{\nu_\mu} : m_{\nu_\tau} = m_u : m_c : m_t$.

There are different methods for the assessment of neutrino mass by experiment. The best limits have been obtained by kinematic analysis of the beta-decay of tritium, and the decay of charged pions and τ-leptons. They are currently assumed to be $m_{\nu_e} < 4.5$ eV [29, 30], $m_{\nu_\mu} < 160$ keV [31], and $m_{\nu_\tau} < 29$ MeV [32] respectively. Experiments designed to detect double neutrinoless β-decay, neutrino decay, additional peaks in the nuclear β-spectrum or oscillations of neutrinos from reactors and accelerators as well as analysis of neutrino events at the SN 1987A supernova failed to confirm the non-zero mass of the neutrino.

Although all experiments appear to provide evidence of the neutrino's zero mass, there is every reason to believe that it actually differs from zero. From the theoretical point of view the absence of the specific long-range forces between leptons suggests that the conservation of the leptons number preservation is not an exact law. In this case, the neutrino mixing leads immediately to the appearance of it mass. On the other hand, three problems: (1) the deficit of solar neutrinos, (2) the deficit of atmospheric neutrinos, and (3) the shortage of matter necessary for the Universe to be closed, are best explained theoretically if neutrinos (the heaviest one ν_τ) have a mass of ~ 10 eV [33] and undergo mixing and oscillations which may experience resonance amplification in matter [34]. The experimental solution of this problem is sought by physicists in different countries by designing and conducting new research projects unparalleled in terms of scale, technical sophistication, and cost [35].

Further progress in understanding neutrino properties is believed to be dependent on the availability of a new generation of detectors which enable a substantial enhancement of sensitivity of measurements in neutrino mass experiments. The highest sensitivity of $\sim 10^{-3} - 10^{-1}$ eV for m_{ν_e} and m_{ν_μ} and < 1 eV for m_{ν_τ} can be achieved in oscillation experiments with two detectors positioned at a large distance from each other in the direction of a neutrino beam [36].

2. Formalism of Dirac and Majorana neutrino masses

Let us formulate the principal concepts and definitions for the description of neutrino physics in terms of the common neutrino Lagrangian which includes Dirac and Majorana mass terms and the weak interaction term relating neutrino generations to gauge bosons. Let us first introduce some mathematical symmetry transformations necessary to construct the Lagrangian describing neutrino fields.

Space-time symmetry transformations:

1. The uniform Lorentz transformation in the form of a linear transformation of coordinates $x = x_\mu$ $(\mu = 1, 2, 3, 4)$ of a four-dimensional space-time,

$$x'_\mu = L_{\mu\lambda} x_\lambda \,, \tag{2.1}$$

retaining the invariant interval

$$x'_\mu x'_\mu = L_{\mu\lambda} x_\lambda L_{\mu\rho} x_\rho = \delta_{\lambda\rho} x_\lambda x_\rho = x_\lambda x_\lambda = \text{inv} \tag{2.2}$$

with $L_{\mu\rho}$ denoting elements of the 4×4 matrix of the Lorentz transformation L satisfying the orthogonality

$$L_{\mu\lambda} L_{\mu\rho} = \delta_{\lambda\rho} \tag{2.3}$$

and unimodularity

$$\det L = 1 \tag{2.4}$$

conditions. The set of matrices L forms the Lorentz orthogonal group O (3.1).

2. Discrete transformations described by Dirac matrices γ^μ in the representation

$$\gamma^0 = \begin{pmatrix} 1 & 0 \\ 0 & -1 \end{pmatrix}, \quad \gamma^i = \begin{pmatrix} 0 & \sigma_i \\ -\sigma_i & 0 \end{pmatrix}, \quad i = 1, 2, 3 \,,$$

$$\gamma_5 = -\mathrm{i}\gamma^0\gamma^1\gamma^2\gamma^3 = -\begin{pmatrix} 0 & 1 \\ 1 & 0 \end{pmatrix}, \tag{2.5}$$

where σ_i are Pauli matrices:

$$\sigma_1 = \begin{pmatrix} 0 & 1 \\ 1 & 0 \end{pmatrix}, \quad \sigma_2 = \begin{pmatrix} 0 & -\mathrm{i} \\ \mathrm{i} & 0 \end{pmatrix}, \quad \sigma_3 = \begin{pmatrix} 1 & 0 \\ 0 & -1 \end{pmatrix}. \tag{2.6}$$

Dirac matrices are 4×4 matrices written as block 2×2 matrices satisfying the anticommunication relation

$$\gamma^{\mu\lambda} + \gamma^{\lambda\mu} = 2g^{\mu\lambda} \,, \qquad \mu, \lambda = 0, 1, 2, 3 \,. \tag{2.7}$$

Discrete transformations:

(a) The transformation $P(x^0, \mathbf{x}) = (x^0, -\mathbf{x})$ of spatial reflection, where $\mathbf{x}$ is the three-dimensional vector, described by the representation

$$S(P) = \eta_P \gamma^0 \,, \qquad \psi'(x^0, -\mathbf{x}) = S(P)\psi(x^0, \mathbf{x}) \tag{2.8}$$

with the phase factor $\eta_P = \pm\mathrm{i}$ or $\eta_P = \pm 1$.

(b) The transformation $T(x^0, \mathbf{x}) = (-x^0, \mathbf{x})$ of temporal reflection described by the representation

$$S(T) = \eta_T \gamma^0\gamma^1\gamma^3 \,, \quad \psi'(-x^0, \mathbf{x}) = S(T)\bar{\psi}^{\mathrm{T}}(x^0, \mathbf{x}), \tag{2.9}$$

where $\bar{\psi}(x^0, \mathbf{x}) = \psi^{\mathrm{H}}(x^0, \mathbf{x})\gamma^0$, $\psi^{\mathrm{H}}(x^0, \mathbf{x})$ is a hermit-conjugate bispinor, and the phase factor η_T meets the condition $|\eta_T| = 1$.

(c) The transformation $R(x^0, \mathbf{x}) = T(x^0, \mathbf{x})P(x^0, \mathbf{x}) = (-x^0, -\mathbf{x})$ described by the operator

$$S(R) = S(T)S(P) \,. \tag{2.10}$$

In addition to the space-time transformations, let us define the transformation of charge conjugation as

$$\psi^{\mathrm{C}} = \eta_{\mathrm{C}} C \bar{\psi}^{\mathrm{T}} \,. \tag{2.11}$$

The matrix C satisfies the conditions

$$C\bar{\gamma}^\mu C^{-1} = -\gamma^\mu \,,$$
$$C^{\mathrm{T}} = -C \tag{2.12}$$

and the requirement of unitarity:

$$C^{\mathrm{H}} = C^{-1} \,. \tag{2.13}$$

Here $\bar{\gamma}^\mu = (\gamma^\mu)^{\mathrm{T}}$ are the transposed Dirac matrices.

In the above representation of Dirac matrices the C matrix is

$$C = \gamma^0\gamma^2 \,. \tag{2.14}$$

The Lagrangian

$$L_\psi = \bar{\psi}(x)(\gamma^\mu \mathrm{i}\partial_\mu - m)\psi(x) \tag{2.15}$$

for a free fermion with mass leads to the Dirac equation

$$(\mathrm{i}\gamma^{\mu}\partial_{\mu} + m)\psi(x) = 0\,. \tag{2.16}$$

Its complex conjugate

$$\left[-\mathrm{i}(\gamma^{\mu})^{\mathrm{T}}\partial_{\mu} - m\right]\bar{\psi}^{\mathrm{T}}(x) = 0 \tag{2.17}$$

may be represented in the form

$$(\mathrm{i}\gamma^{\mu}\partial_{\mu} - m)\psi^{\mathrm{C}}(x) = 0\,, \tag{2.18}$$

where $\psi^{\mathrm{C}}(x) = C\bar{\psi}(x)$ stands for the charge-conjugate field.

The spatial parities (η_{P}) of a particle and $(\eta_{\mathrm{P}})^{\mathrm{C}}$ of an antiparticle satisfy the relation

$$\eta_{\mathrm{P}}(\eta_{\mathrm{P}})^{\mathrm{C}} = -1\,, \tag{2.19}$$

and therefore particles and antiparticles are of the same spatial parity if $\eta_{\mathrm{P}} = \pm\mathrm{i}$, and of opposite parities if $\eta_{\mathrm{P}} = \pm 1$.

Finally, let us introduce operators

$$P_{\mathrm{L}} = \frac{1+\gamma_5}{2}\,, \quad P_{\mathrm{R}} = \frac{1-\gamma_5}{2}\,, \tag{2.20}$$

of projection on particle helicity. They satisfy relations

$$P_{\mathrm{L}} + P_{\mathrm{R}} = 1\,, \qquad P_{\mathrm{L,R}}^2 = P_{\mathrm{L,R}}\,. \tag{2.21}$$

The general solution of the Dirac equation (2.16) for a fermionic field is a linear combination of flat waves with the amplitudes $a(p,s)$ and $b^{+}(p,s)$:

$$\psi(x) = \sum_{p,s=\pm 1/2} \frac{1}{\sqrt{2k}}\big[a(p,s)u(p,s)\exp(-\mathrm{i}px) + b^{+}(p,s)u^{\mathrm{C}}(p,s)\exp(\mathrm{i}px)\big]\,. \tag{2.22}$$

Here summation runs over all possible values of the momentum $\mathbf{p}$ from $-\infty$ to ∞ and all permissible spin projections s, $p = (\mathbf{p}^2 + m^2)^{1/2}$, and $u(p,s)$ and $u^{\mathrm{C}}(p,s) = C\,\bar{u}(p,s)$ are the amplitudes of the Fourier expansion normalized by the condition $\bar{u}u = 2m$ and having the form

$$u(p,s) = \begin{pmatrix} \sqrt{k+m}\;\chi(s) \\ \sqrt{k-m}\;\cdot\mathbf{n}\chi(s) \end{pmatrix}, \tag{2.23}$$

where $\mathbf{n} = \mathbf{p}/|\mathbf{p}|$, and $\chi(s)$ is the two-component spinor whose helicity states

$$\chi\left(\frac{1}{2}\right) = \begin{pmatrix}1\\0\end{pmatrix}, \quad \chi\left(-\frac{1}{2}\right) = \begin{pmatrix}0\\1\end{pmatrix}$$

correspond to projections $s = \pm 1/2$ of the spin on the quantization axis $\mathbf{n}$: $(\cdot\mathbf{n})\chi(s) = 2s\chi(s) = \pm\chi(s)$.

The free neutrino state ν_{L} may be determined via the action of the operator P_{L} given by (2.20) on the wave function $v(x) = u(p,s)\exp(-\mathrm{i}px)$:

$$\nu_{\mathrm{L}} = \frac{1}{2}\begin{Bmatrix} (\sqrt{k+m} - \sqrt{k-m}\;\cdot\mathbf{n})\chi(s) \\ -(\sqrt{k+m} - \sqrt{k-m}\;\cdot\mathbf{n})\chi(s) \end{Bmatrix}\exp(-\mathrm{i}px)$$

$$\simeq \sqrt{k}\begin{Bmatrix} \dfrac{1-\cdot\mathbf{n}}{2}\chi(s) \\ -\dfrac{1-\cdot\mathbf{n}}{2}\chi(s) \end{Bmatrix}\exp(-\mathrm{i}px)\,. \tag{2.24}$$

The approximate equality corresponds to the ultrarelativistic limit $k \gg m$ (e.g. at $m = 0$), and spinor ν_{L} is non-zero only for the left polarization of the neutrino corresponding to the helicity eigenvalue $\lambda = 2s = -1$ when the spin is oriented oppositely to the momentum. The right-handed chirality state $\nu_{\mathrm{R}} = P_{\mathrm{R}}\nu(x)$ of the neutrino in the case of $k \gg m$ has a non-zero wave function only at $\lambda = 1$ and can not be observed in the laboratory. Only left-handed chirality states of the neutrino have been reported to occur in experiments.

Now, let us substitute the left and right-handed chirality fields

$$\nu_{i\mathrm{L}} = \frac{1}{2}(1+\gamma_5)\nu_i\,, \quad \nu_{i\mathrm{R}} = \frac{1}{2}(1-\gamma_5)\nu_i \quad (i = \mathrm{e},\mu,\tau) \tag{2.25}$$

of the neutrino into the fermionic Lagrangian (2.15). In the case of a massless neutrino it takes the form

$$L_{\nu} = \sum_{i}^{n}(\bar{\nu}_{i\mathrm{L}}\gamma^{\mu}\mathrm{i}\partial_{\mu}\nu_{i\mathrm{L}}) + \sum_{i}^{n}(\bar{\nu}_{i\mathrm{R}}\gamma^{\mu}\mathrm{i}\partial_{\mu}\nu_{i\mathrm{R}}) \tag{2.26}$$

and leads to chiral symmetry with respect to the transformation

$$\nu'(x) = \exp\left(-\frac{\mathrm{i}\gamma_5\omega}{2}\right)\nu(x)\,, \quad \bar{\nu}'(x) = \bar{\nu}(x)\exp\left(-\frac{\mathrm{i}\gamma_5\omega}{2}\right), \tag{2.27}$$

where ω is the wave number. Since matrix γ_5 anti-commutes with all γ^{μ}, the exponents in the Lagrangian (2.26) undergo reduction and it becomes chirally invariant.

The introduction of the mass term in the form $m_{\nu}(\bar{\nu}\nu)$ breaks the symmetry of the Lagrangian (2.26) with respect to chiral transformations.

The most general form of the Hermitian and Lorentz-invariant neutrino-mass Lagrangian can be represented as a sum

$$L_{\mathrm{D}} = M_{\mathrm{D}}(\bar{\nu}_{\mathrm{L}}\nu_{\mathrm{R}} + \bar{\nu}_{\mathrm{R}}\nu_{\mathrm{L}}) = M_{\mathrm{D}}(\bar{\nu}\nu) \tag{2.28}$$

of Dirac type mass terms relating the left and right-handed chiral components of the same field $\nu = \nu_{\mathrm{L}} + \nu_{\mathrm{R}}$ to the eigenstate of the mass matrix, and of the Majorana type

$$L_{\mathrm{LM}} = M_{\mathrm{LM}}(\bar{\nu}_{\mathrm{L}}^{\mathrm{C}}\nu_{\mathrm{L}} + \bar{\nu}_{\mathrm{L}}\nu_{\mathrm{L}}^{\mathrm{C}}) = M_{\mathrm{LM}}(\bar{\nu}'_{\mathrm{L}}\nu'_{\mathrm{L}})\,,$$

$$L_{\mathrm{RM}} = M_{\mathrm{RM}}(\bar{\nu}_{\mathrm{R}}^{\mathrm{C}}\nu_{\mathrm{R}} + \bar{\nu}_{\mathrm{R}}\nu_{\mathrm{R}}^{\mathrm{C}}) = M_{\mathrm{RM}}(\bar{\nu}'_{\mathrm{R}}\nu'_{\mathrm{R}})\,, \tag{2.29}$$

relating the left and right-handed chiral components of the conjugate fields in the form of self-conjugate fields

$$\begin{aligned} \nu'_{\mathrm{L}} &= \nu_{\mathrm{L}} + \nu_{\mathrm{L}}^{\mathrm{C}}\,, \quad \nu_{\mathrm{L}}^{'\mathrm{C}} = \nu'_{\mathrm{L}}\,, \\ \nu'_{\mathrm{R}} &= \nu_{\mathrm{R}} + \nu_{\mathrm{R}}^{\mathrm{C}}\,, \quad \nu_{\mathrm{R}}^{'\mathrm{C}} = \nu'_{\mathrm{R}} \end{aligned} \tag{2.30}$$

to the eigenstates of the mass matrix.

In the space of spinors

$$\nu = \begin{pmatrix} \nu'_{\mathrm{L}} \\ \nu'_{\mathrm{R}} \end{pmatrix}$$

it is possible to pass to a new basis

$$\xi_1 = \frac{\nu'_{\mathrm{L}} + \nu'_{\mathrm{R}}}{\sqrt{2}}\,, \quad \xi_2 = \frac{\nu'_{\mathrm{L}} - \nu'_{\mathrm{R}}}{\sqrt{2}}\,, \tag{2.31}$$

in which the 'semi-spinors' ξ_1 and ξ_2 are independently transformed by the Lorentz transformations and turn into each other ($\xi_1 \to \xi_2$ and $\xi_2 \to \xi_1$) in the case of spatial reflection $P(x^0, \mathbf{x}) = P(x^0, -\mathbf{x})$.

The neutrino-mass Lagrangian can be written in the matrix form as

$$L_{\mathrm{M}} = \frac{1}{2}(\bar{\nu}_{\mathrm{L}}, \bar{\nu}_{\mathrm{R}}^{\mathrm{C}}) \begin{pmatrix} M_{\mathrm{LM}} & M_{\mathrm{D}} \\ M_{\mathrm{D}}^{\mathrm{T}} & M_{\mathrm{RM}} \end{pmatrix} \begin{pmatrix} \nu_{\mathrm{L}}^{\mathrm{C}} \\ \nu_{\mathrm{R}} \end{pmatrix} + N\text{s}. \tag{2.32}$$

where ν_{L} is a three-component vector of left-handed neutrinos arising as a component of the electroweak lepton doublet

$$l_{\mathrm{L}}(x) = \begin{pmatrix} \nu_{\mathrm{L}}(x) \\ e_{\mathrm{L}}(x) \end{pmatrix}$$

and undergoing transformations as a component of a spinor under the action of SU(2) in the case of global rotations of isotopic space, ν_{R} is the vector of dimension n of right-handed neutrino electroweak singlets, M_{LM} is the 3×3 matrix of left-handed Majorana masses with $3(3+1) = 12$ parameters, M_{RM} is the $n \times n$ matrix of right-handed Majorana masses with $n(n+1)$ parameters, and M_{D} is the matrix of dimension $3 \times n$ of Dirac masses with $2(3 \times n)$ parameters. All the matrices in (2.32) are largely complex ones.

The anticommutation property of fermion fields and the assumption

$$M_{\mathrm{LM}} = M_{\mathrm{LM}}^{\mathrm{T}}, \qquad M_{\mathrm{RM}} = M_{\mathrm{RM}}^{\mathrm{T}} \tag{2.33}$$

of Majorana matrix symmetry allow the complete mass matrix of dimension $(3 \times n)(3 \times n)$ in (2.32) to be diagonalized by means of double unitary transformations, i.e. for any mass matrix M to find unitary U- and H-matrices such, that

$$U^{\mathrm{H}} M H = M_{\mathrm{diag}} \tag{2.34}$$

is a diagonal matrix with $3+n$ positive eigenvalues of mass neutrino states M_i:

$$M_{\mathrm{diag}} = \begin{pmatrix} M_1 & 0 & 0 \\ 0 & M_2 & 0 \\ 0 & 0 & M_3 \end{pmatrix}, \quad M_i > 0\,. \tag{2.35}$$

The operator $M_i = M_{i\mathrm{L}} + M_{i\mathrm{R}}$ in the diagonal matrix M_{diag} describes a Majorana particle with mass m_i while the operators $M_{i\mathrm{L}}$ and $M_{i\mathrm{R}}$ are its projections having certain chirality, i.e. eigenstates of the charge-conjugation operator (2.14) and operator (2.20). The fields M_i are eigenstates of the Lagrangian. As a result, there is a relationship

$$\bar{\nu}_{\mathrm{L}} M \nu_{\mathrm{R}} = (\bar{\nu}_{\mathrm{L}} U)(U^{\mathrm{H}} M H)(H^{\mathrm{H}} \nu_{\mathrm{R}}) = \bar{\nu}'_{\mathrm{L}} M_{\mathrm{diag}} \nu'_{\mathrm{R}} \tag{2.36}$$

between gauge states of the neutrino involved in a weak interaction and the eigenstates of the mass matrix with eigenvalues M_i, with

$$\nu_{\mathrm{L}} = U\nu'_{\mathrm{L}}, \quad \nu_{\mathrm{R}} = H\nu'_{\mathrm{R}}\,. \tag{2.37}$$

If the consideration is confined to one generation of fermions, the Lagrangian (2.32) contains only one flavour component, e.g. $\nu_{\mathrm{L}} \equiv \nu_{\mathrm{eL}}$, and there are two eigenvalues

$$M_i = M_{1,2} = (M_{\mathrm{LM}} + M_{\mathrm{RM}}) \pm \left[(M_{\mathrm{LM}} - M_{\mathrm{RM}})^2 + M_{\mathrm{D}}^2\right]^{1/2}, \tag{2.38}$$

of the mass matrix corresponding to the eigenvectors

$$\begin{pmatrix} \nu_1 \\ \nu_2 \end{pmatrix} = \begin{pmatrix} \cos\theta & \sin\theta \\ -\sin\theta & \cos\theta \end{pmatrix} \begin{pmatrix} \nu'_{\mathrm{L}} \\ \nu'_{\mathrm{R}} \end{pmatrix}, \tag{2.39}$$

where the mixing angle θ is expressed through parameters of the original Lagrangian:

$$\tan(2\theta) = \frac{2M_{\mathrm{D}}}{M_{\mathrm{LM}} - M_{\mathrm{RM}}}\,. \tag{2.40}$$

The diagonal states ν_1 and ν_2 with certain masses M_1 and M_2 are orthogonal superpositions of the states ν'_{L} and ν'_{R} and describe Majorana neutrinos.

Explicit expression of the Dirac and Majorana mass terms in (2.38) and (2.40) yields

$$\begin{aligned} M_{\mathrm{D}} &= (M_1 - M_2)\sin(2\theta)\,, \\ M_{\mathrm{LM}} &= M_1 \cos^2\theta + M_2 \sin^2\theta\,, \\ M_{\mathrm{RM}} &= M_1 \sin^2\theta + M_2 \cos^2\theta\,. \end{aligned} \tag{2.41}$$

It follows from these expressions that the mass term in the Lagrangian (2.32) describes two Majorana particles with different masses. In the limit $M_{\mathrm{LM}} = M_{\mathrm{RM}} = 0$ (at $\theta = \pi/4$) the mass term is diagonal, having the eigenvalue $\pm M_{\mathrm{D}}$. The negative, non-physical sign of the mass can be changed by the chiral transformation

$$\gamma_5 \begin{pmatrix} \nu'_{\mathrm{L}} \\ \nu'_{\mathrm{R}} \end{pmatrix}.$$

Upon transition to the new basis (2.31), the fields

$$\begin{aligned} \xi_1 &= \frac{1}{\sqrt{2}}(\nu_{\mathrm{L}} + \nu_{\mathrm{L}}^{\mathrm{C}} + \nu_{\mathrm{R}} + \nu_{\mathrm{R}}^{\mathrm{C}})\,, \\ \xi_2 &= \frac{1}{\sqrt{2}}\left[\gamma_5(\nu_{\mathrm{L}} + \nu_{\mathrm{L}}^{\mathrm{C}}) - \gamma_5(\nu_{\mathrm{R}} + \nu_{\mathrm{R}}^{\mathrm{C}})\right] \\ &= \frac{1}{\sqrt{2}}\left[-\nu_{\mathrm{L}} + \nu_{\mathrm{L}}^{\mathrm{C}} - \nu_{\mathrm{R}} + \nu_{\mathrm{R}}^{\mathrm{C}}\right] \end{aligned} \tag{2.42}$$

will correspond to one and the same eigenvalue M_{D}. Such a degeneration allows for the use of any field combination obtained by a turn at the plane $\xi_1\xi_2$. The bilinear form

$$M_{\mathrm{D}}(\bar{\xi}_1\xi_1 + \bar{\xi}_2\xi_2) \tag{2.43}$$

corresponds to the mass term in (2.28); hence, the Dirac neutrino corresponds to the degenerate limit $M_{\mathrm{LM}} = M_{\mathrm{RM}} = 0$ of a more general case of two Majorana particles. The Majorana mass terms M_{LM} and M_{RM} in (2.29) lead to the non-conservation of the lepton quantum number L transferred by the ν field, violating the conservation law by two units: $|\Delta L| = 2$.

In the case of two fermion generations, the neutrino fields have the form

$$\nu'_{\mathrm{L}} = \begin{pmatrix} \nu_{\mathrm{eL}} + \nu_{\mathrm{eL}}^{\mathrm{C}} \\ \nu_{\mu\mathrm{L}} + \nu_{\mu\mathrm{L}}^{\mathrm{C}} \end{pmatrix}, \quad \nu'_{\mathrm{R}} = \begin{pmatrix} \nu_{\mathrm{eR}} + \nu_{\mathrm{eR}}^{\mathrm{C}} \\ \nu_{\mu\mathrm{R}} + \nu_{\mu\mathrm{R}}^{\mathrm{C}} \end{pmatrix}, \tag{2.44}$$

and the diagonalization of the mass matrix in the Lagrangian (2.32) [25] leads to two even eigenstates relative to the charge-conjugation operator (2.14) whose eigenvalues are eigenvalues of the operator $M_{\mathrm{D}} + (M_{\mathrm{LM}} + M_{\mathrm{RM}})$, and to two odd states relative to the operator C with the eigenvalues corresponding to the eigenvalues of the operator

$M_D - (M_{LM} - M_{RM})$. Therefore, there are four Majorana eigenstates of the mass term; in this case, the mixing matrix is a unitary 4×4 matrix. The flavour eigenstates ν_e and ν_μ and the corresponding antiparticles ν_e^C and ν_μ^C are expressed through the same set of four Majorana mass states.

Measurements of the Z^0-boson decay width at the LEP-collider in the ALEPH [37], OPAL [38], DELPHI [39], and L3 [40] experiments have demonstrated that there are only three left-handed neutrinos (to be precise: $N_\nu = 2.985 \pm 0.023 \pm 0.004$ [41]) which contribute to the reaction $Z^0 \to \nu\bar{\nu}$ if $m_\nu < m_Z/2$. This accounts for the field

$$\nu'_L \equiv \begin{pmatrix} \nu_{eL} + \nu^C_{eL} \\ \nu_{\mu L} + \nu^C_{\mu L} \\ \nu_{\tau L} + \nu^C_{\tau L} \end{pmatrix} \tag{2.45}$$

in the case of three fermion generations; there are nine Majorana mass eigenstates with the possibility of existence of n sterile SU(2)⊗U(1) singlets ν'_R with $n \times n$ mass eigenstates. The three mass matrices M_D, M_{LM} and M_{RM} in the Lagrangian (2.32) may be represented as a single $2(3 \times 2n)$ matrix of the form

$$\begin{pmatrix} M^{ik}_{LM} & M^{ik}_{D} \\ (M^{ik}_{D})^T & M^{ik}_{RM} \end{pmatrix}. \tag{2.46}$$

The diagonalization procedure for such a matrix is described at greater length in [42–45] and can be reduced to a search of a unitary $2(3 \times 2n)$ matrix U which expresses a specific variety of neutrino ($l = e, \mu, \tau$) through the $3 + n$ diagonal Majorana states.

Left-handed neutrino components may be written as

$$(\nu_{lj})_L = \sum_i U_{ji} (\nu_i)_L , \tag{2.47}$$

where ν_i are the mass eigenstates, ν_{lj} ($l = e, \mu, \tau, j = 1, 2, 3$) are the eigenstates of the electroweak component of the lagrangian, and U_{ji} is a mixing matrix which, in the case of three lepton generations whose left-handed components participate in the electroweak interaction, can be parametrized in a form analogous to the Kobayashi – Maskawa quark mixing matrix [46]:

$$\begin{pmatrix} \nu_e \\ \nu_\mu \\ \nu_\tau \end{pmatrix} = \begin{pmatrix} C_1 & S_1 C_3 & S_1 S_3 \\ -S_1 C_2 & K_1 & K_2 \\ S_1 S_2 & K_3 & K_4 \end{pmatrix} \begin{pmatrix} \nu_1 \\ \nu_2 \\ \nu_3 \end{pmatrix}. \tag{2.48}$$

Here $S_i = \sin\theta_i$, $C_i = \cos\theta_i$, $K_1 = C_1 C_2 C_3 - S_1 S_3 \exp(i\varphi)$, $K_2 = C_1 C_2 S_3 - S_2 C_3 \exp(i\varphi)$, $K_3 = -C_1 S_2 C_3 - S_2 S_3 \exp(i\varphi)$, and $K_4 = -C_1 S_2 S_3 + C_2 C_3 \exp(i\varphi)$, $i = 1, 2, 3$.

Such a matrix contains four parameters: three mixing angles θ_1, θ_2, θ_3 ($0 < \theta_i < \pi/2$) and a complex phase φ ($-\pi \leqslant \varphi \leqslant \pi$). At $\varphi \neq 0$, this leads to CP-parity violation due to the complex vertices described by the Lagrangian of interaction between charged lepton currents in the standard weak interaction theory:

$$L^{CC}_{int} = \frac{G_F}{\sqrt{2}} \left(J^+_\mu W^-_\mu + J^-_\mu W^+_\mu \right). \tag{2.49}$$

Here $G_F = 1.166 \times 10^{-5}$ GeV^{-2} is the Fermi constant, $W^\pm_\mu$ are the boson fields, and

$$J^+_\mu = \bar{\nu}_{lL} \gamma^\mu l^-_L = \frac{1}{2} \sum_l^n \bar{\nu}_l \gamma^\mu (1 + \gamma_5) l^- \tag{2.50}$$

is the left lepton current which can now be expressed through the neutrino mass states:

$$J^+_\mu = \bar{\nu}'_L U^H \gamma^\mu l^-_L . \tag{2.51}$$

All reactions involving neutrinos can be interpreted as a non-coherent sum of all the channels i for neutrinos ν_i ($i = 1, 2, 3$) with kinematically permissible mass m_i and weight $|U_{ij}|^2$. Therefore, the weak interactions are non-diagonal if expressed through mass eigenstates. It is quite possible that the matrix U is close to diagonal, i.e. $|U_{ii}| \geqslant |U_{ik}|$, $i \neq k$ (this does not mean that $m_{\nu_i} > m_{\nu_k}$).

3. Neutrino mass in gauge theories

3.1 Neutrino mass in the standard model

In the standard model of the electroweak interaction based on the $SU(3)_L \otimes SU(2) \otimes U(1)$ group [12, 47], the generation of mass fermions is described by the Yukawa-type interaction between scalar Higgs fields $\varphi(x)$ and a fermionic field conserving parity and fermion flavours. The corresponding Lagrangian is

$$L_{int} = f^{ij}_e \bar{e}_{iR} (\varphi^+ l_{iL}) + f^{ij}_\nu \bar{\nu}_{iR} \left((\varphi^C)^+ l_{iL} \right) + \ldots, \tag{3.1}$$

where

$$l_{iL} = \begin{pmatrix} \nu_{iL} \\ e_{iL} \end{pmatrix} \tag{3.2}$$

are weak left-handed lepton doublets ($i = e, \mu, \tau$ — lepton flavours) which are transformed as components of SU(2) spinors during a global rotation of an isotopic space and are weak eigenstates, $e_{iR}(x)$ and $\nu_{iR}(x)$ are right-handed singlets, f^{ij}_e and f^{ij}_ν are matrices of dimensionless constants which define the lepton masses.

In the case of spontaneous $SU(2) \otimes U(1)$ symmetry breaking, the vacuum average of the scalar isodoublet

$$\varphi = \begin{pmatrix} \varphi^+ \\ \varphi^0 \end{pmatrix}$$

differs from zero. Namely

$$\langle \varphi(x) \rangle = \frac{1}{\sqrt{2}} \begin{pmatrix} 0 \\ V \end{pmatrix}, \tag{3.3}$$

where

$$V = \left(\frac{1}{\sqrt{2} G_F} \right)^{1/2} \simeq 250 \text{ GeV}. \tag{3.4}$$

The substitution of fields $\varphi(x)$ in the form (3.3) into the Lagrangian (3.1) leads to

$$\begin{aligned} L_{int} &= \frac{V}{\sqrt{2}} \left[f_{ij} (\bar{e}_i e_i) + f_{ij} (\bar{\nu}_i \nu_i) \right] \\ &= m_{ij} \left[(\bar{e}_i e_i) + (\bar{\nu}_i \nu_i) \right], \end{aligned} \tag{3.5}$$

where

$$\bar{\nu}_i \nu_i = \bar{\nu}_R \nu_L + \bar{\nu}_L \nu_R , \quad \bar{e}_i e_i = \bar{e}_R e_L + \bar{e}_L e_R , \tag{3.6}$$

and

$$m_{ij} = \frac{V}{\sqrt{2}} f_{ij} \quad (i, j = e, \mu, \tau) \tag{3.7}$$

is the fermion mass matrix whose elements define the lepton masses of all flavours, e.g.

$$m_e = \frac{f_e V}{\sqrt{2}}, \quad m_\nu = \frac{f_\nu V}{\sqrt{2}}, \tag{3.8}$$

and are arbitrary parameters which can not be computed because of the infinite renormalization of both the mass and the coupling constant of the gauge theory.

The lepton mass matrix is proportional to the Yukawa interaction constant matrix and can be diagonalized:

$$L_{\text{int}} = m_i[\bar{e}'_i e'_i + \bar{\nu}'_i \nu'_i]. \tag{3.9}$$

Here the primed fields are the mass matrix eigenstates.

In the standard $SU(2) \otimes U(1)$ theory, the neutrino masses (both Dirac and Majorana ones) must be zero since the Higgs sector structure leads to a global symmetry corresponding to lepton number conservation. This symmetry forbids the appearance of Majorana mass terms in the bilinear form $f\,\bar{\nu}_L^C \nu_L$ violating conservation of the lepton number L with the selection rule $\Delta L = 2$. The Dirac mass terms conserve the total lepton number, but all the $f_{ij} \equiv 0$ since right-handed neutrinos ν_{iR} are non-existent in nature; hence, $m_{ij} \equiv 0$. To summarize, the zero mass of the neutrino in the standard theory is conditioned by the limited number of particles' fields which create the simplest representation of $SU(2) \otimes U(1)$. In GUTs described by groups of a higher dimension and corresponding to a more complete unification, the number of fields increases and neutrino mass terms appear.

There are several possibilities to extend the standard model in which the neutrino mass arises in the non-contradictory mode.

3.2 Extension of the Higgs sector and generation of Majorana mass

It is possible to postulate a triplet of Higgs fields **H** with a hypercharge $Y = 2$ [48, 49] in addition to (3.3) and present it in the form

$$\cdot\mathbf{H} = \begin{pmatrix} H^+ & \sqrt{2}H^{++} \\ \sqrt{2}H^0 & -H^+ \end{pmatrix}. \tag{3.10}$$

This gives rise to additional terms of the Yukawa interaction in the fermionic Lagrangian:

$$L_{\text{int}}^{\text{M}} = f_{ij}\,\bar{l}_{iL}^C l_{jL}(\cdot\mathbf{H}) + Ns \tag{3.11}$$

The substitution of the non-zero vacuum average

$$\langle\cdot\mathbf{H}\rangle = \begin{pmatrix} 0 & 0 \\ V_H & 0 \end{pmatrix} \tag{3.12}$$

of field **H** into (3.11) leads to a Majorana neutrino term of the form

$$(f_{ij}V_H)\,\bar{\nu}_{iL}^C \nu_{jL} \tag{3.13}$$

with the Majorana mass

$$M_M = \frac{f_{ij}V_H}{\sqrt{2}}. \tag{3.14}$$

The vacuum average V_H can not be too large because the average of the isotriplet field makes different contributions to the $W^{\pm}$- and Z-boson masses:

$$\frac{\Delta M_W^2}{M_W^2} = \frac{2V_H^2}{V^2}, \quad \frac{\Delta M_Z^2}{M_Z^2} = \frac{4V_H}{V}. \tag{3.15}$$

Here $V = 250$ GeV is the standard doublet vacuum average. In order to have the relation $M_W = M_Z \cos\theta_W$ fulfilled with an accuracy corresponding to experimental data (of the order of 1%), the condition $V_H \leqslant 0.1V$ is necessary, e.g. $V_H \leqslant 25$ GeV.

Such a model with the Higgs field triplet also predicts the existence of a massless particle, the majoron [48]. It results from the non-orthogonal transformation of global symmetry of the original Lagrangian relative to the gauge U(1)-symmetry transformation. Concurrently, the imaginary part of component H^0 of the field $\mathbf{H} = (H^{++}, H^+, H^0)$ mixes with the imaginary part of the Higgs doublet field φ. This leads to the formation of a non-physical field

$$\psi = \frac{V\,\text{Im}\,\varphi + 2V_H\,\text{Im}\,H^0}{\sqrt{V^2 + 4V_H^2}} \tag{3.16}$$

absorbed by a massive Z^0-boson while the orthogonal combination

$$\chi = \frac{V\,\text{Im}\,\varphi - 2V_H\,\text{Im}\,H^0}{\sqrt{V^2 + 4V_H^2}} \tag{3.17}$$

describes a massive Goldstone boson, the majoron. This is a real physical object arising from the extension of the Higgs sector in the standard model with a non-zero vacuum average and is responsible for double neutrinoless beta-decay [50].

3.3 Extension of the lepton sector and generation of Dirac mass

The leptonic sector can be extended at the electroweak level by introducing left-handed neutrino fields ν_R which can either be singlets of group $SU(2) \otimes SU(1)$ or may be coupled to e_R into doublets, similar to ν_L and e_L [51]. In this case, the Lagrangian (3.1) contains an additional mass term

$$L_{\text{int}}^{\text{D}} = M_D \bar{\nu}_L \nu_R + \text{H.c}, \tag{3.18}$$

where

$$M_D = \frac{1}{\sqrt{2}} f_\nu V \tag{3.19}$$

is the Dirac mass which appears as a result of the spontaneous symmetry breaking caused by the non-zero vacuum average $\langle\varphi\rangle = V/\sqrt{2}$. This, however, does not explain why in the absence of additional contributions to the neutrino mass matrix the interaction of the neutrino field with the Higgs field φ is a few orders of magnitude weaker than interaction of the electron field with φ. The difference between the interaction constants for particles of one generation ($f_e/\sqrt{2} = m_e/V \simeq 10^{-5}$, $f_\nu/\sqrt{2} = m_\nu/V = 0$ or $m_\nu/V = 10^{-10}$ if $m_\nu \simeq 10$ eV) with the same field φ can not be accounted for in the framework of the standard model.

3.4 Extension of the Higgs and lepton sectors in the 'see-saw' model

The assumption of the existence of a right-handed neutrino ν_R and a scalar Higgs field χ, which is additive to the doublet

$$\varphi = \begin{pmatrix} \varphi^+ \\ \varphi^0 \end{pmatrix}$$

and a singlet with respect to the standard group $SU(2) \otimes U(1)$, leads to the appearance of both Dirac and Majorana terms in the interaction Lagrangian:

$$L_{\text{int}} = M_{\text{D}} \bar{\nu}_{\text{L}} \nu_{\text{R}} + M_{\text{M}} \bar{\nu}_{\text{R}}^{\text{C}} \nu_{\text{R}} + Ns \tag{3.20}$$

In this case, the Dirac mass

$$M_{\text{D}} = \frac{1}{\sqrt{2}} \langle \varphi(x) \rangle f_{\text{L}} \tag{3.21}$$

is of the same order of magnitude as the mass of a charged fermion (lepton or quark with electric charge $Q = 2/3$), while the Majorana mass

$$M_{\text{M}} = \frac{1}{\sqrt{2}} \langle \chi(x) \rangle f_{\text{R}} \tag{3.22}$$

is close to the energy scale at which symmetry of the group describing a GUT is broken and is reduced to the group $SU(3)_{\text{L}} \otimes SU(2) \times U(1)$. The Majorana mass M_{M} appears due to the neutrality of ν_{R} with respect to the $SU(2) \otimes U(1)$ transformations. In this case, the interaction $f_{\text{R}} \bar{\nu}_{\text{R}} (\chi^{\text{C}})^+ \nu_{\text{R}}$ does not affect the symmetry of the theory, and the lepton number is conserved if a double lepton charge is ascribed to the field χ. The spontaneous $U(1)_{\text{L}}$ symmetry breaking [this group is associated with lepton number conservation and is external relative to the gauge group $SU(2) \otimes U(1)$] leads to the appearance of the Majorana mass M_{MR} of the right-handed neutrino by virtue of the non-zero vacuum average of the Higgs field χ and is accompanied by the appearance of a massless majoron whose field is described by the imaginary component $2^{-1/2} \operatorname{Im} \chi$ [52].

Diagonalization of the mass matrix

$$(\bar{\nu}_{\text{L}}, \bar{\nu}_{\text{R}}^{\text{C}}) \begin{pmatrix} 0 & M_{\text{D}} \\ M_{\text{D}}^{\text{T}} & M_{\text{M}} \end{pmatrix} \begin{pmatrix} \nu_{\text{L}}^{\text{C}} \\ \nu_{\text{R}} \end{pmatrix}$$

in the Lagrangian (2.32) is performed trivially, and the states

$$\nu_{\text{L}}' = \nu_{\text{L}} + \nu_{\text{L}}^{\text{C}}, \quad \nu_{\text{R}}' = \nu_{\text{R}} + \nu_{\text{R}}^{\text{C}},$$

which are involved in weak interactions, are a superposition of two Majorana mass eigenstates:

$$\nu_1 \approx \nu_{\text{L}}' - \frac{M_{\text{D}}}{M_{\text{M}}} \nu_{\text{R}}', \qquad \nu_2 \approx \nu_{\text{R}}' + \frac{M_{\text{D}}}{M_{\text{M}}} \nu_{\text{L}}'. \tag{3.23}$$

The neutrino ν_{L}' is largely a light neutrino with a mass

$$m_{\nu_{\text{L}}'} \approx \frac{M_{\text{D}}^2}{M_{\text{M}}} = \frac{(M_1 - M_2)^2 \sin(2\theta)}{M_1 \sin^2\theta + M_2 \cos^2\theta} \tag{3.24}$$

of the same order as the fermion mass, with a small admixture,

$$\sim \frac{(M_1 - M_2)^2 \sin(2\theta)}{M_1 \sin^2\theta + M_2 \cos^2\theta}, \tag{3.25}$$

of a heavy neutrino with a mass

$$m_{\nu_{\text{R}}'} \approx M_1 \sin^2\theta + M_2 \cos^2\theta. \tag{3.26}$$

Light and heavy neutrinos mix up at an angle

$$\tan^2\theta \approx \frac{m_{\text{f}}^2}{M_{\text{GUT}}}. \tag{3.27}$$

The mechanism underlying neutrino mass generation with two scales of masses (m_{f}, M_{GUT}) which determine the mass matrix in the GUT is referred to as the 'see-saw' mechanism [53].

In the minimal SU(5)-based GUT which comprises the strong, weak, and electromagnetic interactions [54], the right-handed neutrino ν_{R} is absent, as in the standard model, so there is no Dirac mass. The Majorana mass is equally impossible because of the appearance of $\Delta(B - L) = 2$ transitions following the spontaneous $U(1)_{(B-L)}$ symmetry breaking. This symmetry is of global nature for group SU(5) and is associated with the conservation of the difference between barion and lepton charges $(B - L)$. As in the standard model, the non-zero neutrino mass in the minimal GUT – SU(5) theory can be obtained by additionally introducing ν_{R} and extending the Higgs sector. All predictions for the mass are analogous to the estimates (3.24) – (3.27) with $M_{\text{GUT}} = M_{\text{SU(5)}} = 4 \times 10^{14}$ GeV.

Quite a different situation arises in the SO(10)-based GUT. In this theory, the conservation of the charge $B - L$ is associated with gauge symmetry which is not exact because of the absence of the second massless boson, a photon analog, interacting with charge $B - L$ with a coupling constant equivalent to the electromagnetic one. In the case of spontaneous gauge $(B - L)$-symmetry breaking, massless bosons are absorbed through the Higgs mechanism and the corresponding gauge field acquires mass [55, 56].

In this theory, Dirac neutrino mass states arise naturally, as of charged fermions, because fields ν_{L} and ν_{R} are included in the fundamental representation of group SO(10), in **16** plet [57 – 59]. The Dirac mass of the neutrino must be of the order of upper quark masses of the corresponding generation:

$$m_{\nu_i} \sim m_{q_i} \quad (\nu_i = \nu_{\text{e}}, \nu_{\mu}, \nu_{\tau};\ q_i = \text{u}, \text{c}, \text{t}). \tag{3.28}$$

For instance, ν_{e} masses have a value of $\sim$ MeV. However, such a situation is obviously in conflict with experimental findings because in this case, the Dirac mass $M_{\text{D}} \equiv m_{\nu_i}$ is the eigenvalue of the eigenstate ν_i of the original Lagrangian (2.32).

The generation of the Majorana mass in the SO(10)-based model may occur in case of spontaneous gauge symmetry breaking when the Higgs sector is described by the **126**-representation of SO(10) [60]. The vacuum average $\langle H \rangle$ of the Higgs field carries a double lepton charge and is of the same value as the unification scale of interactions $M_{\text{GUT}} = 10^{15} - 10^{19}$ GeV. The interaction of $\langle H \rangle$ with Majorana term $f \bar{\nu}_{\text{R}}^{\text{C}} \nu_{\text{R}} \langle H \rangle$ leads to two diagonal mass states

$$M_1 = \frac{M_{\text{D}}^2}{M_{\text{M}}}, \qquad M_2 = M_{\text{M}} \sim M_{\text{GUT}} = 10^{15} \text{ GeV} \tag{3.29}$$

of neutrinos [see expressions (3.24), (3.26)], the former of which is light and the latter heavy. Experimentally observed left-handed neutrinos largely represent the light mass state with a small admixture of the heavy state, and the following mass hierarchy holds:

$$m_{\nu_{\text{e}}} : m_{\nu_{\mu}} : m_{\nu_{\tau}} = m_{\text{u}}^2 : m_{\text{c}}^2 : m_{\text{t}}^2. \tag{3.30}$$

Relation (3.30) does not explicitly contain the dependence of the neutrino mass on the unification scale M_{GUT} and the quark mass m_q; it implies independence on the Majorana mass M_M. A more exact relationship for neutrino masses, free from the above defects, was obtained in [61, 62]:

$$\frac{m_e}{m_{\nu_\mu}} = \left(\frac{\lambda_u(M_{GUT})}{\lambda_c(M_{GUT})}\right)^2 \frac{M_2}{M_1} \approx \left(\frac{m_u}{m_c}\right)^2 \frac{M_2}{M_1}\,, \tag{3.31}$$

$$\frac{m_{\nu_\mu}}{m_{\nu_\tau}} = \left(\frac{\lambda_c(M_{GUT})}{\lambda_t(M_{GUT})}\right)^2 \frac{M_3}{M_2} = \left(\frac{\lambda_c(m_t)}{\lambda_t(m_t)}\right)^2 \left(1 - \frac{\lambda_t^2(m_t)}{\lambda_L^2}\right) \frac{M_3}{M_2}$$
$$= \left(\frac{m_c}{\eta_c m_t}\right)^2 \left[1 - \left(\frac{m_t}{190}\right)^2\right] \frac{M_3}{M_2}\,. \tag{3.32}$$

The following quantities are introduced into the expressions (3.31), (3.32):

$$m_u = m_u(1\ \text{GeV}) = 5.1 \pm 1.5\ \text{MeV}\,,$$
$$m_c(m_c) = 1.27 \pm 0.05\ \text{GeV}\,,$$
$$M_M \equiv \text{diag}(M_1, M_2, M_3)\,,$$
$$\eta_c = \frac{m_c(m_c)}{m_c(m_t)} \approx 1.9 \ \text{ in the } \alpha_3(M_Z) \text{ region}\,,$$
$$\frac{\lambda_t(m_t)}{\lambda_L} \approx \frac{m_t}{190}\ \text{GeV}, \tag{3.33}$$

where λ_u, λ_c, λ_t are running Yukawa coupling constants for quarks, λ_L is the limiting value of the Yukawa coupling constant for the t-quark, and α_3 is the strong interaction constant.

In principle, the 'see-saw' mechanism can predict neutrino mixing parameters at low energies, by analogy with the Kabayashi-Maskawa quark matrix. In this case, however, the situation is much more complicated because mass generation is described by the 6×6 'see-saw' matrix, which must be known. It can be assumed, without loss of generality, that at low energies heavy neutrinos are described by the symmetric diagonal mass matrix M_ν, and there is a basis in which the charged lepton mixing matrix is diagonal while matrix U diagonalizing M_ν contains relative mixing angles and, in the case of a very small angle $\theta_{e\tau}$, is parameterized in the form

$$U \approx \begin{pmatrix} 1 & \theta_{e\mu} & 0 \\ \theta_{e\mu} & 1 & \theta_{\mu\tau} \\ 0 & \theta_{\mu\tau} & 1 \end{pmatrix}. \tag{3.34}$$

The following phenomenological relations are valid for mixing angles [58, 59]:

$$\theta_{e\mu} = \left(\frac{m_{\nu_e}}{m_{\nu_\mu}}\right)^{1/4}, \quad \theta_{\mu\tau} = \left(\frac{m_{\nu_\mu}}{m_{\nu_\tau}}\right)^{1/2}, \quad \theta_{e\tau} \approx 0\,. \tag{3.35}$$

Expressions (3.31) and (3.32) and the form of matrix (3.34) may be used to express neutrino mixing angles through quark masses and neutrino mass states:

$$\sin^2(2\theta_{e\mu}) = 4\left(\frac{m_u}{m_c}\right)\left(\frac{M_2}{M_1}\right)^{1/2}, \tag{3.36}$$

$$\sin^2(2\theta_{\mu\tau}) = 4\left(\frac{m_c}{\eta_c m_t}\right)^2 \left[1 - \left(\frac{m_t}{190}\right)^2\right] \frac{M_3}{M_2}\,. \tag{3.37}$$

These expressions are convenient for comparison with experimental data.

Calculations using these three formulae at $M_3/M_2 = 10$, $m_{\nu_\mu} = 2 \times 10^{-3}$ eV and in the t-quark mass range $90 \leqslant m_t \leqslant 150$ GeV [63,64] yield τ-neutrino mass values in the range

$$4.7 \leqslant m_{\nu_\tau} \leqslant 27 \ \text{ eV} \tag{3.38}$$

and parameters of $\nu_\mu \to \nu_\tau$ mixing in the ranges

$$3.0 \times 10^{-4} \leqslant \sin^2(2\theta_{\mu\tau}) \leqslant 1.7 \times 10^{-3}\,, \tag{3.39}$$

$$22 \leqslant \Delta m^2_{\nu_\mu \to \nu_\tau} \leqslant 715 \ \text{ eV}^2\,. \tag{3.40}$$

Let us now consider supersymmetry models which predict neutrino masses in the framework of the 'flipped see-saw' mechanism. Let us first examine the simplest supersymmetric extension of the standard model in the context of SU(5) group [64–66]. In such a scheme, the 'see-saw' matrix for each generation includes three fields, ν_i, ν_i^C and ϕ_i [67–69]:

$$(\nu_i, \nu_i^C, \phi_i) \begin{pmatrix} 0 & m_{ui} & 0 \\ m_{ui} & \lambda_{9i} M^2_{GUT}/M_{nr} & \lambda_{6i} M_{GUT} \\ 0 & \lambda_{6i} M_{GUT} & \mu_i \end{pmatrix} \begin{pmatrix} \nu_i \\ \nu_i^C \\ \phi_i \end{pmatrix}. \tag{3.41}$$

Here ϕ_i is the SU(5)⊗U(1) singlet field and different states of the matrix are derived from the following field combinations of the supersymmetric SU(5)-theory:

$$\lambda_{ui} F_i \bar{f}_i \bar{\varphi} \to m_{ui} \nu_i \nu_i^C\,, \tag{3.42}$$

$$\lambda_{6i} F_i \bar{H} \phi_i \to \lambda_{6i} \bar{V} \nu_i^C \phi_i \approx \lambda_{6i} M_{GUT} \nu_i^C \phi_i\,, \tag{3.43}$$

$$\lambda_{9i} \frac{1}{M_{nr}} F_i F_i \bar{H}\bar{H} \to \lambda_{9i} \frac{\bar{V}^2}{M_{nr}} \nu_i^C \nu_i^C \approx \lambda_{9i} \frac{M^2_{GUT}}{M_{nr}} \nu_i^C \nu_i^C\,, \tag{3.44}$$

while the mass term is $\mu_i \phi_i \phi_i$. In these expressions, F_i and $\bar{f}_i$ are the usual fields of matter in the representation **10** and $\bar{\mathbf{5}}$, H and $\bar{H}$ are the Higgs fields in the representation **10** and $\bar{\mathbf{10}}$, the neutral component (V_H^C, V_H^C) of which acquires the vacuum average $V = \bar{V} \approx M_{GUT}$ in the case of SU(5)⊗U(1) spontaneous symmetry breaking, and $M_{nr} \approx 10^{18}$ GeV is the scale at which non-renormalizable terms in the superpotential are calculated [70, 71]). Probably, the computation of such non-renormalizable interaction will be feasible in the framework of string models [72].

The light neutrino state in the 3×3 'see-saw' matrix is such that

$$m_{\nu_i} \approx \frac{m_{ui}^2}{M_i}\,, \tag{3.45}$$

$$M_i = \lambda_{6i}^2 \frac{M^2_{GUT}}{\mu_i} \left(1 - \frac{\lambda_{9i}}{\lambda_{6i}^2} \frac{\mu_i}{M_{nr}}\right). \tag{3.46}$$

Neglecting the heavy state, that is assuming $\lambda_{9i} \equiv 0$, gives the following relation between mass states:

$$\frac{M_3}{M_2} = \frac{\lambda_{63}^2}{\lambda_{62}^2} \frac{\mu_2}{\mu_3}\,. \tag{3.47}$$

String models [70–72] assume three generations of Yukawa constants, with the two former being markedly

suppressed: $\sim \mu/M_{\rm nr} \sim 1/10$. The masses μ_i must obey such a hierarchy: if $\lambda_{62}/\lambda_{63} \sim 1/10$, it follows from (3.47) that $M_3/M_2 \sim 1-100$. Now, we have from expressions (3.45), (3.46) that

$$m_{\nu_\tau} = \frac{m_{\rm t}^2(M_{\rm GUT})}{M_3} = m_{\rm t}^2\left[1-\left(\frac{m_{\rm t}}{190}\right)^2\right]^{-1}\frac{1}{\eta M_3}\,, \qquad (3.48)$$

and the value $m_{\nu_\tau} \sim 1-10$ eV is obtained for $M_3 \sim 10^{12}$ GeV (with $\eta = 10$). The value $M_3 \sim \lambda_{63}^2 M_{\rm GUT}^2/\mu_3 \sim 10^{12}$ GeV is obtained for $M_{\rm GUT} \sim 10^{15}$ GeV from expression (3.46).

4. Neutrino mass in cosmology

Massive neutrinos could be formed in the early Universe and survive at later phases of its expansion. Their gravitational interaction with fields of matter at different stages of evolution could play a role in the formation and stability of different structures in the Universe.

The Universe is homogeneous and isotropic at larger scales. Evolution of its scale factor $R(t)$ is described by the Einstein equations [73]:

$$\frac{1}{R}\,\frac{{\rm d}^2R}{{\rm d}t^2} = -\frac{4\pi}{3}\,G_{\rm N}(\rho+3p)+\frac{\Lambda}{3}\,, \qquad (4.1)$$

$$H^2 \equiv \left(\frac{1}{R}\,\frac{{\rm d}R}{{\rm d}t}\right)^2 = \frac{8\pi}{3}\,G_{\rm N}\rho - \frac{K}{R^2}+\frac{\Lambda}{3}\,. \qquad (4.2)$$

Here ρ is the matter energy density in the Universe, p is the pressure of the matter, $G_{\rm N} = M_{\rm P}^{-2}$ is the gravitation constant expressed through the Plank mass $M_{\rm P} = 1.2\times 10^{19}$ GeV,

$$H = \frac{{\rm d}R}{{\rm d}t}\,\frac{1}{R}$$

is the time-dependent Hubble constant, $K = +1, -1, 0$ are the three signatures for the closed, open, and flat Friedman Universe respectively, and Λ is the cosmological constant assumed to be zero.

The Hubble constant in the present epoch

$$H_0 = 100h\ \ {\rm km\ (s\ Mps)^{-1}} \sim h\times 10^{-10}\ {\rm year^{-1}} \qquad (4.3)$$

is defined up to values of h lying in the interval $h = 0.5-1$. For a flat Universe, the matter energy density and the Hubble constant are connected by Eqn. (4.2) with the critical density

$$\rho_{\rm c} = \frac{3H^2}{8\pi G_{\rm N}} = \frac{3H^2M_{\rm P}^2}{8\pi}\,. \qquad (4.4)$$

If density is higher (for a given H), the Universe is closed, while if lower it is open. At present, the critical density of the Universe is

$$\rho_{\rm c} = 1.88\times 10^{-29}\ h^2\ \ {\rm g\ cm^{-3}}\,, \qquad (4.5)$$

and the mean ratio of mean matter density to critical density is characterized by the quantity

$$\Omega = \frac{\rho}{\rho_{\rm c}}\,. \qquad (4.6)$$

Astrophysical observations of luminous parts of galaxies give the value $\Omega_{\rm gal} = 0.01$. In other words, the amount of barion matter in visible stars is two orders of magnitude smaller than is necessary to exclude infinite expansion of the Universe.

Another group of observations is pertinent to the determination of the gravitational mass of spiral galaxies based on their rotational dynamics [74]. The orbital velocities of objects outside such galaxies, on the assumption of a compact center of attraction with mass $M(R)$ inside a sphere of radius R, must decrease with distance:

$$V^2 = \frac{G_{\rm N}M(R)}{R}\,. \qquad (4.7)$$

However, the observable radiation spectrum defined by the Doppler shift of spectral lines corresponding to hydrogen surrounding the galaxies leads to an R-independent value $V = {\rm const}$. The flat rotation curve implies a total mass

$$M_{\rm tot} = G_{\rm N}^{-1}V^2R\,, \qquad (4.8)$$

which is

$$10^{11}M_\odot\left(\frac{V\ [{\rm km\,s^{-1}}]}{200}\right)^2\frac{R\ [{\rm kpc}]}{10}$$

higher than the visible mass $M_{\rm (vis)}$.

The velocity dispersion of groups and clusters of galaxies [75] correlates with the x-ray emission of the hot gas present in these clusters [76] and corresponds to the gravitational potential and the total galactic mass which is an order of magnitude larger than the masses of the galaxies and gas taken together. This discrepancy can be accounted for by the existence of non-luminous matter concentrated at the periphery of galaxies and their clusters with a mean density

$$\Omega_0 \simeq 0.2-0.4\,. \qquad (4.9)$$

The calculation of barionic matter density based on the Universe expansion rate during nucleosynthesis and the comparison of theoretical and observed distributions of relic hydrogen nuclei and the isotopes ^{3}He and ^{4}He yield a barion density [77]

$$\rho_{\rm bar} = (2.82\pm 0.94)\times 10^{-31}\ {\rm g\ cm^{-3}}\,, \qquad (4.10)$$

or only 6% of the critical density:

$$\Omega_{\rm bar} = (0.06\pm 0.02)\,h^{-2}\,. \qquad (4.11)$$

An excess of Ω_0 over $\Omega_{\rm bar}$ indicates that a major part of the Universe mass is condensed in non-luminous matter. It is unlikely that there is a significant amount of invisible non-barion matter, which it can not make a substantial contribution to the dark matter [78] to ensure $\Omega = 1$. Instead, a massive neutrino appears to be the most likely candidate for dark matter in the Universe.

Neutrino mass can be derived from cosmological considerations related to the hot Universe model [78], with due regard for current astrophysical observations of matter density and the microwave background radiation spectrum. This approach was first realized in [80] where an upper estimate for the rest mass of a muon neutrino was computed to be $m_\nu < 400$ eV. This work was followed by a number of reports demonstrating the key role of relic neutrinos in the formation of clustered galaxies and their hidden mass [81, 82].

At early stages of expansion of the hot Universe, neutrinos were in thermodynamic equilibrium with photons, electrons, quarks, and antiparticles. This inference provides

the basis for calculating all parameters of the present neutrino distribution. The particle number density in the radiation Universe is related to temperature by the formula

$$n = (kT)^3 \frac{1}{2\pi^2} \int_0^\infty \frac{x^2\,\mathrm{d}x}{\exp(x)-1} \left(\sum_{\mathrm{b}} g_{\mathrm{b}} + \frac{3}{4} \sum_{\mathrm{f}} g_{\mathrm{f}} \right) \quad (4.12)$$

for black body radiation [83], where

$$\zeta(3) = \int_0^\infty \frac{x^2\,\mathrm{d}x}{\exp(x)-1} = 1.2$$

is the Riemann function, g_{b} and g_{f} are the numbers of boson and fermion degrees of freedom (helicity states) respectively. For a photon gas $g_{\mathrm{b}} = 2$, while for Majorana and Dirac neutrinos $g_{\mathrm{f}} = 2$ and 4 respectively. The relationship between energy density and pressure is described by the equation for an ultra-relativistic hot gas of particles:

$$\rho = 3p = \frac{\pi^2}{30}(kT)^4 \left[\sum_{\mathrm{b}} g_{\mathrm{b}} + \frac{7}{8} \sum_{\mathrm{f}} g_{\mathrm{f}} \right]. \quad (4.13)$$

At the temperature

$$T_0 = 2.726 \pm 0.005 \text{ K}, \quad (4.14)$$

of relic radiation precisely measured by COBE [84], the current photon density derived from (4.12) is

$$n_\gamma = \frac{2\zeta(3)}{\pi^2}(kT_0)^3 \approx 411 \text{ cm}^{-3}, \quad (4.15)$$

and the corresponding energy density from (4.13) is

$$\rho_\gamma = 4.65 \times 10^{-34} \text{ g cm}^{-3} = 0.26 \text{ eV cm}^{-3}, \quad (4.16)$$

i.e. five orders of magnitude lower than the critical density.

A similar line of reasoning leads to the relic neutrino density. In equilibrium with radiation, the ratio of Majorana neutrino density n_{ν_i} and n_γ in accordance with (4.12) is

$$\frac{n_{\nu_i}}{n_\gamma} = \frac{3}{4} \quad (4.17)$$

for each flavour. This ratio remains unaltered after neutrinos escape thermodynamic equilibrium up to $kT_\nu \simeq 0.2\, m_{\mathrm{e}} c^2$, when $\mathrm{e}^+\mathrm{e}^-$-annihilation started to heat phonon radiation. Conservation of entropy in the Universe leads to a rise in the photon number per unit volume at constant neutrino density by a factor

$$1 + \frac{7}{8} g_{\nu_i} = \frac{11}{4}. \quad (4.18)$$

Then, the present-day density of each flavour of Majorana and Dirac neutrinos must be

$$(n_{\nu_i})_{\mathrm{M}} = \frac{3}{4}\left(\frac{T_{\nu_i}}{T_\gamma}\right)^3 n_\gamma = \frac{3}{11} n_\gamma \simeq 115 \text{ cm}^{-3}, \quad (4.19)$$

and respectively

$$(n_{\nu_i})_{\mathrm{D}} = \frac{6}{11} n_\gamma \simeq 230 \text{ cm}^{-3}. \quad (4.20)$$

Upon transition to neutrino mass eigenstates, the neutrino energy density can be written as

$$\rho_{\nu_i} = \frac{3}{11} n_\gamma \sum_i \frac{g_{\nu_i}}{2} m_i \simeq 2 \times 10^{31} \sum_i \frac{g_{\nu_i}}{2} m_i \quad [\text{eV}]. \quad (4.21)$$

Assuming that massive neutrinos are responsible for the apparent lack of matter in the Universe up to $\Omega = 1$, we get from Eqns (4.5) and (4.21) the upper bound on the neutrino mass:

$$\sum_i \frac{g_{\nu_i}}{2} m_i \quad [\text{eV}] \leqslant 91.8\, h^2. \quad (4.22)$$

In the case of the neutrino mass hierarchy $m_{\nu_\tau} \gg m_{\nu_\mu} \gg m_{\nu_{\mathrm{e}}}$, a major contribution to the dark matter is made by τ-neutrinos with $m_{\nu_\tau} = 23$ eV for $h = 0.5$ and $m_{\nu_\tau} = 91.8$ eV for $h = 1$. The value $m_{\nu_\tau} \approx 30$ eV, preferable from the cosmological point of view, is in good agreement with the predictions of 'flipped see-saw' models. This mass value at $h \geqslant 5$ corresponds to an age

$$t_0 = \frac{1}{H_0} \int_0^1 \left(1 - \Omega_0 + \frac{\Omega_0}{x}\right)^{-1/2} \mathrm{d}x \geqslant 13 \times 10^9 \text{ years} \quad (4.23)$$

of the Universe, which is not at variance with the age of the oldest stars in stellar clusters [$t_0 \geqslant (14-16) \times 10^9$ years] and the estimates by nuclear cosmochronological methods. Analysis of the present-day isotope composition of uranium gives $t_0 > 8 \times 10^9$ years [85] and a study of radioactive Re decay into Os leads to value of $t_0 > (11-18) \times 10^9$ years [86].

Now let us consider the cosmological role of neutrinos in the formation of the large-scale structure of the Universe. This problem is most comprehensively reviewed in [87–91].

The evolution of the Universe described by the equation for the state of a hot ultrarelativistic gas of particles (photons, electrons, neutrinos, quarks, and their antiparticles) with a pressure $p = \rho/3$ leads to the scale-factor values

$$\left[\frac{\mathrm{d}R(t)}{\mathrm{d}t}\right]^{-2} \sim t. \quad (4.24)$$

It follows from (4.2) that

$$|\Omega - 1| = \frac{|\rho(t) - \rho_{\mathrm{c}}|}{\rho_{\mathrm{c}}} = \left[\frac{\mathrm{d}R(t)}{\mathrm{d}t}\right]^{-2}. \quad (4.25)$$

In order that the present-time Ω value lies in the interval

$$0.1 \leqslant \Omega \leqslant 2, \quad (4.26)$$

it is necessary that the inequality

$$|\Omega - 1| \leqslant 10^{-59} \frac{M_{\mathrm{P}}}{T^2} \quad (4.27)$$

be fulfilled at an early stage of evolution of the hot Universe.

At a temperature $T \sim M_{\mathrm{P}}$ and for the Plank moment $t_{\mathrm{P}} \simeq M_{\mathrm{P}}^{-2}$, the Universe must have had a density close to the critical one, to the accuracy

$$|\Omega - 1| = \left|\frac{\rho}{\rho_{\mathrm{c}}} - 1\right| \leqslant 10^{-59}. \quad (4.28)$$

This scenario is most readily realized at $\Omega = 1$ because in this case the value of Ω remains unity throughout the period

of evolution. The present-day approximate equation $\Omega \approx 1$ implies, in conformity with (4.28), a correspondence to the critical density at Plank scales with an accuracy of 10^{-59}. The solution of this problem has been found in inflation models of the Universe assuming the existence of an unstable vacuum-like state with a high energy density at the earlier stages of evolution [92–95]. In this case, it follows from (4.2) that at large times the Universe undergoes exponential expansion or inflation,

$$a(t) = a_0 \exp\left(\int_0^t H(t)\,\mathrm{d}t\right), \tag{4.29}$$

which continues until the vacuum energy is completely converted to thermal energy. Thereafter, the hot Universe is described by the canonical evolution theory.

A few characteristic scales determining the development of perturbations are distinguished in the evolution of the neutrino Universe. One is directly related to neutrino mass and determines the horizon scale $R_{\mathrm{hor}}(t_\nu) \approx 2ct$ at time $t = t_\nu$ and $3kT_\nu \approx m_\nu c^2$ when neutrinos become non-relativistic. They remain as such until the moment $t < t_\nu$, and perturbations at large scales grow according to the law

$$\frac{\delta\rho}{\rho} \propto t\,. \tag{4.30}$$

The boundary between large and small scales is determined by the Jeans scale

$$R_{\mathrm{J}} \approx \frac{2ct}{\sqrt{3}}\,, \tag{4.31}$$

which is close to the horizon scale $R_{\mathrm{hor}}(t_\nu)$. Another characteristic scale is associated with the equilibrium time t_{eq} when matter and radiation are of the same density. At $t > t_{\mathrm{eq}}$, the neutrino density ρ_ν begins to exceed the radiation density, and from this moment, the neutrino becomes the determinant of the general expansion and evolution of inhomogeneities according to

$$\frac{\delta\rho}{\rho} \propto t^{2/3} \propto \frac{h^2}{1+Z}\,, \tag{4.32}$$

where Z is the red shift defined by the wavelength ratio of emitted (λ_1) to observed (λ_2) light:

$$1 + Z = \frac{\lambda_2}{\lambda_1}\,. \tag{4.33}$$

Neutrinos come within the horizon practically at the moment of equilibrium which in the linear theory of gravitational instability determines the natural damping scale R of neutrino perturbations which can be expressed through the Jeans mass:

$$M_{\mathrm{J}} = \rho_\nu R_\nu^3 = \frac{M_{\mathrm{P}}^3}{m_\nu^2} = 10^5\, M_\odot \frac{m_\nu}{30} \quad [\mathrm{eV}]\,. \tag{4.34}$$

The Jeans mass (4.34) corresponds to the masses of large-scale structures in the Universe, i.e. superclusters.

The evolution of perturbations on a scale which significantly exceeds the Jeans scale ($M \gg M_{\mathrm{J}}$) is described by the non-linear gravitational instability theory [96] and ensures the development of the structure of the Universe filled with both massive and massless neutrinos. The evolution of density perturbations growing in compliance with (4.32) can be described by an approximate non-linear solution in the form of the dependence of the Euler particle coordinates r_i on the Lagrangian coordinates q_i and time:

$$r(\mathbf{q}, t) = (1 - Z)^{-1}\left[q_i - B(Z)S_i(\mathbf{q})\right]. \tag{4.35}$$

Here, the factor $(1 - Z)^{-1}$ is a growing function of time defining the overall expansion of the Universe, $B(Z)$ is an increasing time function which describes the perturbation growth, and $S_i(\mathbf{q})$ is the potential vector field giving the initial perturbation as a function of the Lagrangian coordinates. The solution (4.35) predicts the appearance of strongly flattened clouds of compressed gas and neutrinos ('pancakes'). Neutrino and gas pancakes evolve simultaneously and are bounded by a caustic, i.e. a surface of infinite density. Such a border is subject to erosion under the influence of the initial thermal dispersion of neutrino velocities which maintains a maximum density at the level [97]

$$\rho_{\max} \approx (10{-}20)\langle\rho_\nu\rangle\,. \tag{4.36}$$

The structure of the neutrino Universe is defined by a single small parameter, the metric perturbation amplitude $h_\nu \approx 10^{-4}$. According to the equation $p \propto \rho_\nu^2$ for the neutrino gas state this parameter limits the achievable neutrino density at the moment of pancake formation [98]:

$$\rho_{\max} \approx h_\nu^{-1/3}\,. \tag{4.37}$$

On the whole, the non-linear stage of perturbation evolution is responsible for the structure of the Universe in the form of gas and neutrino clouds whose mass and size correspond to galactic superclusters. Therefore, neutrinos with mass $m_\nu \approx 30$ eV fairly well define the typical structure at scales corresponding to (4.34), and fragmentation of superclusters into galaxies occurs during their rotation.

Information about the neutrino density perturbation spectrum can be obtained from measurements of the large-scale mode of temperature fluctuations of relic radiation. Hydrogen recombination in the Universe at $T \approx (3{-}4) \times 10^3$ K arrests interactions between radiation and matter. However, this process is very slow in the neutrino Universe with a low density of baryons and impairs temperature fluctuations of the relic radiation [91] which are minimal in the present structure of the Universe at scales ≈ 100 Mps. The COBE satellite experiment designed to measure the quadrupole mode in relic radiation anisotropy independently of the motion of the Sun, Earth, and satellite gave the value [99]

$$Q = 17 \times 10^{-6}\ \mathrm{K}. \tag{4.38}$$

If the temperature-dependent deviation of the relic radiation spectrum from the equilibrium thermal distribution (4.14) is related to the gravitational effect of inhomogeneities of the neutrino component in the form of massive neutrinos, it is possible to calculate the invariant amplitude in the perturbation spectrum at different times, as shown in Fig. 1 [33].

At horizon scales, the density perturbations are

$$\left(\frac{\delta\rho}{\rho}\right)_{\mathrm{hor}} = \frac{9\sqrt{3}}{2\sqrt{5}}\,\frac{Q}{T} = 2.15 \times 10^{-5}\,. \tag{4.39}$$

The amplitude of these perturbations increases during the matter predominance stage in accordance with (4.32) by a

factor $(1+Z_{eq})$, where $Z_{eq}=2.77\times10^4h^2$ is the red shift at equilibrium. Therefore, the value of

$$\left(\frac{\delta\rho}{\rho}\right)_{Z_f}=\frac{0.6}{1+Z_f}\,h^2 \tag{4.40}$$

at Jeans scales in the epoch of formation of the large-scale structure with $Z_f\approx3$ is always less than unity [100].

To conclude, the hot dark matter (HDM) [100] model which makes up for the lack of density in the Universe up to $\Omega=1$ in the form of massive neutrinos with mass $m_\nu\simeq30$ eV [101, 102] does not, for all its attractiveness, ensure the amplitude necessary to trigger the non-linear stage of evolution so that the present-day perturbation spectrum correlates with the results of the COBE experiment [99]. An artificial rise in the perturbation amplitude by introducing perturbations of constant curvature in the form of cosmic strings [103, 104] does not solve the problem because additions to the amplitude are insignificant. The amplitude in (4.40) can effectively be increased by introducing cold dark matter (CDM). The candidate particles (neutralino, axion, and axino) occur in the Minimal Supersymmetric Standard Model (MSSM). However, pure CDM also fails to account for perturbation spectra because the CDM curve in Fig. 1 can not simultaneously fit observations at long and short wavelengths by the COBE and IRAS satellites [105]. The best agreement with experimental findings is obtained for the perturbation spectrum calculated in the framework of the mixed dark matter (MDM) model [106] with densities $\Omega_{CDM}=0.69$, $\Omega_{HDM}=0.3$ and $\Omega_{bar}=0.01$ when the cold matter consists of neutralinos and the hot matter of neutrinos (in all probability, ν_τ) [107]. Now,

$$\frac{m_\nu}{91.8}=\Omega_\nu h^2\,, \tag{4.41}$$

in accordance with Eqn. (4.22) [33]. Hence, to-day the most stringent cosmological limitation on neutrino mass has the form

$$m_\nu=7\ \text{eV}\quad\text{for}\quad\Omega_\nu=0.3\quad\text{and}\quad h=0.5\,. \tag{4.42}$$

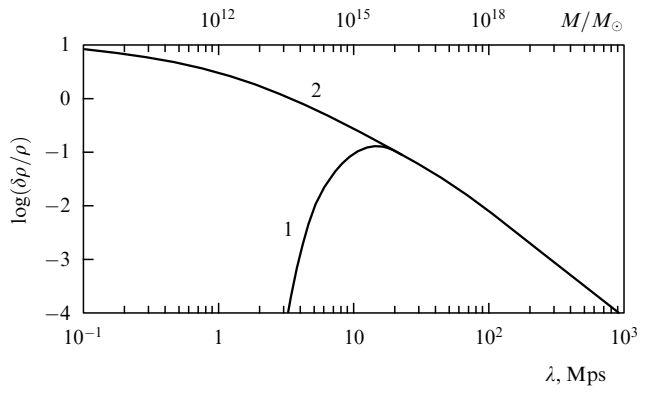

Figure 1. Perturbation spectrum in the present epoch normalized in compliance with COBE findings. Curve *1*: hot dark matter constituted by neutrinos, curve *2*: cold dark matter. The amplitude maximum for hot dark matter is $\delta\rho/\rho\sim0.1$, i.e. smaller than is necessary for the initiation of the the non-linear stage of evolution [33].

5. Experimental measurement of neutrino mass

5.1 Kinematic analysis of weak decays

The most sensitive method for measuring the electron neutrino mass (that of $\bar\nu_e$, to be precise) is the reconstruction of the shape of the electron energy spectrum near the final point of tritium beta-decay:

$$^3\text{H}\rightarrow{}^3\text{He}+e^-+\bar\nu_e\,. \tag{5.1}$$

The advantage of using tritium is the small amount of energy radiation in the reaction (5.1): $E_e^{max}\simeq18.6$ keV. Experimental results are usually presented in the form of a linearized spectrum referred to as the Curie plot:

$$K(E_e)\equiv\left[\frac{dN}{dP_e}\frac{1}{P_e^2F(E_e)}\right]^{1/2}$$
$$\sim(E_e^{max}-E_e)^{1/2}\left[(E_e^{max}-E_e)^2-m_{\nu_e}^2\right]^{1/4}. \tag{5.2}$$

Here $F(E_e)$ is the Coulomb repulsive factor and P_e and E_e are electron momentum and energy respectively. In such a representation, the spectrum (5.2) for zero neutrino mass ends in a straight line while in the case of $m_\nu\neq0$ this spectrum has a vertical tangential component. A major difficulty encountered when using this method originates from the presence of tritium in molecular compounds and the dependence of the resulting spectrum structure on molecular excitations with a typical scale of ~10 eV which are difficult to calculate.

The first studies carried out by Bergkvist and co-workers using a magnetic β-spectrometer and a thin Al-target with implanted molecular tritium yielded spectral characteristics of massless neutrinos. They were followed by a series of experiments performed by a group headed by Lubimov at the Institute of Theoretical and Experimental Physics, Moscow, which suggested a non-zero mass of the neutrino lying in the range 17 to 40 eV. The experiments were conducted on a toroidal spectrometer with a thin film of tritiated valine ($C_5H_{11}NO_2$) as the source [109, 110]. However, further works of different authors failed to confirm the above findings. Specifically, Kundig et al. [111] at Zurich obtained ($m_{\bar\nu_e}<18$ eV), at variance with what was reported in [109, 110], despite using a spectrometer similar to that employed by Lubimov and co-workers. Recent estimates of ν_e mass from the β-decay rate of ^{3}H show a consistent trend to lower the upper limit: $m_{\bar\nu_e}<13.1$ eV [112] <11.7 eV [113], <9.3 eV [114], <7.2 eV [115]. The best result currently available ($m_{\bar\nu_e}<4.5$ eV) has been reported by Lobashev's group at Troitsk [29, 30].

The limit for the muon neutrino mass can be found from kinematic analysis of the decay $\pi^+\rightarrow\mu^++\nu_\mu$. The measurement of muon momentum in such a decay, when the pion beam stops in the target, allows the mass of ν_μ to be estimated as

$$m_{\nu_\mu}^2=m_\pi^2+m_\mu^2-2m_\pi\sqrt{m_\mu^2+P_\mu^2}\,. \tag{5.3}$$

The best estimate of muon neutrino mass so far obtained is $m_{\nu_\mu}<160$ keV [31].

The limitation on the τ-neutrino mass was obtained in the reconstruction of the neutrino energy spectrum with mass-

sensitive shape in the low-energy region from kinematic analysis of pion modes of τ-leptonic decay. The best results were reported by the ARGUS group at DESY from the analysis of mode $\tau^- \to 3\pi^- 2\pi^+ \nu_\tau$ ($m_{\nu_\tau} < 31$ MeV [116]), the CLEO group at CESR from the analysis of modes $\tau^- \to 3\pi^- 2\pi^+ \nu_\tau$ and $\tau^- \to 2\pi^- \pi^+ 2\pi^0 \nu_\tau$ ($m_{\nu_\tau} < 32.6$ MeV [117]), and the ALEPH group at LEP ($m_{\nu_\tau} < 29$ MeV [32]).

5.2 Neutrinoless double beta-decay

The existence of the non-zero Majorana mass of a neutrino must lead, with the higher than zero probability, to a double neutrinoless β-decay ($2\beta(0\nu)$)

$$(A, Z) \to (A, Z+2) + e^- + e^- \tag{5.4}$$

of nuclei containing Z protons and $A = Z + N$ nucleons. The double neutrinoless β-decay is the sole process from which it is possible to identify either the Dirac or Majorana nature of the neutrino mass. The theory of this process has been given much attention in the literature and been reviewed in detail in [50, 118, 119]. The probability of decay (5.4) is defined by the relation [120]

$$W \propto \left| \sum_i \eta_i U_{\alpha i}^2 m_{\nu_i} \right|^2 , \tag{5.5}$$

where $\eta_i = \pm 1$ are the eigenvalues of the operator CP, i.e. eigenvalues of Majorana fields, and m_{ν_i} is the neutrino mass eigenstate. The limitation on the neutrino mass resulting from the analysis of the output of double neutrinoless β-decay correlates with the quantity

$$\langle m_\nu \rangle = \left| \sum_i^n U_{\alpha i}^2 m_{\nu_i} \right| . \tag{5.6}$$

Experimental investigation of neutrinoless 2β-decay is a very difficult task because in the case of $2\beta(0\nu)$-decay, if it occurs, the half-life is not less than $10^{21} - 10^{22}$ years and the characteristic energies of decay products do not exceed a few MeV. Indirect experiments allow for the evaluation of the half-lives of isotopes contained in rocks (Te^{130}, Te^{128}, Se^{82}) which undergo conversion to Xe^{130}, Xe^{128}, Kr^{82} respectively in the course of double β-decay. The probability of $2\beta(0\nu)$-decay can be estimated from the comparison of observed and theoretical values. Uncertainties inherent in the assessment of the nuclear matrix element preclude an unambiguous conclusion that Majorana mass of neutrino differs from zero [121]. In direct experiments, limitations on the Majorana neutrino mass were ascertained from the analysis of the transitions $Mo^{100} \to Ru^{100}$ ($m_\nu < 6.6$ eV [122]), $Xe^{136} \to Ba^{136}$ ($m_\nu < 2.8$–4.3 eV [123]), $Ge^{76} \to Se^{76}$ ($m_\nu < 1.5$ eV [124]). The best limit so far obtained for the Majorana neutrino mass from the analysis of transition $Ge^{76} \to Se^{76}$ by the Heidelberg-Moscow Collaboration is $m_\nu < 0.9$ eV [125].

The existence of the Majorana mass of the neutrino must lead to violation of the lepton number, there being no fundamental reason for its conservation by analogy with the quark sector. Lepton number conservation was precisely measured in processes altering flavours. The relative probability of $\mu \to e\gamma$ decay and the process $K_L \to \mu e$ was estimated with an accuracy higher than 4.9×10^{-11} [126] and 3.3×10^{-11} [127] respectively. However, the output of the reaction $\mu \to e\gamma$ must not exceed 10^{-48} if the neutrino mass is below 1 eV.

5.3 Heavy neutrino decay

The process of flavour variation is very close to the decay of heavy neutrinos ν_i [128–130] which could give rise to the weak state upon superposition with light neutrinos ν_α. Such heavy neutrinos can exist with rather small mixing $U_{i\alpha}$ and show as secondary peaks in the spectrum of charged leptons accompanying neutrinos in the leptonic decay of mesons ($\pi \to \mu\nu$, $\pi \to e\nu$, $K \to \mu\nu$) with the intensity $|U_{i\alpha}|^2$, in addition to the main peak corresponding to ν_α. The current view of the possibility of observing a heavy neutrino (17 keV) is discussed in [131]. The upper limit for the parameters of neutrino mixing with the electron and muon $|U_{i\alpha}|^2$ as a function of $m(\nu_i)$ has been measured in many experiments [132, 133]. The best result $|U_{1\alpha}|^2 < 10^{-7}$ at 50 Mev $< m_{\nu_e} < 130$ MeV was obtained in [134] by the analysis of postulated additional peaks in the positron spectrum from the decay $\pi^+ \to e^+ \nu_e$.

Heavy neutrinos are equally possible to detect in beam-dump experiments or using a beam from an accelerator with an intensity proportional to $|U_{i\alpha}|^2$. Neutrinos heavier than 1 MeV were sought in the leptonic channel $\nu_i \to e^+ e^- \nu_e$. However, this attempt failed and resulted in an increased limit on the heavy neutrino mass.

5.4 Neutrinos from supernova CH 1987A

A limit on the neutrino mass can be derived from records of neutrino radiation by underground detectors on 23 February 1987 during the gravitational collapse of a star in the Large Magellanic Cloud. The possibility of such an evaluation was first predicted by Zatsepin more than 20 years ago [138]. If the neutrino mass m_ν is non-zero and the source (e.g. a supernova explosion) emits neutrinos in the energy range ΔE, a detector located at a distance D from the source will first record high-energy neutrinos. Two neutrinos with energies $E_2 > E_1 \gg m_\nu c^2$ simultaneously emitted by a source will be recorded by the detector as signals separated by a time interval

$$\Delta t_\nu = \frac{D}{2c} (m_\nu c^2)^2 \left(\frac{1}{E_1^2} - \frac{1}{E_2^2} \right) . \tag{5.7}$$

If all the parameters in (5.7), except m_ν, are measured in the experiment, it is possible to calculate the mass of the neutrino. In reality, however, a neutrino burst is not momentary but takes a certain finite time. Its initial stage lasts $\sim 10^{-3}$ s and produces electron neutrinos from electron capture leading to gravitational collapse. Thereafter, neutrino radiation is a statistical mixture of ν_e, $\bar{\nu}_e$, ν_μ, $\bar{\nu}_\mu$, ν_τ, $\bar{\nu}_\tau$ and carries away around 10% of the stellar nuclear mass [139]. According to different authors, the total length of the neutrino signal emitted by a collapsed stellar nucleus is $\Delta T = 2$–20 s [139–142]. Such a discrepancy does not allow neutrino mass to be unambiguously evaluated from (5.7). However, it is possible to place a limit on the neutrino mass from the condition $\Delta t_\nu < \Delta T$. That is, the time difference between records of two neutrinos in a detector (Δt_ν) must be less than the characteristic time of the neutrino burst (ΔT). In this case, the neutrino mass does not substantially affect the temporal structure of the integral characteristics of the neutrino signal.

Neutrinos from a supernova explosion can be experimentally detected with the aid of reaction

$$\bar{\nu}_e + p \to e^+ + n , \tag{5.8}$$

and also via elastic scattering

$$\overset{(-)}{\nu}_i + e^- \to \overset{(-)}{\nu}_i + e^- . \quad (5.9)$$

Radiation from the explosion of supernova CH 1987A was recorded by four detectors: Kamiokande II, IMB, LSD, and the Baksan underground scintillation telescope.

Kamiokande is a large closed water Cherenkov detector installed in the 1,000 m deep Kamioka pit (2,700 mwe), 250 km west of Tokyo (western Honshu coast). The Kamiokande project has been elaborated to carry out a wide range of experiments including a study of proton decay, the detection of solar and atmospheric neutrinos and neutrinos from collapsing supernovae. The results are summarized in scientific papers and technical reports [143–146]. The detector consists of two co-axial cylinders, the outer one 19.6 m in diameter and 22.5 m in height and the inner one (diameter 15.6 m, height 16 m), containing 2,140 tons of water. Cherenkov radiation is detected by 948 Hammamatsu R1449 PMTs each having a 508 mm photocathode. They are uniformly spaced 1 m apart at the inner surface of the instrument, looking inward. The sensitive area viewed by PMTs amounts to 20% of the total inner cylinder surface. Water serves as both the target for passing neutrinos and the Cherenkov radiator for charged interaction products. The water layer between the cylinders is also used as a radiator of Cherenkov photons viewed by 123 PMTs and a counter of anticoincidences. Such an anticoincidence system protects against gamma-radiation, neutrons, and cosmic muons.

A relativistic particle that traverses the bulk of the detector with a coefficient of refraction $n \approx 1.33$ generates a Cherenkov radiation cone with an angle

$$\theta_C = \arccos\frac{1}{n\beta} \approx 40^\circ . \quad (5.10)$$

The number of emitted photons is

$$N_{ph} \approx 370 \sin^2\theta_C \approx 200 \ \text{photon cm}^{-1} . \quad (5.11)$$

The electronics of Kamiokande record signals with an amplitude exceeding the output energy of 0.35 photoelectrons. The detector is triggered when more than 20 PMTs fire in $\tau = 100$ ns, i.e. at the electron energy threshold 7.5 MeV. The energy released and the angles of particle tracks can be derived from the information from each activated PMT about the pulse arrival time and amplitude proportional to Z^2 (Z is the particle's charge). The vertex of a (5.8)-like event is reconstructed with an error of $1\sigma \approx 1.7$ m for an electron having an energy of 10 MeV in the entire detector volume. During the CH 1987A collapse, the Kamiokande detector was adjusted to record solar ^{8}B-neutrinos and had a threshold sensitivity for electrons $E_{e,thr} = 9$ MeV. Neutrinos from the collapse had an energy of around 10 MeV and were readily recorded by the detector.

IMB (Illinois–Michigan–Brookhaven) is a large Cherenkov detector of the closed type located at the bottom of an abandoned salt-mine near Cleveland, Oh, USA, at a depth of 600 m (1,570 mwe). The construction of the detector, the programme of physical research, and the recording procedure were described at length in [147–150]. The latest version of the detector (IMB-3) is a rectangular tank ($22.5 \times 17 \times 18$ m^3) filled in with purified water. The active volume of about 5,000 m^3 is instrumented with 2048 Hammamatsu R4558 PMTs having 200 mm diameter photocathodes arranged on an approximate 1 m grid. Water is both the target for incoming neutrinos and the Cherenkov light radiator, as in the Kamiokande detector. The recording system is triggered by any event firing at least 25 PMTs within $\tau = 50$ ns. The time, configuration, and amplitude of signals from the PMTs are analysed by a computer to reconstruct the neutrino interaction point, and to track the direction and energy of secondary charged particles in each event. The IMB-3 detector has a higher energy threshold for neutrino events compared with Kamiokande (~ 20 MeV) due to the lower efficiency of Cherenkov light collection (14%). Its capacity increases to 90% at energies of 50 MeV.

The LSD is a liquid scintillation detector designed to record stellar collapses in the Galaxy. It is installed in the Mont Blanc tunnel at a depth of 5,200 mwe [151–153]. The construction is a three-storeyed parallelepiped with a base area of 6×7 m^2 and 4.5 m in height. It consists of 72 counters ($1 \times 1.5 \times 1$ m^3 each) filled with scintillation fluid (white spirit). The total active mass of the detector is 90 tons. Each module is viewed by three 49B PMTs with photocathodes 150 mm in diameter. The energy release in a module is analysed when the PMT signals coincide within $\tau = 200$ ns. The energy threshold is 5–7 MeV.

The Baksan underground neutrino telescope is a liquid scintillation detector located at a depth of 850 mwe in the Andyrchi massif, North Caucasus [154, 155]. It is designed to continuously record stellar collapses in the Galaxy. The detector is a four-tiered cube shape of honeycomb geometry with the 14 m sides. Each of the 3,130 $0.7 \times 0.7 \times 0.3$ m^3 modules is filled with white spirit and viewed by a 495-PMT with photocathodes of 150 cm in diameter. The energy threshold is 10 MeV.

Analysis of the neutrino events originating from the collapse of supernova CH 1987A and recorded by the underground detectors Kamiokande, IMB, LSD, and the Baksan neutrino telescope is presented in [139–142, 156, 157]. The main characteristics of neutrino events are summarized in Table 1.

The data obtained in the Kamiokande, IMB, and Baksan experiments are synchronized while the LSD-recorded events were 4.7 hr ahead and may not be associated with the CH 1987A collapse.

The upper bound for the neutrino mass can be estimated based on relation (5.7) and the data of Table 1. Taking the distance to the Large Magellanic Cloud to be $D = 50$ Kpc, the characteristic values $\Delta T = 10–15$ s, $E_{min} = 10$ MeV, and $E_{max} = 20$ MeV and assuming the condition $\Delta t_\nu < \Delta T$ to be satisfied, the limit on the mass will be $m_\nu < 23–28$ eV [139]. This estimate is compatible with the limits calculated in the experiments discussed in Subsections 5.1–5.3. According to Bachall and Glashow [158], there is no correlation between the energy released in the event with time, as should have been expected in the case of a finite neutrino mass.

Analysis of the subtle structure of a neutrino burst on the assumption of special physical processes led certain authors [159–163] to a more conservative estimate $m_\nu < 14–16$ eV.

Hopefully, the forthcoming generation of neutrino detectors described below will provide a better opportunity for examining the neutrino radiation of the next supernova, and a statistical analysis of the results will ensure a more reliable evaluation of the neutrino mass.

Table 1. Characteristics of neutrino events from supernova CH 1987A.

Detector	Energy threshold, MeV	Number of events	Electron energy, MeV		Time interval, s
			Minimal	Maximal	
Kamiokande II [143]	7–14	11	7.5±2.0	35.4±8.0	12.4
IMB [149]	20–15	8	20.0±5.0	40.0±10.0	5.6
LSD [152, 153]	5–7	5	6.2±0.7	7.8±0.9	7.0
Baksan telescope [154, 155]	10	6	12.0±2.4	23.0±4.7	14.0

6. Neutrino oscillations: general formalism

6.1 Vacuum oscillations

Neutrino oscillations are a periodical process during which a beam of neutrinos of a certain flavour ν_l traveling in a vacuum is wholly or partially converted to a neutrino beam of a different flavour $\nu_{l'}$ ($\nu_l \leftrightarrow \nu_{l'}$). In Section 3, we considered the neutrino states ν_e, ν_μ, ν_τ formed during weak interactions which are stationary states of a free Lagrangian. For oscillations to occur, neutrinos must have a mass. In this case, the mass matrix in the Lagrangian expressed through weak eigenstates is non-diagonal and complex. Weak states have no definite mass; they are a linear combination (2.47) of mass eigenstates which diagonalize the Lagrangian (2.32). Such a mixing when a neutrino state ν_l exists as a combination of several eigenstates of the Lagrangian is another condition for the existence of oscillations.

The wave function $|\nu_l\rangle$ describing the free neutrino distribution can be expanded in wave functions of mass states. Different mass states $|\nu_l\rangle$ have different velocities when propagating in a vacuum; as a result, the relative phases in the expansion coefficients change with time. Therefore, neutrino oscillations arise from the difference between the phase velocities of states having masses, i.e. eigenstates of the Lagrangian (2.32).

Let us consider a case of neutrino oscillations when the mixing matrix is parametrized in the form (2.48). The wave function of the neutrino (e.g. ν_e) born in a weak process at the moment $t = 0$ can be represented as a superposition of eigenstates of the mass matrix:

$$|\nu_e(0)\rangle = C_1|\nu_1\rangle + S_1C_3|\nu_2\rangle + S_1S_3|\nu_3\rangle\,. \tag{6.1}$$

Evolution of the wave function in time is defined by the corresponding eigenstates of the energy operator

$$E_i = \sqrt{p_\nu^2 + m_i^2} \tag{6.2}$$

provided all the neutrinos in the beam have an identical fixed momentum p_ν. Then,

$$|\nu_e(t)\rangle = C_1\exp(-\mathrm{i}E_1t)|\nu_1\rangle + S_1C_3\exp(-\mathrm{i}E_2t)|\nu_2\rangle + S_1S_3\exp(-\mathrm{i}E_3t)|\nu_3\rangle\,. \tag{6.3}$$

The probability that at time t a neutrino will remain in the initially weak state $|\nu_e(0)\rangle$ can be found from the relation

$$\begin{aligned} P(\nu_e \leftrightarrow \nu_e) &= |\langle\nu_e(0)|\nu_e(t)\rangle|^2 \\ &= 1 - 2C_1^2S_1^2C_3^2\big[1-\cos(E_1-E_2)t\big] \\ &\quad - 2C_1^2S_1^2S_3^2\big[1-\cos(E_1-E_3)t\big] \\ &\quad - 2S_1^4S_3^2C_3^2\big[1-\cos(E_2-E_3)t\big]\,. \end{aligned} \tag{6.4}$$

In the general case, the probability of transition from state $|\nu_l\rangle$ to state

$$|\nu_{l'}(t)\rangle = \sum_l U_{l'i}\nu_i\exp(-\mathrm{i}E_it) \tag{6.5}$$

is

$$\begin{aligned} P(\nu_l \leftrightarrow \nu_{l'}) &= |\langle\nu_l(0)|\nu_{l'}(t)\rangle|^2 \\ &= \sum_{ij} U_{l'i}U_{li}^*U_{l'j}^*U_{lj}\exp\big[-\mathrm{i}(E_i-E_j)t\big]\,. \end{aligned} \tag{6.6}$$

The least possible value of the averaged probability can be found by minimizing a functional of the form

$$F = \sum_i\left(|U_{l'i}|^2\right)^2 + \lambda\left[\left(\sum_i|U_{l'i}|^2\right) - 1\right], \tag{6.7}$$

which leads to

$$\langle P(\nu_l \leftrightarrow \nu_{l'})\rangle = -\frac{\lambda}{2} = \frac{1}{N}\,, \tag{6.8}$$

where $N = 3$ is the total number of neutrino flavours. Therefore, an original beam of neutrinos with three flavours may undergo a 3-fold reduction when propagating in a vacuum.

Experiments usually analyse the explicit solution of the problem of neutrino oscillations with two flavours. For this reason, the mixing matrix can be written in the form of an orthogonal combination

$$U = \begin{pmatrix} \cos\theta & \sin\theta \\ -\sin\theta & \cos\theta \end{pmatrix} \tag{6.9}$$

with one parameter, the mixing angle θ, and the state of the flavour in the form

$$\begin{pmatrix} \nu_e \\ \nu_\mu \end{pmatrix} = U\begin{pmatrix} \nu_1 \\ \nu_2 \end{pmatrix}. \tag{6.10}$$

Then, the evolution of the wave function in time is described by the state vectors

$$\begin{aligned} |\nu_e(t)\rangle &= \exp(-iE_it)|\nu_e(0)\rangle = \exp(-\mathrm{i}E_1t)\cos\theta|\nu_1\rangle \\ &\quad + \exp(-\mathrm{i}E_2t)\sin\theta|\nu_2\rangle\,, \end{aligned} \tag{6.11}$$

where E_1 and E_2 are energies of two mass states with similar momenta. Let us now turn to flavour states:

$$\begin{aligned} |\nu_e(t)\rangle &= |\nu_e\rangle\big[\cos^2\theta\exp(-\mathrm{i}E_1t) + \sin^2\theta\exp(-\mathrm{i}E_2t)\big] \\ &\quad + |\nu_\mu\rangle\big[\exp(-\mathrm{i}E_2t) - \exp(-\mathrm{i}E_1t)\big]\sin\theta\cos\theta\,. \end{aligned} \tag{6.12}$$

The probability of a neutrino initially in the weak state $|\nu_e\rangle$ remaining in this state for a time t is

$$P(\nu_e \leftrightarrow \nu_e) = |\langle \nu_e | \nu_e \rangle|^2 = 1 - \sin^2(2\theta) \sin^2 \left[\frac{1}{2}(E_2 - E_1)t \right]. \tag{6.13}$$

It can be assumed, to a good approximation, that $E_i \gg m_i$; hence,

$$E_i \simeq p_\nu^2 + \frac{m_i^2}{2p_\nu^2}. \tag{6.14}$$

Then,

$$E_2 - E_1 = \frac{m_2^2 - m_1^2}{2E_\nu} = \pm \frac{\Delta m^2}{2E_\nu}, \tag{6.15}$$

where Δm^2 is always a positive quantity. Now, the relation (6.13) may be regarded as

$$P(\nu_e \leftrightarrow \nu_e) = 1 - \sin^2(2\theta) \sin^2 \left(\frac{\pi L}{L_{vac}} \right), \tag{6.16}$$

where $L = ct$ is the distance covered by a neutrino in a time t (in experiments, this is the distance between the source and the detector) and

$$L_{vac} = 2\pi \frac{2p_\nu}{m_2^2 - m_1^2} \simeq 2\pi \frac{2E_\nu}{\Delta m^2} \tag{6.17}$$

is the vacuum oscillation length which reflects the periodic dependence of a signal in the detector on the distance L for each mass pair (m_1, m_2). The use of units convenient for calculations in oscillation experiments, when E_ν is measured in MeV and Δm^2 in eV^2, yields

$$L_{vac}\ [\mathrm{m}] = 2.48 \frac{E_\nu}{\Delta m^2}. \tag{6.18}$$

The probability of a neutrino in the original weak state $|\nu_l\rangle$ at a distance L from the source turning into $|\nu_{l'}\rangle$ due to the oscillation effect is

$$P(\nu_l \leftrightarrow \nu_{l'}) = \sin^2(2\theta) \sin^2 \left(\frac{\pi L}{L_{vac}} \right) = \sin^2(2\theta) \sin^2 \left(\frac{1.27 L \Delta m^2}{E_\nu} \right). \tag{6.19}$$

Expressions (6.16) – (6.19) describe the model of neutrino oscillations with two flavours in which the amplitude of the process depends on one mixing angle θ while the phase, and hence the probabilities of oscillations, depends on $L\Delta m^2/E_\nu$. For this reason, experiments in search of neutrino oscillations are intended to determine the quantity $\Delta m^2 = |m_i^2 - m_j^2|$ included in expressions (6.17), (16.8) for the vacuum oscillation length and the region of permissible mixing angles θ, rather than the neutrino mass. It follows from (6.19) that the ratio L/E_ν depends on the neutrino mass to which the experiment is sensitive. In order to find the least possible values of Δm^2_{min},

$$\Delta m^2_{min} \sin(2\theta) = \frac{1}{1.27} \frac{E_\nu}{L} \sqrt{\Delta P(\nu_l \leftrightarrow \nu_{l'})}, \tag{6.20}$$

where $\Delta P(\nu_l \leftrightarrow \nu_{l'})$ is the minimal probability, i.e. the minimal difference between flavour compositions in the original and experimentally detected neutrino beams, measurements should be made at the highest possible L/E_ν values. The sensitivity of different experiments to the value of Δm^2 is illustrated in Table 2.

Table 2. Ranges of possible L/E values in experiments searching for vacuum oscillations.

Type of experiment	L/E, m MeV^{-1}
Accelerator	$10^{-3} - 10^{1}$
Meson fabric	$10^{0} - 10^{1}$
Reactor	$10^{0} - 10^{2}$
Atmosphere	$10^{2} - 10^{4}$
Sun	$10^{10} - 10^{11}$
Supernova	$10^{19} - 10^{20}$

Experimental findings are usually presented as boundaries of permissible regions of the oscillation parameter values $(\sin^2(2\theta), \Delta m^2)$ being examined. Figure 2 shows the regions of possible values of oscillation parameters obtained in experiments at high-energy accelerators, reactors, and with solar or atmospheric neutrinos.

6.2 Neutrino oscillations in matter with constant density

The presence of matter in the path of a beam can greatly affect the oscillation patterns because neutrinos undergo refraction when passing through the matter. The coefficient of refraction n for a neutrino with flavour l and momentum p_ν is defined by the optical theorem

$$p_\nu^2 (n - 1) = 2\pi N f_l(0), \tag{6.21}$$

where $f_l(0)$ is the forward scattering amplitude arising from the weak interaction and N is the scattering center density. The imaginary part of the refraction coefficient is related to the cross-section of neutrino absorption in matter which is small and may be neglected. The real part of the scattering amplitude consists of two components. One is common for neutrinos of any flavour and described by the Feynman diagram as shown in Fig. 3a. The other is related to the non-symmetry of interactions of electron neutrinos and neutrinos of other types (ν_μ and ν_τ) with electrons of the medium due to the charged current contribution to scattering $\nu_e e \to \nu_e e$ (Fig. 3b).

It follows from computation of the diagrams in Figs 3a,b that the scattering amplitude of electron neutrinos from electrons of the medium exceeds the scattering amplitude of ν_μ and ν_τ by

$$\Delta f(0) = f_e(0) - f_{\mu,\tau}(0) = -\sqrt{2} \frac{G_F p_\nu}{2\pi}, \tag{6.22}$$

where $G_F = 10^{-5} M_p^{-2}$ is the Fermi constant and M_p is the photon mass.

The value of (6.22) was first obtained by Wolfenstein [164, 165] who demonstrated the difference between oscillations of a neutrino beam in matter and vacuum oscillations. These studies were continued in [34, 166 – 168].

The contribution of (6.22) to the scattering amplitude leads to an additional term W in the energy operator (6.14) which is the potential energy of electron neutrino in a

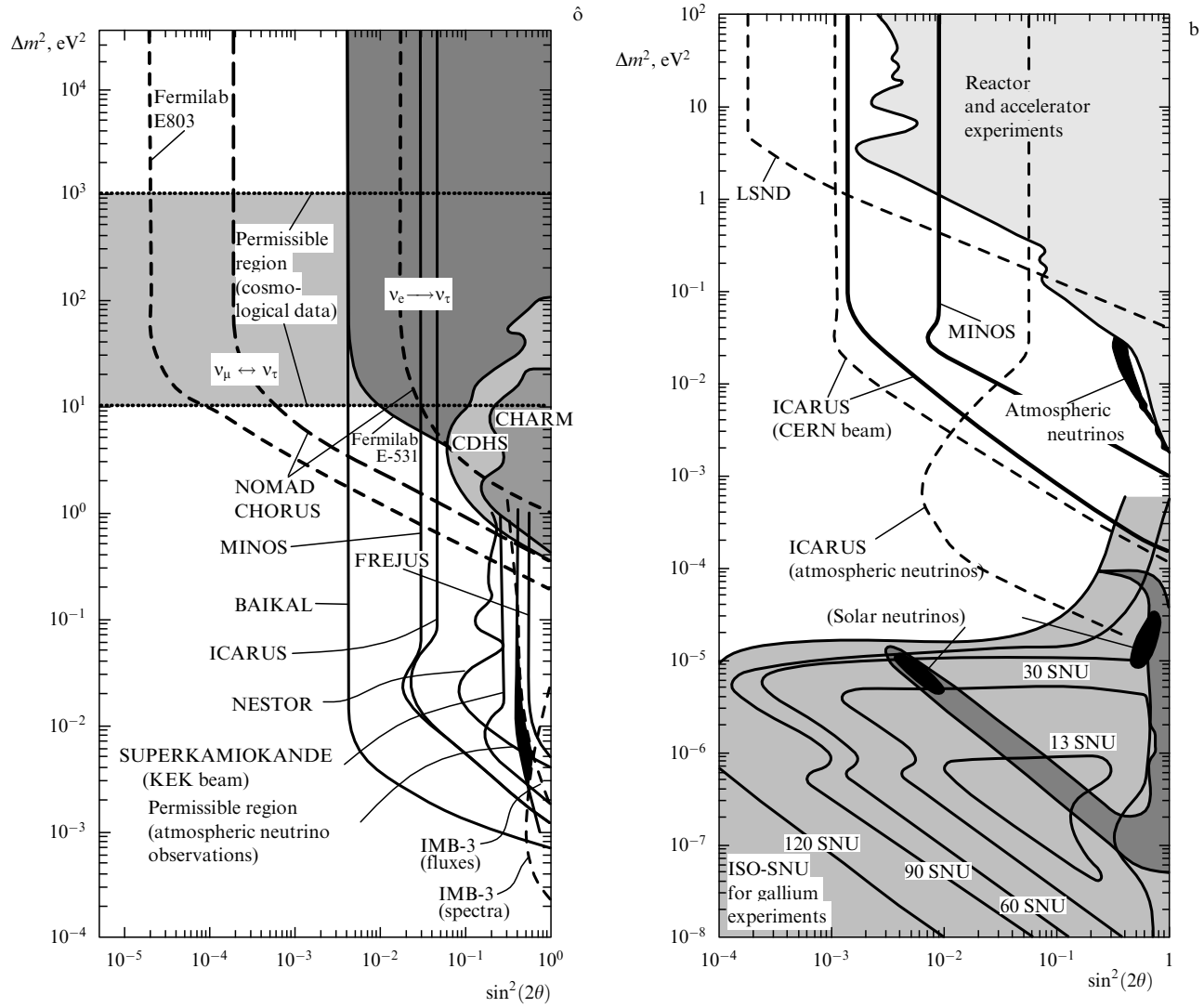

Figure 2. Boundaries of oscillation parameter regions obtained in different experiments and attainable in the near future. The excluded region is to the right of the curves. (a) mode $\nu_\mu \leftrightarrow \nu_\tau$ and $\nu_e \leftrightarrow \nu_\tau$ experiments, (b) mode $\nu_\mu \leftrightarrow \nu_e$ experiments.

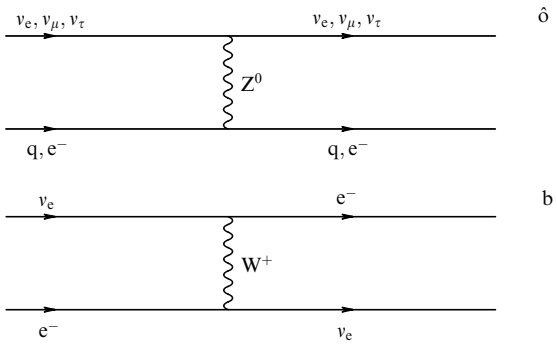

Figure 3. Feynman diagrams describing neutrino-matter interactions: (a) the NC contribution to the forward scattering amplitude is common for all types of neutrinos and changes the phase of all components of the neutrino beam in a similar way, (b) the CC-contribution which holds for ν_e but not ν_μ and ν_τ

medium:

$$E_i \simeq p_\nu + \frac{m^2}{2p_\nu} + W = p_\nu + \frac{m^2}{2p_\nu} + \sqrt{2}\, G_F N_e \,. \tag{6.23}$$

Here N_e is the electron density in the medium and

$$W = -\frac{2\pi\Delta f(0) N_e}{p_\nu} \,. \tag{6.24}$$

Then, the evolution of the wave function (6.11) is described by the state vector

$$|\nu_e(t)\rangle = \exp\left[-\mathrm{i}t\left(\frac{m^2}{2p_\nu} + \sqrt{2}\, G_F N_e\right)\right] |\nu_e(0)\rangle \,. \tag{6.25}$$

The oscillations $\nu_e \leftrightarrow \nu_{\mu,\tau}$ in the medium may be described by the Shrödinger equation for the two-component amplitude $\left|\begin{smallmatrix}\nu_e\\ \nu_{\mu,\tau}\end{smallmatrix}\right\rangle$:

$$\mathrm{i}\frac{\mathrm{d}}{\mathrm{d}t}\left|\begin{matrix}\nu_e\\ \nu_{\nu,\tau}\end{matrix}\right\rangle = H\left|\begin{matrix}\nu_e\\ \nu_{\nu,\tau}\end{matrix}\right\rangle , \tag{6.26}$$

$$H \equiv E_i \,. \tag{6.27}$$

While the solution of Eqn. (6.26) in a vacuum yields eigenvalues of energy in the form (6.15), the energy eigenvalues in matter, when oscillations $\nu_e \leftrightarrow \nu_{\mu,\tau}$ are examined, are

described by the expression

$$E_2 - E_1 = \pm\left[\left(\pm\frac{\Delta m^2\cos(2\theta)}{2E} - \sqrt{2}\,G_F N_e\right)^2 + \left(\pm\frac{\Delta m^2\sin(2\theta)}{2E}\right)^2\right]^{1/2}. \quad (6.28)$$

The Wolfenstein length characterizing the length of the neutrino-electron interaction is

$$L_0 = \frac{2\pi}{\sqrt{2}\,G_F N_e} \simeq \frac{1.6\times 10^4\ [\mathrm{km}]}{\rho}. \quad (6.29)$$

Then, the expression for the probability $P(\nu_e \leftrightarrow \nu_e)$ for an electron neutrino remaining as such for a time t during the interaction of ν_e with medium of constant density $\rho = \mathrm{const}$ is given by [164]

$$P(\nu_e \leftrightarrow \nu_e) = 1 - \frac{\sin^2(2\theta)}{\omega^2}\sin^2\left(\frac{\omega\pi L}{L_{vac}}\right), \quad (6.30)$$

whereas the probability of oscillating into another flavour is

$$P(\nu_e \leftrightarrow \nu_{\mu,\tau}) = \frac{\sin^2(2\theta)}{\omega^2}\sin^2\left(\frac{\omega\pi L}{L_{vac}}\right), \quad (6.31)$$

where the notation

$$\omega = \left[1 - 2\cos(2\theta)\frac{L_{vac}}{L_0(\rho)} + \left(\frac{L_{vac}}{L_0(\rho)}\right)^2\right]^{1/2} \quad (6.32)$$

is introduced. Comparison of expressions (6.16) and (6.19) for the probability of oscillations in the vacuum and the corresponding expressions (6.30) and (6.33) for their probability in matter yields the effective mixing angle and oscillation length taking into account the matter effect:

$$\sin(2\theta_m) = \frac{\sin(2\theta)}{\omega}, \quad L_m = \frac{L_{vac}}{\omega}. \quad (6.33)$$

The probability of a $P(\nu_e \leftrightarrow \nu_{\mu,\tau})$ transition in matter may be significantly different from that in vacuum. Matter can both suppress (at $\cos(2\theta) \simeq 0$) and enhance oscillations. Three limiting cases are conceivable.

1. $L_{vac}/L_0 \ll 1$. In this case, matter practically does not affect oscillations and they are reduced to vacuum oscillations. It follows from (6.29) that for vacuum oscillations to be studied, the experiment should be carried out with a sufficient distance between the source and the detector that ensures fulfillment of the condition $L \ll L_0 \ll (1-2)\times 10^3$ km.

2. $L_{vac}/L_0 \gg 1$. In this case, the oscillation amplitude is suppressed by the factor $\simeq L_{vac}/L_0$.

3. Resonance amplification of the oscillations,

$$\frac{L_{vac}}{L_0} = \cos(2\theta), \quad (6.34)$$

referred to as the Mikheev–Smirnov–Wolfenstein (MSW) effect [34, 168]. If this condition is satisfied, $\omega = \sin(2\theta)$ and the oscillation amplitude is unity at any mixing angle θ. Accordingly, experimentally obtained limitations on the parameters Δm^2 and $\sin^2(2\theta)$ at a given level of observation of the probability of transition $P(\nu_e \leftrightarrow \nu_{e'})$ are different from those for vacuum oscillations.

It is worthwhile to note that the resonance condition (6.34) in the Earth's matter takes the form

$$\frac{L_{vac}}{L_0} = \frac{E_\nu \rho}{1.4\times 10^4 \Delta m^2} \quad (6.35)$$

and is satisfied for a wide range of Δm^2 and $\sin^2(2\theta)$ values permissible in the light of current experimental findings and for a variation of neutrino beam energy in the range $1 < E_\nu < 10^3$ GeV. The Wolfenstein length at densities $\rho \simeq 3-10$ g cm^{-3} characteristic of the Earth's matter is $L_0 \simeq 3.5\times 10^3 - 1.2\times 10^4$ km and determines the optimal path of neutrino flight for experiments verifying the effect of matter on oscillation parameters.

6.3 Neutrino oscillations in matter with variable density

The oscillation effect is especially pronounced when the density of matter traversed by a neutrino beam is variable: a neutrino of one flavour may be completely converted to a neutrino of a different flavour. Oscillations in the medium with variable electron density can be described by the Shrödinger equation (6.26) with the operator H in the form [169]

$$H(\tau) = (\tau)\cdot, \quad (6.36)$$

where $\tau = \pi L/L_{vac}$, $(\tau) = (-\sin(2\theta), 0, \cos(2\theta) - L_{vac}/L_0(\tau))$, and are the Pauli matrices or, in the explicit form,

$$H = \pi\begin{pmatrix} \dfrac{\cos(2\theta)}{L_{vac}} - \dfrac{1}{L_0(t)} & -\dfrac{\sin(2\theta)}{L_{vac}} \\ -\dfrac{\sin(2\theta)}{L_{vac}} & -\dfrac{\cos(2\theta)}{L_{vac}} + \dfrac{1}{L(t)} \end{pmatrix}, \quad (6.37)$$

where $t = L/c = L$; then

$$\begin{vmatrix} \nu_l(t) \\ \nu_{l'}(t) \end{vmatrix} = T\exp\left[-\mathrm{i}\int_0^t H(t)\,\mathrm{d}t\right]\begin{vmatrix} \nu_l(0) \\ \nu_{l'}(0) \end{vmatrix}. \quad (6.38)$$

Now, let us exclude the component $|\nu_l\rangle$ (following [169]) and reduce (6.38) to a second order equation

$$\frac{\mathrm{d}^2\xi}{\mathrm{d}t^2} + f(t)\xi = 0, \quad (6.39)$$

$$f(t) = \pi^2\left[\frac{1}{L_0^2(t)} - \frac{2\cos(2\theta)}{L_{vac}L_0(t)} + \frac{1}{L_{vac}^2}\right] + \mathrm{i}\pi\frac{\mathrm{d}}{\mathrm{d}t}\frac{1}{L_0(t)} \quad (6.40)$$

for the amplitude $|\nu_{l'}\rangle \equiv \xi$ with the initial conditions (for the original beam $\nu_{l'}$)

$$\xi(0) = 0, \quad \frac{\mathrm{d}\xi(0)}{\mathrm{d}t} = \mathrm{i}\sin(2\theta). \quad (6.41)$$

The solution of Eqns (6.39), (6.40) with the initial conditions (6.41) yields the probability

$$P(\nu_l \leftrightarrow \nu_{l'}) = \left|\xi(t)\right|^2 \quad (6.42)$$

of $\nu_l \leftrightarrow \nu_{l'}$ transition. In the case $\rho(t) = \rho = \mathrm{const}$ of constant density $\mathrm{d}\rho/\mathrm{d}t \equiv 0$ and for the probability of oscillations Eqn. (6.42) gives (6.31).

The sign of the scattering amplitude $\bar\nu_l l \leftrightarrow \bar\nu_l l$ is opposite to that of the scattering amplitude $\nu_l l \leftrightarrow \nu_l l$ which is equivalent to the change of sign of the characteristic Wolkenstein length $L_0 \to -L_0$. Accordingly, the resonance

effect holds either for a neutrino or antineutrino but not for both particles at the same time. This means that, in principle, observation of oscillations in matter permits the determination of the sign of

$$L_{\text{vac}} \propto \left(|m_2^2 - m_1^2|\right)^{-1} . \tag{6.43}$$

Figure 4 compares changes in vacuum oscillations (6.12) and oscillations of neutrinos traveling in matter as described by Eqns (6.39)–(6.41), with the density distribution in the Earth according to [170]. Ref. [171] reports the estimated achievable levels of oscillation parameters for a muon neutrino beam with energy $\langle E_{\nu_\mu} \rangle \simeq 30$ GeV propagating along an Earth chord 4,200 km in length and for a beam traveling in a vacuum. It follows that the presence of matter allows movement some 20% farther to a region of smaller mixing angles and practically does not influence the attainable limit on Δm^2, even at maximum mixing angles.

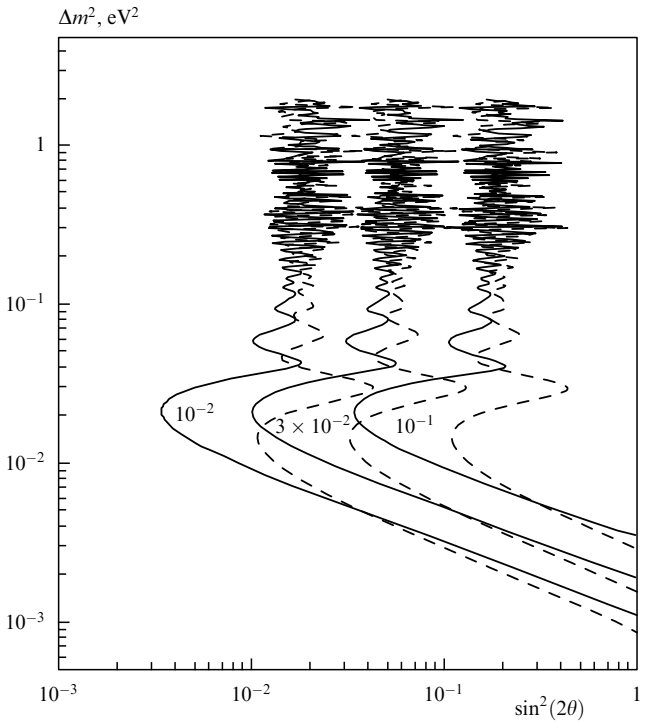

Figure 4. Calculated attainable values of oscillation parameters (ranges right of the corresponding curves) for muon neutrinos with energies of $\langle E_{\nu_\mu} \rangle \simeq 30$ GeV (estimate of the $P(\nu_\mu \leftrightarrow \nu_\tau)$ transition probability with accuracy 1, 3, 10 %). The solid lines correspond to calculations taking the matter effect into account; the dotted lines are vacuum oscillations.

7. Neutrino oscillation studies at low energies: reactor experiments

The sensitivity of experiments to measuring the oscillation parameter Δm^2 is described by expression (6.20). In the approximation of maximum mixing ($\sin^2(2\theta) \simeq 1$), the sensitivity of experiments is unambiguously related to the E_ν/L ratio. Therefore, oscillations are better observed using sources which emit neutrinos with minimal energy and are located at a maximum distance from the detector [172].

Nuclear reactors are powerful artificial sources of electron antineutrinos with energies $E_{\bar{\nu}_e} \leqslant 8$ MeV which can be detected in the process

$$\bar{\nu}_e + p \to n + e^+ . \tag{7.1}$$

A search for oscillations in reactor experiments is based on recording the 'annihilation' of a primary neutrino (or rather, an antineutrino) beam via the inclusive channel $\bar{\nu}_e \to x$ when the flux ν_e is observed (or is not observed) to decrease with the distance from the source faster than is expected from the results of calculations based on the beam configuration, on the assumption of the absence of oscillations.

There are two methods for recording the oscillation effect: absolute and relative. The absolute method consists in the comparison of observed and calculated intensities of neutrino interactions. Measurements of the cross-section of the reaction (7.1) in a detector located at a distance L from the reactor are compared with the calculated cross-section σ_{exp} averaged over the antineutrino spectrum. As a result, the probability of (6.16) in the presence of oscillations must be other than unity:

$$\begin{aligned} \langle P(\bar{\nu}_e \leftrightarrow x) \rangle &= \frac{\langle \sigma_{\text{exp}} \rangle}{\langle \sigma_{\text{cal}} \rangle} = 1 - \sin^2(2\theta) \left\langle \sin^2 \frac{1.27 \Delta m^2 L}{E_{\bar{\nu}}} \right\rangle \\ &= 1 - \sin^2(2\theta) \int_{E_{\text{thr}}}^{E_{\max}} \sigma(E) N_{\bar{\nu}} \frac{1.27 \Delta m^2 L}{E_{\bar{\nu}}} \, \mathrm{d}E_{\bar{\nu}} \\ &\times \left[\int_{E_{\text{thr}}}^{E_{\max}} \sigma(E) N_{\bar{\nu}}(E) \, \mathrm{d}E_{\bar{\nu}} \right]^{-1} . \end{aligned} \tag{7.2}$$

Here, integration is carried out from the $\bar{\nu}_e$ recording threshold $E_{\text{thr}} = M_n + m_e - M_p = 1.8$ MeV in the reaction (7.1) to the upper limit $E_{\max}$ of energy possible for neutrinos from the reactor. A major difficulty encountered in this method is the necessity of exactly calculating the neutrino spectra of all fissionable isotopes contained in the nuclear fluid of the reactor. These spectra are obtained by the summation of partial spectra of fission products and depend on the fragment composition, decay patterns, and a number of other factors. The accuracy of reconstruction of the neutrino spectra can be increased by restoring (from the same computed data) the electron spectra of fission fragments and comparing them with experimental measurements.

If the experiment is not intended to determine the cross-section of (7.1), σ_{exp}, evaluation of the oscillation effect is based on the comparison of integral positron outputs:

$$\langle P(\bar{\nu}_e \leftrightarrow x) \rangle = \int N_{\text{exp}}(E_{e^+}) \, \mathrm{d}E_{e^+} \left[\int N_{\text{cal}}(E_{e^+}) \, \mathrm{d}E_{e^+} \right]^{-1} . \tag{7.3}$$

Here the first integral defines the number of positrons detected in the reaction (7.1) in the energy range $\mathrm{d}E_{e^+}$ and the expression in square brackets gives the number of positrons calculated on the assumption of the absence of oscillations and takes into account the response function of the detector.

Most of the difficulties caused by the uncertainty of reactor neutrino spectra are obviated by using the relative method for the detection of oscillations. In this method, two identical detectors are placed at distances L_1 and L_2 respectively from the active reactor zone. Alternatively, one detector is used which can be removed and installed at different distances from the reactor. The presence of oscillations is indicated by a relative change in the cross-section

$\sigma_{exp}(L_1)/\sigma_{exp}(L_2)$ or by a deformity of the integral positron spectrum in the reaction (7.1), depending on the distance from the reactor $\int N_{exp}(E_{e^+}, L_1)\, dE_{e^+} [\int N_{exp}(E_{e^+}, L_2)\, dE_{e^+}]^{-1}$.

Neutrino detectors used in experiments at various reactors have similar structures allowing the recording of time-correlated signals from positrons and neutrons in reaction (7.1). Positrons are recorded in a honeycomb counter containing a liquid scintillator which simultaneously serves as a proton target (high-proton scintillators are normally employed for the purpose) and a neutron moderator. Each cell is viewed by a PMT, and the positron energy is measured from the signal amplitude. ^{3}He-filled wire proportional chambers are placed between sections of the counter to record neutrons. The necessary background conditions are provided by active and passive shielding, that is, a neutrino detector surrounded by effective anticoincidence counters is placed in a concrete bunker with a several polyethylene or water layers and layers of radiopure lead. The results obtained when the reactor is stopped are taken to be the background of the instrument.

Permissible oscillation parameters are calculated by the maximum likelihood method for various values of $\sin^2(2\theta)$, Δm^2 in the anticipated neutrino spectrum. The boundaries of the permissible oscillation parameter region correspond to the best description of an experimental spectrum in which the quantity $\chi^2(\sin^2(2\theta_i), \Delta m_j^2)$ for each parameter being fitted has a minimum value. The limitation on the quantity Δm^2 is usually imposed assuming the maximum mixing to be $\sin^2(2\theta) = 1$:

$$\Delta m^2 = \frac{\sqrt{\langle P(\bar{\nu}_e \leftrightarrow x)\rangle}}{1.27\langle L/E_{\bar{\nu}_e}\rangle}\,. \qquad (7.4)$$

A detailed description of the methods for investigating oscillations in reactor experiments, the construction and geometry of neutrino detectors sensitive to reaction (7.1) products, the procedure for the reconstruction of positron and neutrino spectra, and algorithms for determining the parameters $\sin^2(2\theta)$, Δm^2 can be found in monographs [173, 174]. The limits on parameters obtained in reactor experiments are presented in Table 3.

Results of reactor experiments (excepting those obtained at Bugey which do not yield an unambiguous interpretation) give evidence of the absence of neutrino oscillations for a wide range of the parameters $\sin^2(2\theta) = 0.1 - 1$ and $\Delta m^2 = 2 \times 10^{-2} - 10^{-1}$.

The objective of forthcoming reactor neutrino experiments will be a search of oscillations at large distances from the reactor. The smooth spectrum of reactor neutrinos in conjunction with their pathlength $L \simeq 1$ km allows the sensitivity to the parameter Δm^2 to be increased up to $\simeq 10^{-3} - 10^{-4}$ at large mixing angles especially in the case of the MSW effect [6, 34]. Such experiments need a new generation of high-capacity neutrino detectors. It has been proposed to construct a detector with 5 tons of scintillation fluid containing gadolinium to be set 1 km from two new French reactors. The organization of a group to construct a similar detector to search for oscillations in a neutrino beam from the reactor at San Onofre, Ca, is underway [184].

Table 3. Results obtained by leading groups in search of neutrino oscillations at detectors exposed to electron antineutrino beams from reactors.

Reactor location	Distance between reactor and detector, m	Constraints on the parameter Δm^2 at $\sin^2(2\theta) = 1$ eV	References
Grenoble	8.76	< 0.15	[175, 176]
Gosgen	37.9/45.9	< 0.016	[177]
Gosgen	37.9/45.9/64.7	< 0.019	[178]
Bugey	13.6/18.3	$6 \times 10^{-2} - 10^{-1}$	[179]
Rovno	18.5/25	< 0.04	[180]
Rovno	32.8/92.3	< 0.0083	[181]
Savannah River	18.5/23.7	< 0.02	[182, 183]

8. Neutrino oscillation studies at high energies: accelerator experiments

The 'see-saw' mechanism in the GUT implies a hierarchy of neutrino masses $m_{\nu_{e,\mu,\tau}} \simeq (m_{u,c,t})^2/M_{GUT}$ in which the τ-neutrino is the heaviest ($m_{\nu_e} \ll m_{\nu_\mu} \ll m_{\nu_\tau}$) and the mixing angles are $\theta_{e\mu} = (m_{\nu_e}/m_{\nu_\mu})^{1/4} \gg \theta_{\mu\tau} = (m_{\nu_\mu}/m_{\nu_\tau})^{1/2} \gg \theta_{e\tau} \simeq 0$. It was shown in Section 3 that the oscillation parameter region $\nu_\mu \to \nu_\tau$ permits the values $\sin^2(2\theta_{\mu\tau}) = 2 \times 10^{-3} - 3 \times 10^{-4}$, $\Delta m^2_{\mu\tau} = 22 - 715$ eV^2 [63, 64] if the mass of the τ-neutrino lies in the range 5 to 30 eV; for oscillation $\nu_\mu \leftrightarrow \nu_e$ the most probable parameters values are $\sin^2(2\theta_{\mu e}) = (0.3 - 1.0) \times 10^{-2}$, $\Delta m^2_{\mu e} = (0.5 - 1.2) \times 10^{-3}$ eV^2 [185–187]. In this scheme, both the τ-neutrino mass and the mixing angle $\theta_{\mu\tau}$ occur in the oscillation parameter region which can be investigated in accelerator experiments. That is why studies of oscillations in muon neutrino beams from CERN, FNAL, and UNK-1 accelerators are largely intended to examine the mode $\nu_\mu \leftrightarrow \nu_\tau$.

Proton accelerators produce muon neutrino beams with broad energy spectra containing an admixture of one to a few percent of neutrinos with different flavours. ν_μ arises from the decay of secondary π and K-mesons generated in the interaction of protons with the target and focused into a parallel beam. Neutrino beams from accelerators are amenable to control; their energy, intensity, time-structure and direction being well-known. Thus, their spectra and admixtures of background neutrinos (largely electron neutrinos) are easy to calculate with high accuracy. However, experiments must be carried out in a monochromatic neutrino beam if their sensitivity is to be at the level $P(\nu_\mu \leftrightarrow \nu_{e,\tau}) \simeq 10^{-4}$.

Experiments on accelerator neutrino beams allow both the 'annihilation' ($\nu_\mu \leftrightarrow x$) and inclusive 'creation' ($\nu_\mu \leftrightarrow \nu_e$ and $\nu_\mu \leftrightarrow \nu_\tau$) modes to be investigated. For direct recording excessive ν_e in a flux ν_τ, the energy E must be higher than the rest mass of an electron (τ-lepton) formed through the reaction

$$\nu_{e(\tau)} N \to e^-(\tau^-)\, X \qquad (8.1)$$

being detected, where N is the nucleon of detector matter and X is the final hadronic state.

Electrons in the reaction (8.1) are identifiable by virtue of an electromagnetic shower developing in the material of the detector, electromagnetic calorimeter, bubble chamber or other part of the experimental unit. There are two options for recording τ-leptons in the reaction (8.1). One is direct observation of the lepton's flight between the creation and decay points ($c\tau \simeq 91$ μm) using a tracking detector with a resolution of $\sigma \leqslant 10$ μm, e.g. nuclear photoemulsions, bubble chambers with a holographic information retrieval system, or targets of scintillating fibers. The other method for recording τ-leptons is a kinematic analysis of the reaction (8.1) products,

i.e. an evaluation of the transverse momenta disbalance between the τ-lepton and hadronic flux. The measurements are made with a precision calorimetric detector.

Let us now discuss at greater length the experimental units used in neutrino oscillation studies and the limits on the parameters $\sin^2 2\theta$, Δm^2 obtained in these experiments.

The oscillations $\nu_\mu \leftrightarrow$ x were investigated in the CERN PS neutrino beam of mean energy $\langle E_\nu \rangle = 1.5$ GeV, at CHARM and CDHS, and in the $E_\nu = 40-230$ GeV FNAL neutrino beam at CCFR. All experiments were carried out using two detectors positioned at different distances from the neutrino channel target. Neutrino interactions in the neutral current (NC) channel recorded by the detectors had similar cross-sections for all flavours and can not be used for labeling the neutrino flavour. On the contrary, charged current (CC) interactions were characterized by different charged leptons in the final state. Therefore, the oscillations $\nu_\mu \leftrightarrow$ x must result in a smaller number of CC-events

$$\nu_\mu + \mathrm{N} \to \mu^- + \mathrm{X} \tag{8.2}$$

containing muons compared with that calculated on the assumption of the absence of oscillations. Increasing the distance to the detector also leads to a decrease in the (8.2)-type events. The oscillation parameters $\sin^2(2\theta)$, Δm^2 are determined by comparing the observed neutrino fluxes in both the near and far detectors. Thereafter, the region of oscillation parameters $\nu_\mu \leftrightarrow$ x excluded from a given experiment is found by the maximum likelihood method. The results are summarized in Table 4.

The oscillations $\nu_\mu \leftrightarrow \nu_e$ have been extensively studied at the CERN PS, BNL, AGS, FNAL, and U-70 accelerators. The method of detecting the electron neutrino ν_e 'creation' channel in a beam of muon neutrinos ν_μ is based on the comparison of the experimentally observed ν_e- ν_μ-events ratio

$$R^{\exp} = \frac{N^{\exp}_{\nu_e}}{N^{\exp}_{\nu_\mu}} = \frac{n_{\nu_e}\langle P(\nu_e \to \nu_e)\sigma_{\nu_e}\rangle + n_{\nu_\mu}\langle P(\nu_\mu \to \nu_e)\sigma_{\nu_e}\rangle}{n_{\nu_\mu}\langle P(\nu_\mu \to \nu_\mu)\sigma_{\nu_\mu}\rangle + n_{\nu_e}\langle P(\nu_e \to \nu_\mu)\sigma_{\nu_\mu}\rangle} \tag{8.3}$$

with the R^{cal} value calculated on the assumption of the absence of oscillations. In expression (8.3), n_{ν_i} is the initial number of neutrinos of the i-th flavour ($i = \mathrm{e}, \mu$), σ_{ν_i} is the cross-section of the νN-interaction in the charged current channel for a neutrino of the i-th flavour, and averaging is over the original neutrino spectrum. The n_{ν_e}/n_{ν_μ} ratio on the assumption

$$\frac{\sigma_{\nu_e}}{E_{\nu_e}} = \frac{\sigma_{\nu_\mu}}{E_{\nu_\mu}} = \mathrm{const}$$

can be obtained from on the computed number of ν_e and ν_μ events and the averaged energy of neutrinos of a given flavour:

$$\frac{n_{\nu_e}}{n_{\nu_\mu}} = \frac{N^{\mathrm{cal}}_{\nu_e}\langle E_{\nu_e}\rangle^{-1}}{N^{\mathrm{cal}}_{\nu_\mu}\langle E_{\nu_\mu}\rangle^{-1}} = R^{\mathrm{cal}}\frac{\langle E_{\nu_e}\rangle}{\langle E_{\nu_\mu}\rangle}\,. \tag{8.4}$$

Then, expression (8.3) can be rewritten in the form

$$R^{\exp} = \frac{R^{\mathrm{cal}}\langle E_{\nu_\mu}\rangle\langle E_{\nu_e}\rangle^{-1}\langle [1 - P(\nu_\mu \to \nu_e)]E_{\nu_e}\rangle + \langle P(\nu_\mu \to \nu_e)E_{\nu_\mu}\rangle}{\langle [1 - P(\nu_\mu \to \nu_e)]E_{\nu_\mu}\rangle + R^{\mathrm{cal}}\langle E_{\nu_\mu}\rangle\langle E_{\nu_e}\rangle^{-1}\langle P(\nu_\mu \to \nu_e)E_{\nu_e}\rangle}\,. \tag{8.5}$$

In the presence of $\nu_\mu \leftrightarrow \nu_e$ oscillations, the $R^{\exp}/R^{\mathrm{cal}}$ ratio must be other than unity. The limit set on $P(\nu_\mu \leftrightarrow \nu_e)$, and hence on the ratio of the oscillation parameters $\sin^2(2\theta)$ and Δm^2 compatible with $R^{\exp}$ at a given confidence level, is derived from (8.5). The results of a search for $\nu_\mu \leftrightarrow \nu_e$ oscillations are presented in Table 5.

The $\nu_\mu \leftrightarrow \nu_\tau$ oscillations were first studied in neutrino experiments in the BEBC bubble chamber at CERN and the 15-foot FNAL chamber. In these early experiments, vertices from τ-leptonic decays could not be visualized. Therefore, the oscillation parameters were found on the assumption that part of the neutrino events with electrons in the final state is due to interactions of τ-neutrino in the reaction $\nu_\tau + \mathrm{N} \to \tau^- + \mathrm{X}$ followed by the $\tau \to \mathrm{e}^-\nu_\tau\bar{\nu}_\mathrm{e}$ decay of a τ-lepton. Such a method for a search of $\nu_\mu \leftrightarrow \nu_\tau$ oscillation parameters requires a high accuracy of distinction between background and ν_e interactions and kinematic cuts for separating the desired mode of the τ-leptonic decay.

Table 4. Results of oscillation $\nu_n \leftrightarrow x$ experiments using accelerators.

Accelerator, experiment	Detector structure	Distance between target and detectors, m	Δm^2 at $\sin^2(2\theta) = 1$, eV^2	$\sin^2(2\theta)$	References
CERN PS, CHARM	Segmented calorimeter: a sandwich of marble plates interleaved with scintillation counters, proportional drift tubes (PDT), and streamer tubes. Muon spectrometer: magnetized iron plates alternating with PDT.	123 (Near) 903 (Distant)	<0.29 or >22	<0.17 ($\Delta m^2 = 0.7-9.0\ \mathrm{eV}^2$)	[188]
CERN PS, CDGS	Toroidally magnetized iron sheets alternating with scintillation plates and drift chambers	130 (Near) 885 (Distant)	<0.23 or >100	<0.1 ($\Delta m^2 = 1.0-10.0\ \mathrm{eV}^2$)	[189]
FNAL, CCFR	Segmented calorimeter with muonic spectrum	715 (Near) 1115 (Distant)	<8 or >1250	<0.02 ($\Delta m^2 = 110\ \mathrm{eV}^2$)	[190]

Table 5. Results of $\nu_\mu \leftrightarrow \nu_e$ oscillation studies with accelerators.

Accelerator, experiment	Detector structure	Distance between target and detectors, m	Δm^2 at $\sin^2(2\theta) = 1$, eV^2	$\sin^2(2\theta)$	References
CERN, BEBS	Large bubble chamber	850	< 0.09	$< 2 \times 10^{-2} (\Delta m^2 \simeq 2$ eV$^2)$	[191]
CERN PS, CHARM	Structured target calorimeters placed at two distances; muon absorber	123 (Near) 903 (Distant)	< 0.19	$< 8 \times 10^{-3}$ ($\Delta m^2 \geqslant 30$ eV^2)	[188]
BNL AGS, E-734	Segmented calorimeter: liquid scintillator planes, iron sheets, and proportional drift chambers; shower counters	96	< 0.43	$< 3.4 \times 10^{-3}$	[192] [193]
FNAL	15-feet bubble chamber	1056	< 2.2	$< 1.1 \times 10^{-2}$	[194]
ç-70 ¾ÀÇ	Large bubble chamber	270	< 1.3	$< 2.5 \times 10^{-3}$	[195]

In the later experiments E-531 and E-564 using nuclear photoemulsions, it was possible to directly record τ-leptons. This significantly increased the sensitivity of experiments to $\nu_\mu \leftrightarrow \nu_\tau$ oscillation parameters. Of special note is the CARM-II experiment in search of the quasielastic reaction

$$\nu_\tau N \rightarrow \tau^- (\pi^- \nu_\tau) N'$$

against the background of single-ray events in the charged current reaction $\nu_\mu N \rightarrow \nu_\mu N' \pi^-$. The results of all these experiments are summarized in Table 6.

At present, neutrino interactions are recorded in the CERN SPS ν_μ beam for the statistical purposes of the CHORUS experiment (CERN Hybrid Oscillation Research ApparatUS) [201, 202]. The experiment employs a magnetic spectrometer composed of arrays of scintillating fiber trackers [203] which help to locate the vertices of events to be scanned in the 800 kg photoemulsion target. The experiment is also aimed at detecting CC-interactions $\nu_\tau N \rightarrow \tau^- X$ followed by the τ-leptonic decay. Muon tracks are extrapolated to the emulsion using coordinates derived from the fiber target [204]. The signature for the τ-lepton decay is 'kink'-like single-ray event. All these events (τ-neutrino interaction candidates) are kinematically selected based on calorimetric information [205]; the photoemulsion is examined with totally automated microscopes. The preliminary results of a statistical analysis are reported in [202].

The CERN SPS beam will also be used in the NOMAD experiment (Neutrino Oscillation Magnetic Detector). In this experiment, a precise vertex detector is absent, and the signal from ν_τ is separated based on the known kinematic criteria taking advantage of an extensive tracking system which comprises 15 drift chambers inside the UA (1) magnet [202, 206].

The sensitivity of the CHORUS and NOMAD experiments to the mixing parameter $\sin^2(2\theta)$ was computed in [64] to be $\sin^2(2\theta) > 2 \times 10^{-4}$ for the case of $m_{\nu_\tau} > 7$ eV at the 90% confidence level.

9. Oscillations of long-baseline neutrinos

Further progress in measuring the neutrino mass and improving the sensitivity of experiments to the order of $m_{\nu_\mu} \simeq 10^{-3} - 10^{-1}$ eV and $m_{\nu_\tau} < 1$ eV depends on oscillation studies using long-baseline neutrinos and a new generation of detectors with large sensitive masses. The term long-baseline neutrinos has been coined to denote neutrinos recorded at distances of ≃1 km from the accelerator. The long path and large amount of matter traversed by a neutrino traveling from

Table 6. Results of $\nu_\mu \leftrightarrow \nu_\tau$ oscillation experiments using accelerators.

Accelerators, experiment	Detector structure	Distance between neutrino source and detectors, m	Δm^2 at $\sin^2(2\theta) = 1$, eV^2	$\sin^2(2\theta)$	References
CERN PS, BEBC	Large bubble chamber	850	< 6	$< 5 \times 10^{-2}$	[196]
FNAL	15-foot bubble chamber	1056	< 3	$< 6 \times 10^{-2}$	[197]
FNAL, E-531	Hybrid spectrometer: nuclear photoemulsion, time-of-flight system	951	< 0.9	$< 4 \times 10^{-3}$	[198]
FNAL, E-564	Nuclear photoemulsion inside a 15-foot bubble chamber	1466	< 4.5	$< 6 \times 10^{-2}$	[199]
CERN SPS, CHARM II	Structured target calorimeter placed at two distances; muon spectrometer	123 (near) 903 (distant)	< 0.5	$< 5 \times 10^{-3} (\Delta m^2 \simeq 50$ eV$^2)$	[200]

the source to the detector allows an increase in the sensitivity of the experiment to oscillation parameters and to check the influence of the MSW effect on the oscillation mechanism.

Long-baseline neutrino beams for oscillation experiments are expected to be generated at CERN SPS, FNAL (Fermilab Main Injector), KEK (Japan), and UNK-600 (Protvino, Russia). Long-baseline neutrino projects are extensively discussed in the literature [35, 36, 207–210]. New types of detectors to be used in further oscillation experiments have been described in [35, 36, 211, 212].

All known methods for the detection of neutrino oscillations will be used in the near future:

1. Measurement of the variation of a fraction of events mediated through charged current interactions (CC-events) with the distance between the accelerator and the detector (L_D) or with a neutrino energy at a fixed distance L_D. These studies require the neutrino spectrum to be well-known.

2. Recording changes in the ratio of the number of events via neutral current (NC-events) to that of CC-events with the distance L_D or with the neutrino energy at a fixed L_D (NC/CC method).

3. Direct records of alien neutrinos in a neutrino flux of a different nature (e.g. the detection of 'excess' ν_e, ν_τ in a ν_μ-flux, the measurement of the relative number of equilibrium muons).

4. Measurement of a flux of equilibrium muons formed in the matter in front of the detector (measurements of intensity, momentum spectrum, and charge ratio at a fixed distance L_D).

The prospects of having a long-baseline neutrino beam from CERN SPS (energy of protons incident on the target is 450 GeV, intensity 2×10^{13}, period 14.4 s) are discussed in detail in [213]. It is hoped to direct the beam onto detectors of the laboratory at Gran-Sasso located at a depth of 4,500 mwe in an underground excavation (the Apennines) 120 km east of Rome and 730 km from CERN. The laboratory has a system of several large detectors designed for astrophysical studies and a search for protons. Some of them are described below.

ICARUS (Imaging Cosmic and Rare Underground Signals) is an ideal detector for examining rare events including neutrino interactions [35, 36, 214, 215]. It belongs to a new generation of detectors and is in fact a time-projection chamber (TPC) consisting of three 5 ton modules each filled with liquid argon and equipped with an electronic readout system. ICARUS identifies neutrino iteractions by recording recoil electrons from secondary charged particles. Owing to electron drift in the uniform electric field, reading planes recognize the charge and produce a three-dimensional image. Two spatial coordinates of each point on the track are analysed upon arrival of drifting electrons at the readout plane. The main difficulty encountered in obtaining an image in the liquid argon detector is associated with the long-range drift of ionized electrons. This problem has been solved using a 3 ton prototype detector [214]. ICARUS has a high spatial resolution (from $\pm$ 1 mm to hundreds of μm) and a good energy resolution ($\simeq 3\,\%$ for $e^{\pm}$ and γ with the energy of 1 MeV). The first module is tentatively planned to be ready for experimentation in 1998 [216].

Neutrino oscillations can be investigated by two methods. One measures the ratio of the number of non-muonic NC-events to that of CC-events containing one muon in the final state [36]:

$$R_1 \simeq 0.31\left[1 + 1.95\sin^2(2\theta)(\Delta m^2 \cdot 1.27 L_D)^2\langle E^{-2}\rangle\right], \quad (9.1)$$

where the following relations hold for the CERN SPS proton beam with an energy of $E_p = 450$ GeV:

$$\frac{\sigma_{NC}^{\mu}}{\sigma_{CC}^{\mu}} \simeq 0.31\,, \quad \frac{\sigma_{NC}^{\tau}}{\sigma_{CC}^{\mu}} \simeq 0.5\,. \quad (9.2)$$

An advantage of the 'creation' method is in that it does not require a near detector and is less sensitive to the flux size.

The other technique (the 'annihilation' method) measures the ratio of muons recorded by the near detector located in the vicinity of CERN (their number is proportional to that of ν_μ in the beam) to interactions of neutrinos of any flavour recorded by ICARUS. The total sensitivity of ICARUS in both methods is $\sin^2(2\theta) = 1.5 \times 10^{-3}$ and $\Delta m^2 = 1.5 \times 10^{-4}$ for $\nu_\mu \leftrightarrow \nu_e$ oscillations and $\sin^2(2\theta) = 5.0 \times 10^{-2}$ and $\Delta m^2 = 2.0 \times 10^{-3}$ eV^2 for $\nu_\mu \leftrightarrow \nu_\tau$ oscillations.

The LVD (Liquid Volume Detector) is a high-capacity detector recording light flashes from recoil electrons of $\nu - e$ scattering in a liquid scintillator [217]. It is intended for the solution of a wide spectrum of problems including observation of neutrino radiation from our galaxy, studies on neutrino fluxes from collapsed stars, and recording neutrinos from accelerators. The detector consists of two parts: the underground neutrino observatory which contains 1.8×10^3 tons of a liquid scintillator and a tracking system made of 1.6×10^4 alternately horizontal and vertical streamer tubes. The total number of detecting channels is 10^5. A basic module of the LVD consists of $1 \times 1 \times 1.5$ m^3 elements each filled with a scintillation fluid and viewed by three 49B PMTs. The total number of modules is close to 200. The size of the detecting system is $10 \times 5 \times 44$ m^3. To augment the target mass, each module is sandwiched between iron plates. The number of free electrons in the working matter of the detector is 7×10^{32}.

MACRO is intended for recording γ-radiation, muons, and neutrinos from galactic and extra-galactic sources and can also be used to detect neutrinos from accelerators [218]. The detector, $72 \times 12 \times 9$ m^3 in size, is an assembly of 12 m long horizontal liquid scintillators stacked together in blocks (a total volume of about 100 m^3), vertical scintillators, horizontal and vertical streamer tubes, lead absorbers (for muon absorption), and supplementary tracking devices. The instrument is expected to record annually as many as 1,000 neutrino events from CERN SPS.

NOE (Neutrino Oscillation Experiment) is a new type of calorimeter for the search of neutrino oscillations [219, 220]. It is modular and easily extendible. Blocks of 10^3 tons ($8 \times 6.4 \times 8$ m^3) are composed of $0.3 \times 0.3 \times 8$ m^3 basic modules each surrounded by streamer tubes and logically divided into four calorimetric elements. Each element is realized as a target made by an 8 m long bar of an iron-concrete mixture with 400 fibers as active components distributed throughout the bar. The fibers are 2 mm in diameter and have a light attenuation length of 5 to 6 m. The fiber readout is in two coordinates. The third coordinate should be provided by an independent tracking system made of streamer tubes. The particle identification is helped by the measurement of $\Delta E/\Delta l$ ionization along the track in each counter.

GENIUS (GEV Neutrino Induced Underground Shower) is a large 17 ton fine-grained magnetic calorimeter for neutrino oscillation studies [221]. The instrument will have both near and distant detectors of $3 \times 3 \times 10$ m^3 and $12 \times 10 \times 24$ m^3 respectively. Each detector is an array of

4 cm thick iron sheets separated by 2 cm thick active elements nominally planned to be resistive plate counters (RPC) made of proportional or streamer tubes. The detectors are closed with toroidal magnets which generate a 20 kGs field. Using the CERN SPS neutrino beam, as many as 4×10^4 CC-events are expected from the 2 year run which is sufficient for detecting the oscillation effect at the 1% confidence level.

Experiments with neutrinos having longer paths are planned, in addition to Gran Sasso detectors, to take advantage of the CERN SPS beam. A most interesting and promising project for the search of neutrinos of galactic and extra-galactic origin is the NESTOR experiment to be carried out in the underwater neutrino laboratory located 1,676 km from CERN.

NESTOR (Neutrinos from Supernovae and Tevsources Ocean Range) is a large water Cherenkov detector now under construction at a depth of 3,800 m near the island of Pylos (south-west of the Greek coast). In this detector, water is used as a Cherenkov radiator, neutrino target, and cosmic ray absorber and filter. The basic element is a horizontal hexagon with pairs of 15 inch photomultipliers, one looking up and the other down. By stacking 12 hexagons vertically, a tower with radius 16 m is being built. The distance between hexagons is 20–30 m. The total number of photomultipliers is 1,176. They will be viewing an effective volume of 10^4 m^3 with an angular resolution of 1°. The oscillation effect will be deduced from the time distribution of NC muonless events and CC-events containing a muon in the final state. The detector will be able to distinguish them because muon-generated Cherenkov light comes earlier than that from a hadronic cascade or a magnetic shower. The systematics of such a statistical separation will be controlled to better than 10% [222]. With the 450 GeV baseline CERN SPS neutrino beam running for one year, NESTOR will, with one tower only, produce a few thousand events.

The KEK experiment in Japan is designed to study oscillations of 'distant' neutrinos to be recorded by the Superkamiokande detector placed 250 km from the accelerator. The neutrino beam is expected to be available by 1999. The following three detectors will be installed in the path of the beam: a 1.7×10^3 ton near detector 0.5 km from the target, an intermediate detector 25 km from the target, and the main (Superkamiokande) detector.

The Superkamiokande water Cherenkov detector is the extension of the Kamiokande experiment described in Section 5 [223, 224]. The mass of its active volume varies from 22×10^3 tons for recording solar neutrinos (with an energy threshold of 5 MeV) to 32×10^3 tons to observe neutrinos from supernovae and the accelerator. That is, the detector is about ten times as large as Kamiokande. The total of 1.1×10^4 Hammamatsu PMTs each having a 50 cm diameter photocathode will provide effective coverage of 40% of the inner surface of the steel vessel containing purified water to provide the active area of the detector. The counting rate of Superkamiokande is calculated to be 400 CC-events/day at a beam energy $E_\nu = 1.4$ GeV.

Another Japanese project whose development is currently underway is a water Cherenkov detector to be deployed at a depth of 1,000 m in lake Motossu 150 km from Tokyo [225]. Its fiducial mass is 20×10^3 tons. The active volume ($30 \times 30 \times 23$ m^3) filled with filtered water is separated from the lake water by light-proof walls. The Cherenkov light will be collected by a sandwich structure of 20 inch Hammamatsu PMTs.

Several experiments have been proposed in the USA using BN2 AGS and FNAL accelerators.

The BNL experiment (E889) is aimed at examining the 'annihilation' of a high-intensity 1 GeV ν_μ-neutrino beam generated by AGS [226]. The experiment will use 4 identical water Cherenkov detectors placed 1, 3, 24, and 68 km from the target at an angle of 1.5° to the beam axis. The two latter detectors are expected to see 9×10^3 and 1×10^3 CC-events respectively for 1.5 years. It was calculated that the beam intensity difference across the first and second detectors will amount to 33% and 10% respectively, and be insignificant for the two latter detectors. The cosmic ray background is negligibly small.

One of the detectors operated today in search of neutrino interactions is the Soudan II intended to receive 120 GeV neutrinos from the Main injector of FNAL.

Soudan II is a multifunctional detector assembled at the bottom of an abandoned iron-mine (2,090 mwe) near lake Superior, Minn, USA. The bulk of its mass consists of 224 identical 4.3 ton calorimetric modules. Each module is an assembly of 240 steel sheets ($1 \times 1 \times 16$ m^3) with 7,560 drift tubes inserted in between [227]. The detector is designed to record muons, electrons, and γ-quanta. Soudan is being completed by increasing its mass which grew from 275 tons in 1988 to 1,000 tons in 1991 and must eventually be $7-8 \times 10^3$ tons to enable the detector to accept the FNAL neutrino beam.

At present, joint projects are being elaborated by leading laboratories in the USA, UK, and Russia to construct a full-scale oscillation experiment. This will require digging a new shaft 75 m long and 14 m wide close to the hall which accommodates Soudan II. The shaft will harbor a new MINOS detector.

MINOS (Main Injector Neutrino Oscillation Search) is an experiment to investigate $\nu_\mu \to \mu_e$ and $\nu_\mu \to \nu_\tau$ oscillations using the new neutrino beam from the Main injector of FNAL with an energy in excess of τ-lepton creation energy threshold [228]. The oscillation effect will be identified from the difference between signals in near and far detectors. The former is at FNAL and the latter 730 km apart in the direction of the Soudan underground laboratory at a depth of 713 m (2,090 mwe). MINOS is a 36 m and 8 m wide sandwich construction containing six hundred 4 cm thick octagonal iron sheets interleaved with 1 cm streamer tubes. The total area of the active element is 32,000 m^2. The readout is accomplished by 48,000 strips and anode wires. An opening aligned with the detector axis harbors an electromagnet coil which generates a 1.5 T toroidal magnetic field. The total detector mass is around 10^4 tons. The near detector will be identical with the far one in terms of structure and detecting systems and will have a transverse size comparable with the beam diameter.

The experiment will use both a broad spectrum beam with energy up to $E_\nu \simeq 30$ GeV and a narrow neutrino beam tunable to have any energy in the range $E_\nu = 10-30$ GeV with dispersion $\sigma_{E_\nu} = \pm 15\%$.

Analysis of the oscillation effect in the wide beam experiment will be performed using traditional techniques; i.e. comparison of the ratios of CC-events to the total number of interactions in the near and far detectors, comparison of CC-events in the two detectors in terms of energy distribution, observation of the $\tau \to \nu +$ hadrons signature, investigation of the energy distribution of NC-events, etc. It is expected that 2,100 ν_μ-events will be recorded annually in the CC-

channel per 10^3 tons of effective mass using the wide neutrino beam with E_ν energies up to 30 Gev and about 300 ν_τ-CC-events per 10^3 tons at the maximum mixing $\nu_\mu \leftrightarrow \nu_\tau$.

The narrow beam provides new research opportunities, viz. measurement of the total energy of events containing muons in the final state (for ν_τ interactions with subsequent $\tau \to \mu\nu\nu$ decay); the same for electron-containing events in case of $\tau \to e\nu\nu$ decay; and comparison of energy distributions in the near and far detectors.

The sensitivity of the experiment is sufficient to examine oscillation parameters up to $\Delta m^2 \simeq 0.002$ eV^2 and $\sin^2(2\theta) \simeq 0.01$.

Apart from purely oscillation experiments BNL (E-889) and FNAL (MINOS), American scientists plan to exploit the large-volume water Cherenkov detectors DUMAND, AMANDA, and GRANDE to tackle a variety of astrophysical problems. Specifically, they will be used to observe main injector neutrino oscillations and address unresolved traditional questions of neutrino and gamma-astronomy.

DUMAND (Deep Underwater Muon and Neutrino Detector) is a project with a very long history that dates back to the 1970s [229]. It was originally planned to submerge the detector near the Hawaiian Islands. The prototype was designed to have a mass of a few hundred megatons. Thereafter, it was repeatedly upgraded which has eventually led to a more realistic modification DUMAND II. The detector was due to be placed at a depth of 4,800 m east of Hawaii. It consists of 9 vertical strings arranged at the edges and the center of an equilateral octagon with 40 m long sides. A total of 216 optical modules each having a 15 inch photomultiplier with temporal resolution $\simeq 2$ ns are attached to the strings. Each string carries 24 modules spaced at 10 m intervals. The volume of the detector (240 m in height and 106 m in diameter) contains about 2 megatons of water. DUMAND is expected to identify neutrino interactions both inside and outside the volume by detecting muons formed in ν_μ-neutrino interactions. The high water transparency in the study area (light absorption length 50 m) allows the strings to be set 40 m apart while the high temporal resolution of the PMTs and electronics enables the detector to measure the pathlengths of muons to an angular resolution of 0.01 rad.

DUMAND II has been optimized for detecting $\simeq 100$ GeV neutrinos. However, its recording efficiency for the FNAL beam with $\langle E_\nu \rangle \simeq 10$ GeV at a distance $L_D = 6283$ km from the accelerator remains sufficiently high to study oscillations [230]. Two strings mounted on a submarine were put to the test in 1992. Rough waters in the test area proved to be an insuperable difficulty which made the participants of the experiment practically give up further work.

AMANDA is a large Cherenkov detector with an effective mass of 10^7 tons [209]. It is to be installed at the South Pole and use polar ice as a Cherenkov radiator. The high purity of the ice is expected to ensure the long-range transmission of the Cherenkov light. At present, one of the vertical strings carrying photomultipliers is ready to be deployed. The pathlength of the neutrino beam from FNAL to AMANDA is about 12,000 km, i.e. longer than in any other long-baseline neutrino experiment. Around 10^5 neutrino events are expected from the AMANDA one year run, with the target being exposed to a total of $I_p = 2 \times 10^{20}$ protons.

GRANDE is a 10^5 ton universal water Cherenkov detector to be plunged into an artificial water-body near Little Rock, Ark, USA [231]. It is a 50 m high cylinder 196 m in diameter viewed by 1,600 photomultipliers each equipped with a 9 inch photocathode. The sensitive volume of the detector is filled with filtered water and shielded from the environment by a black plastic film. The distance between FNAL and GRANDE is about 800 km.

The UNK-1 accelerating storage system presently under construction at Protvino near Moscow will generate protons with energies of $E_p = 600$ GeV [232] and is intended for physical research having the study of neutrino oscillations as a priority objective [233]. The project envisages generation of a long-baseline neutrino beam with broad and narrow energy spectra [210]. An important task is to select the proper direction of the beam towards an available detector of long-baseline neutrinos. Today, the most advanced stage of the project in terms of the choice of configuration of the experiment and collection of statistical data refers to the proposed oscillation studies with UNK-I neutrinos to be detected by the NT-200 neutrino telescope in lake Baikal [234] and the detectors at Gran Sasso [235].

NT-200, a deep-water facility for detecting muons and neutrinos, is to be deployed at a depth of 1 km in the southern part of lake Baikal approximately 3.5 km offshore [236, 237]. At this depth, the Baikal water is known to have minimal natural luminescence and the absorption length of light is 20 m at $\lambda = 420$ nm. The first part of the telescope will consist of 196 optical Cherenkov modules arranged on 9 vertical strings mounted on a rigid frame, with one in the center and the others around it. The frame consists of 7 arms each 21.5 m long. This umbrella-like construction will be positioned 300 m above the bottom. The deployment will be carried out in wintertime when the lake is covered with a thick ice layer. The Cherenkov radiation will be recorded by the Kvazar photoelectronic system which is an assembly of a 115M PMT and an opto-electronic preamplifier equipped with a spherical electrocathode 37 cm in diameter. The optical modules are grouped in pairs along the string looking alternately upward and downward. The distance between pairs looking face to face is 7.5 m. The trigger logic of the array provides an angular resolution of $1 - 1.5^\circ$ for a single muon, depending on its tracklength across the detector. The effective volume of the NT-200 is $\simeq 10^5$ m^3. It has an active area of around 2,880 m^2 which can be enlarged to $\simeq 17500$ m^2 by increasing the number of detecting systems.

The Baikal neutrino detector is 4,200 km from UNK-1. The near detector will be placed 650 m from the end of the decay channel of the accelerator in order to avoid systematic errors introduced by unstable beam intensity. This detector consists of 60 magnetized ($B \simeq 1.5$ T) 10 cm thick iron plates (3×3 m^2 transverse size). The plates are interleaved with alternate horizontal and vertical 3 m long proportional counters (0.06×0.06 m^2). The triggering signal is generated by scintillation counters regularly arranged along the entire length of the detector. Such a structure enables the calorimeter to have an energy resolution for a hadronic shower of $\Delta E/E = 0.7/\sqrt{E[\text{GeV}]}$. The trigger is tailored to events due to the passage of neutrinos through the CC-channel and must have tracks crossing more than 300 cm of iron ($\simeq 15$ nuclear lengths) without apparent interaction (this corresponds to the path of a muon with energy $E_\mu \geqslant 5$ GeV). This would provide for separation of a muon track from the nuclear hadronic cascade created in neutrino interactions.

A similar construction for the near detector has been proposed for the UNK-1 neutrino beam which is to be directed to the laboratory at Gran Sasso [210]. In this case,

the neutrino pathlength will be 2,200 km. Taken together, the calculations made for different modes of beam generation indicate that up to 10^3 CC-interactions will be recorded by the Baikal detector and ICARUS during a working session of the accelerator (1–2 months) [210, 234, 235]. The anticipated oscillation parameter region is $\Delta m^2 \leqslant 10^{-3}$ eV^2 in the case of complete mixing at $\Delta m^2 \simeq 2 \times 10^{-2}$ eV^2, depending on the experimental conditions.

Even if only some of the above long-baseline neutrino projects are realized, we may soon have an answer to the intriguing question whether neutrino oscillations exist or not.

10. Solar neutrino oscillations

The main source of the Sun's energy in the standard solar model [238–240] is hydrogen burning

$$4p \rightarrow {}^4He + 2e^+ + 2\nu_e + 26.7 \text{ MeV}. \quad (10.1)$$

This process is a sequence of exothermal thermonuclear reactions resulting from proton-proton (pp), proton-electron-proton (pep), and carbon-nitrogen (CNO) cycles. The proton-proton cycle is responsible for 99% of the final states (10.1) and always involves two initial reactions:

$$p + p \rightarrow {}^2H + e^+ + \nu_e + 0.42 \text{ MeV}, \quad (10.2)$$

$$^2H + p \rightarrow {}^3He + \gamma + 5.49 \text{ MeV}. \quad (10.3)$$

The process further proceeds along the main line and two by-lines. The former is completed by the reaction

$$^3He + {}^3He \rightarrow {}^4He + 2p + 12.86 \text{ MeV}, \quad (10.4)$$

which occurs in 86% of all cases. The assembly of four protons into the helium nucleus results in the emission of two positrons which annihilate with two electrons and thus contribute $2m_ec^2$ to the total energy released through the reaction (10.1). Concurrently, two electron neutrinos are produced, each carrying away the energy $E_{\nu_e} \leqslant 0.42$ MeV. The side-reaction is

$$^3He + {}^4He \rightarrow {}^7Be + \gamma + 1.59 \text{ MeV}, \quad (10.5)$$

instead of (10.4) and continues as

$$^7Be + e^- \rightarrow {}^7Li + \nu_e + \gamma + 0.86 \text{ MeV}, \quad (10.6)$$

$$^7Li + p \rightarrow {}^4He + {}^4He + 17.35 \text{ MeV} \quad (10.7)$$

in 99.89% of the cases and as

$$^7Be + p \rightarrow {}^8B + \gamma + 0.14 \text{ MeV}, \quad (10.8)$$

$$^8B \rightarrow {}^8Be^* + e^+ + \nu_e + 14.6 \text{ MeV}, \quad (10.9)$$
$$\hookrightarrow 2{}^4He + 3 \text{ MeV}$$

in the remaining cases.

The ultimate result of side-reactions (10.5)–(10.7) and (10.5), (10.8), (10.9) is the same as that of (10.4), but they give rise to higher-energy neutrinos. Reactions (10.8), (10.9) create the so-called boron neutrinos with energies of up to 14 MeV. It is these neutrinos that are recorded in the majority of experiments even though the said side-reactions are relatively rare (one per 5×10^3 final states [101]).

The so-called hep-reaction occurs instead of (10.4) and (10.5) in 2×10^{-5}% of cases:

$$^3He + p \rightarrow {}^4He + e^+ + \nu_e + 18.8 \text{ MeV}, \quad (10.10)$$

giving rise to solar neutrinos with the highest energy (up to 18.8 MeV).

The initial reaction in a pep-cycle is

$$p + e + p \rightarrow {}^2He + \nu_e + 1.44 \text{ MeV}, \quad (10.11)$$

[instead of (10.2)] which further proceeds similarly to a pp-cycle. Reaction (10.11) generates monoenergy neutrinos with $E_{\nu_e} = 1.4$ MeV which are easier to detect than neutrinos produced through the initial reaction of the pp-cycle (10.2). It is worth noting that the pp/pep neutrino output ratio is independent of the version of the Solar Model. This makes recording neutrinos in the reaction (10.11) equivalent to detecting them in (10.2) if the experiment is designed to measure the rates of the main reactions in thermonuclear synthesis.

This line of reasoning leads to the conclusion that the energy threshold of selected experiments determines the possibility of detecting the following neutrino species differing in terms of energy:

(a) neutrinos from the initial reaction of the pp-cycle (< 0.42 MeV);

(b) neutrinos from the initial reaction of the pep-cycle (< 1.42 MeV);

(c) neutrinos from reaction (10.6) of the pp and pep-cycles (< 0.86 MeV);

(d) boron neutrinos (< 14.6 MeV);

(e) neutrinos from the hep-reaction (< 18.6 MeV).

The CNO cycle involves the carbon and nitrogen isotopes ^6C and ^{14}N, the nuclei of which are catalysts of thermonuclear synthesis (10.1). The amount of these isotopes in the cycle remains unaltered. The total energy released in the CNO cycle is the same as in pp and pep-cycles (26.7 MeV); the neutrinos carry away an energy of $\leqslant 1.2$ MeV through the reaction

$$^{13}N \rightarrow {}^{13}C + e^+ + \nu_e \quad (10.12)$$

and $E_{\nu_e} \leqslant 1.73$ MeV in the reaction

$$^{15}O \rightarrow {}^{15}N + e^+ + \nu_e. \quad (10.13)$$

The standard solar model [328–240] allows solar neutrino fluxes to be computed with an accuracy of 2%. The computed values and experimental findings are expressed in solar neutrino units (SNU), i.e. as the product of a calculated neutrino flux (cm^2 s^{-1})) and the neutrino absorption section in the target (cm^2). The problem of solar neutrinos arises from the discrepancy between the theoretical probability and the experimentally found number of neutrino interactions in the material of different detectors.

Today, there are several continuously working experimental facilities to record solar neutrinos. The results of independent studies indicate that the intensity of real fluxes of solar neutrinos is lower than that calculated in the framework of the standard solar model.

The chlorine-argon experiment is a classical study of solar neutrinos carried out over a 25 year period by R Davis's group in a mine of the abandoned gold-fields at Homestake, S Dak, USA. This study was described and its results interpreted in numerous publications of which Ref. [241] substantiates the experiment, Ref. [242] presents its philosophy, and Refs [243–244] discuss the results of observations. All these aspects are reviewed in [157].

Davis and his co-workers detected solar neutrinos taking advantage of the reaction

$$\nu + {}^{37}_{17}\mathrm{Cl} \rightarrow {}^{37}_{18}\mathrm{Ar} + e^- , \tag{10.14}$$

which produces ^{37}Ar with a half-life of $\tau_{1/2} = 35.1$ days and a decay energy of $Q = 3$ keV, sufficient to record individual events. Reaction (10.14) has the threshold $E_\nu = 0.81$ MeV which makes it possible to record only ^{8}B and ^{7}Be neutrinos.

The target detector is a 400 m^3 tank filled with 615 tons of liquid perchlorethylene containing 133 tons of ^{37}Cl (2.2×10^{30} atoms). It is located at a depth of 4,100 mwe. Following a 3-month exposure, ^{37}Ar atoms are non-trivially extracted to be counted in a precision proportional counter. The experimental technique is described in [157]. Because a pure gauging experiment with the Sun 'switched off' is impossible, much attention is given to the improvement of methodology for evaluating the efficiency of ^{37}Ar extraction, the separation of $^{37}Ar^+$ ions, background measurements, etc.

The frequency of solar neutrino captures in the ^{37}Cl-detector calculated in the framework of the standard solar model is [240]

$$R_{\mathrm{cal}} = (7.9 \pm 2.6)\,\mathrm{SNU} , \tag{10.15}$$

and that measured experimentally in more than 90 exposures is

$$E_{\mathrm{exp}} = (2.1 \pm 0.9)\,\mathrm{SNU} . \tag{10.16}$$

The errors in (10.15) and (10.16) correspond to three standard deviations.

GALLEX is an experimental facility of the underground laboratory at Gran Sasso in which solar neutrinos are detected from their capture in the reaction

$$ {}^{71}_{31}\mathrm{Ga} + \nu_e \rightarrow {}^{71}_{32}\mathrm{Ge} + e^- \tag{10.17}$$

with threshold energy $E_\nu = 0.23$ MeV [245]. The detector holds 30 tons of $^{71}_{31}$Ga in a $GaCl_3$ solution and can detect about 70% of the pp-neutrinos produced in the main reaction (10.2). The method for selecting $^{71}_{32}$Ge atoms and recording them has much in common with that used by Davis and co-workers. Exposures over a few last years have revealed a deficit of solar neutrinos; their calculated quantity for the gallium detector turns out to be [240]

$$R_{\mathrm{cal}} = 132^{+20}_{-17}\,\mathrm{SNU} \tag{10.18}$$

which is significantly higher than the experimental result

$$R_{\mathrm{exp}} = (79 \pm 10^{+8}_{-5})\,\mathrm{SNU} . \tag{10.19}$$

Recent calibration of GALLEX against a ^{51}Cr source confirmed previous measurements of neutrino fluxes [246].

SAGE, a detector at the Baksan underground laboratory, has a 60-ton target of metallic $^{71}_{31}$Ga and uses at reaction (10.17) [247]. Preliminary data confirm the previous observations of the solar neutrino deficit which proves to be even more prominent than in the GALLEX experiment [248]:

$$\frac{R_{\mathrm{exp}}}{R_{\mathrm{cal}}} = 0.55 \pm 0.14_{\mathrm{exp}} \pm 0.03_{\mathrm{cal}} . \tag{10.20}$$

The Kamiokande detector described in Section 5.4 detects neutrinos produced through the reaction

$$\nu_e + e^- \rightarrow \nu_e + e^- \tag{10.21}$$

with an energy threshold $E_{\mathrm{thr}} = 7.5$ MeV and analyses only ^{8}B- and hep-neutrino fluxes [249]. Analysis of the experimental results suggests a marked deficit of boron neutrinos [250]:

$$\frac{R_{\mathrm{exp}}}{R_{\mathrm{cal}}} = 0.50 \pm 0.04_{\mathrm{stat}} \pm 0.06_{\mathrm{sist}} \pm 0.07_{\mathrm{cal}} . \tag{10.22}$$

There are several ways to interpret the problem of the solar neutrino deficit which can be categorized into three groups. Considered in terms of nuclear physics, the problem depends on the poor knowledge of (10.4), (10.5) and especially (10.8) cross-sections. More precise gauging experiments are needed to check the validity of calculated reactor outputs. Another group of questions pertains to astrophysical studies and the relevance of the standard solar model used for computation. In this model, the initial conditions are given to include spherical symmetry, chemical homogeneity, and the assumption of hydrostatic equilibrium and radiative energy transfer. The solar evolution is calculated for various initial conditions and the ^{4}He/^{2}H ratio with fixed heavy element distributions. This model is probably incomplete and requires non-trivial solutions. Non-standard solar models and alternative solutions have been described in [157, 251, 252].

Finally, the third group relates to basic aspects of elementary particle physics. The following hypotheses are probably compatible with the measured solar neutrino fluxes:

1. Vacuum oscillations requiring fine adjustment for masses $\Delta m^2_\nu \simeq 10^{-10}$ eV^2 and large mixing angles;

2. A neutrino oscillation model which employs the MSW effect and implies parameters $\Delta m^2 \simeq 10^{-5}$ eV^2 and $\sin^2(2\theta) \simeq 0.01$ or $\sin^2(2\theta) \simeq 0.8$ [34, 168, 252, 253];

3. The existence of a large magnetic momentum of ν_e which facilitates the flip of neutrino spin in the Sun's convective zone and precludes recording its left-handed component [254 – 256];

4. The decay of the heavy mass state of a ν_1-neutrino into a lighter one ν_2 with the emission of a massless scalar boson ϕ: $\nu_1 \rightarrow \nu_2 + \phi$ [257];

5. The radiative decay of massive neutrinos [258, 259];

6. The presence of sterile non-interacting neutrinos in a constant electromagnetic cross-field [260];

7. The existence of weakly interacting particles (WIMP) which are able, after gravitational capture in the Sun, to transfer (independently of photons) a part of the energy and lower the temperature gradient in the center of the Sun; this would in turn decrease the flux of ^{8}B-neutrinos [261].

The oscillation scenario based on the 'see-saw' mechanism of neutrino mass generation and the MSW effect which ensures conversion of electron neutrinos to muon neutrinos looks the most natural and elegant of all the above options. In this case, theoretical calculations of neutrino fluxes based on the standard solar model most perfectly agree with the results of the Homestake, GALLEX, SAGE, and Kamiokande experiments for the oscillation parameters

$$\Delta m^2(\nu_e \leftrightarrow \nu_\mu) = (0.3 - 1.2) \times 10^{-5}\ \mathrm{eV}^2 , \tag{10.23}$$

$$\sin^2(2\theta_{e\mu}) = (0.4 - 1.5) \times 10^{-2} . \tag{10.24}$$

Were oscillations a reality, solar neutrinos with energies in the megaelectronvolt range would be the ideal 'tool' for their study at $\Delta m^2 \simeq 10^{-15}$ eV^2 [263].

Results of solar neutrino experiments may provide unambiguous evidence of oscillations of neutrinos with different flavours, perhaps enhanced by the matter effect, only after their total energy spectrum is measured and the source is exactly identified. This problem can be solved with a new generation of detectors capable of recording ν_μ- and ν_τ-neutrinos, besides ν_e-neutrinos, and their interactions via neutral currents. Some of these detectors were described in Section 9.

Superkamiokande will record the elastic scattering of neutrinos by electrons [35, 36]:

$$\nu_x + e^- \to \nu_x + e^- . \tag{10.25}$$

This device can detect only ^{8}B-neutrinos but is expected to provide good statistics within a real measuring time. Indeed, it is hoped to record 23 (10.25)-events daily ($\simeq 8 \times 10^3$ events per year) in the sensitive volume of the 15×10^3 ton detector, at an electron energy of 7 MeV.

ICARUS will be used to investigate solar ^{8}B-neutrinos by recording two reactions [35, 36]:

(a) elastic ν_ee-scattering

$$\nu_e + e^- \to \nu_e + e^- , \tag{10.26}$$

(b) ν_e-capture

$$\nu_e + {}^{40}\mathrm{Ar} \to {}^{40}\mathrm{K}^* + e^- \tag{10.27}$$

largely by virtue of the permitted transition $^{40}\mathrm{K}^* \to {}^{40}\mathrm{K} + \gamma(2\gamma)$ with the release of 2 MeV of energy. Calculations of neutrino fluxes in the context of the standard solar model suggest the possibility of observing 2.7×10^3 events of the (10.26) type and 3×10^3 Fermi transitions of the reaction (10.27) during a year-long exposure of the detector, at a recoil electron energy threshold of $E_{\mathrm{thr}} = 5$ MeV. The ratio of (10.26) to (10.27) events will be used as a measure of the fraction of ν_e-neutrinos which are likely to undergo transformation to other ν_μ, ν_τ-flavours. This ratio relates to neither the solar model nor the initial flux of neutrinos. The full-scale version of ICARUS will be able to detect solar neutrino oscillations for two years with probability 20%.

It should be noted following [36] that the existence of the neutrino oscillation effect can be verified based on variations of solar neutrino fluxes with changing distance between Earth and Sun. The number of events in a detector N in the absence of oscillations varies in accordance with the relation

$$N \simeq \frac{1}{L^2} , \tag{10.28}$$

where L is the distance between Earth and Sun. In case of vacuum oscillations,

$$N \simeq \frac{1}{L^2}\left[1 - P(\nu_e \to \nu_x)\right] . \tag{10.29}$$

Then,

$$\frac{N(L_{\max})}{N(L_{\min})} = A\frac{L_{\min}^2}{L_{\max}^2} , \tag{10.30}$$

$$A = \frac{1 - \sin^2(2\theta)\langle \sin^2[1.27\Delta m^2 (L_{\max}/E)]\rangle}{1 - \sin^2(2\theta)\langle \sin^2[1.27\Delta m^2 (L_{\min}/E)]\rangle} . \tag{10.31}$$

In expressions (10.30) and (10.31), $L_{\min} = 1.465 \times 10^{11}$ m, $L_{\max} = 1.516 \times 10^{11}$ m and averaging is over the neutrino energy spectrum. In the absence of oscillations

$$\frac{N(L_{\max})}{N(L_{\min})} = 0.934 . \tag{10.32}$$

Experimentally, the oscillation effect will manifest as the difference between amplitudes of annual modulations of neutrino fluxes from the Sun. Their evaluation is illustrated in Fig. 5. If the oscillations are to be recorded by this method, the data from Superkamiokande and ICARUS need to be collected for about two years.

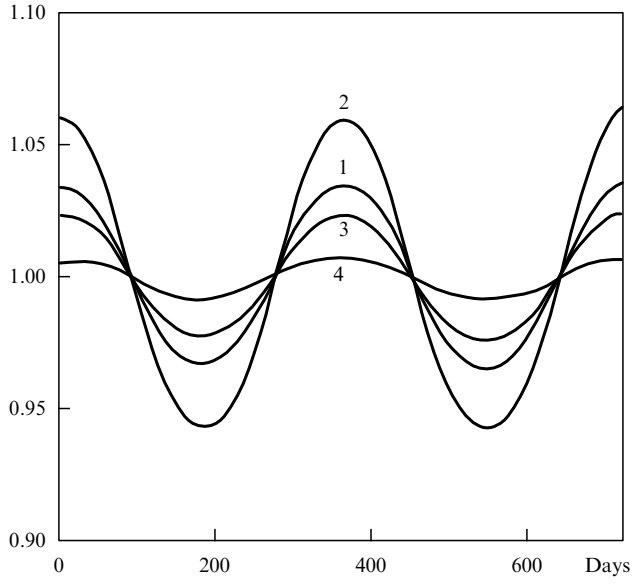

Figure 5. Changes of the normalized number of neutrino events with time for the following cases: (*1*) no oscillations, (*2*) oscillations with parameters $\Delta m^2 = 5 \times 10^{-11}$ eV^2, $\sin^2(2\theta) = 1$; (3) $\Delta m^2 = 8 \times 10^{-11}$ eV^2, $\sin^2(2\theta) = 0.8$; (4) $\Delta m^2 = 1.1 \times 10^{-10}$ eV^2, $\sin^2(2\theta) = 0.9$.

Let us now turn to facilities being specially designed and constructed for solar neutrino investigations in the near future.

SNO (Sadbury Neutrino Observatory) is located at a depth of 2 km in the vicinity of Sadbury, Canada [264]. This is actually a Cherenkov detector with the heavy water D_2O target placed in an acrylic container and shielded from the ionizing radiation of the surrounding rocks by a few layers of ultrapure water and concrete. SNO is intended to study elastic scattering (10.26), CC-events

$$\nu_e + d \to p + p + e^- \ (Q = -1.4 \text{ MeV}) \tag{10.33}$$

and NC-processes

$$\nu_x + d \to p + n + \nu_x \ (Q = -2.2 \text{ MeV}) . \tag{10.34}$$

Electrons produced in the inverse β-decay (10.33) have energies equal to that of neutrinos minus the threshold energy of the reaction; in the case of the MSW effect, there is a correlation between the distortions of electron and ^{8}B-neutrino spectra. Reaction (10.34) has similar cross-sections for all neutrino species (ν_e, ν_μ, ν_τ) and will be identified from

the retention time of an electron resulting from Compton scattering of a γ-quantum emitted when a decelerated neutron is captured. Sensitivity to the process (10.34) will be enhanced by periodic addition (followed by removal) of around 2.5 tons of NaCl into the detector volume to ensure neutron capture from chloride. The resulting proton with an energy of 8.5 MeV will emit Cherenkov light. SNO will count solar neutrino events at the high rate of 20/day, but it will detect only ^{8}B-neutrinos. Nevertheless, the detection of three reactions, (10.26), (10.33), and (10.34), will hopefully allow for the interpretation of experimental data regardless of the calculated neutrino fluxes and the evaluation of all oscillation transition modes.

BOREXINO is an experiment being designed at Gran Sasso with a view to investigating low-energy solar neutrinos in the reaction of electron capture by ^{7}Be [265]. The detector contains 100 tons of a ^{11}B-enriched scintillation fluid for recording recoil electrons in the scattering reaction (10.26). It is expected to ensure the precise measurement of electrons from their kinetic energy. The device is supposed to have record-breaking statistics of up to 50 events per day in the electron energy range 250 to 700 keV. It will be possible to observe oscillations if the neutrino mass varies in the range 10^{-8} eV$^2 > \Delta m^2 > 10^{-11}$ eV^2 [226]. The major difficulty appears to be related to the background control since the low energy threshold of the method requires the use of a highly purified scintillator.

HELLAZ (Helium Liquid Azote temperature) is one more device to be operated at Gran Sasso, capable of recording practically the entire spectrum of solar neutrinos [267]. Neutrinos including those created in the pp-reaction will be detected by measuring elastic scattering in (10.2). The detector will contain a large amount of an He + 2% CH mixture (around 6 tons) at the temperature of liquid nitrogen (77K) and high pressure (5 bars). The detecting module is a time-of-flight TRS chamber sensitive to individual recoil electrons from (10.25). The energy will be measured with an accuracy of $\Delta E_e/E_e = 2-4\%$ (at $E_e = 300$ keV). Better statistics (5×10^3 neutrino-containing events per year) can be achieved at the threshold sensitivity of electron recording 100 keV (217 keV for neutrons).

Precise measurements of neutrino spectra with the above instruments in the low-energy range and reconstruction of the neutrino direction ($\cos\vartheta$) relative to the Sun,

$$E_\nu = m_e\left[\cos\vartheta\left(1+\frac{2m_e}{T_e}\right)^{1/2}-1\right]^{-1}, \qquad (10.35)$$

afford a unique opportunity to solve the problem of solar neutrinos.

11. Atmospheric neutrino oscillations

Atmospherically-produced neutrinos originate from the decay of pions $\pi \to \mu\nu_\mu$ and kaons $K \to \mu\nu_\mu$ formed in interactions of primary cosmic rays with the Earth's atmosphere. The subsequent muonic decay $\mu \to e\nu_e\nu_\mu$ determines the expected ratio of atmospherically produced neutrino fluxes:

$$\frac{R(\nu_\mu)}{R(\nu_e)} = 2\,. \qquad (11.1)$$

Observation of atmospheric neutrino oscillations requires an exact knowledge of their energy spectrum and the paths of flight of each (ν_e, ν_μ) flavour. The majority of atmospherically produced neutrinos have energies below the threshold for τ-lepton formation. Therefore, experiments on the creation of ν_τ appear unrealistic. The sensitivity of experiments with ν_e and ν_μ to the oscillation parameters is largely restricted for statistical reasons when they are intended for determining $\sin^2(2\theta)$ and by the energy E_ν when the objective is to measure Δm^2.

The reconstruction of the spectrum of atmospheric neutrinos and the normalization of their fluxes constitute a non-trivial problem because the absolute fluxes of primary cosmic rays are poorly known and the conditions for the creation of π- and K-mesons in interactions of high-energy protons and light nuclei with atmospheric atoms' nuclei and low-energy photons are uncertain. For this reason, experimental devices are made to measure the ratio of ν_μ to ν_e-neutrino interactions via the CC-channel: $R_{exp} = N_{exp}(\nu_\mu)/N_{exp}(\nu_e)$.

A similar ratio for neutrino fluxes with different flavours emerges from the ratio of the outputs of showerless muon events to the number of events in an electromagnetic cascade:

$$R' = \frac{N(\mu\text{–track})}{N(\text{e–cascade})}\,.$$

This ratio is compared with the value calculated by the Monte Carlo method

$$R_{cal} = \frac{N_{cal}(\nu_\mu)}{N_{cal}(\nu_e)}\,,$$

which takes into account the development of atmospheric cascades, the response function of the detector, etc.

The results of major atmospheric neutrino experiments are presented in Table 7.

Table 7. Experimental to theoretical ratio of atmospheric ν_μ- and ν_e-neutrino fluxes.

Experiment	Exposure, 10^3 ton year^{-1}	R'_{exp}/R_{cal}	Ref.
IMB-3	7.7	a) 0.54±0.05 b) 0.64±0.07	[268]
Kamiokande II	4.92	ô) 0.60±0.06 b) 0.69±0.06	[269]
Frejus	2.0	0.87±0.13	[270]
Soudan II	1.0	0.64±0.19	[271]
NUSEX	0.5	0.96±0.29	[272]

The data in Table 7 indicate that observations of atmospheric neutrinos in underground laboratories using the large water Cherenkov detectors IMB-3 and Kamiokande revealed anomalous CC-interactions in ν_μ and ν_e-channels. They were detected by two methods: (a) from the shape of the Cherenkov ring recorded by PMTs and (b) by recording μ-decay, i.e. from the excess of PMTs working for several microseconds after the scattering event. The table R'_{exp}/R_{cal} ratios obtained by either method using IBM-3 and Kamiokande suggest an approximately 30% – 40% deficit of ν_μ-events and an excess of ν_e-events.

Neutrinos formed in the Earth's atmosphere cover a distance $L = 10-13000$ km before they interact in a detector and have a energy of $E_\nu = 0.3-1.2$ GeV. Therefore, the deficit of ν_μ-neutrinos created in interactions of cosmic rays in the

atmosphere may be interpreted as supporting the existence of $\nu_\mu \leftrightarrow \nu_\tau$ or $\nu_\mu \leftrightarrow \nu_e$ oscillations with the parameters

$$\Delta m^2 = 10^{-2} - 10^{-4}\ \text{eV}^2\,, \tag{11.2}$$

$$\sin^2(2\theta) = 0.3 - 0.6\,. \tag{11.3}$$

On the other hand, calorimetric experiments such as Frejus and NUSEX failed to reveal this effect. However, recent findings obtained with the Soudan II appear to confirm that the $R(\mu)/R(e)$ ratio for the CC-channel is lower than the theoretical ratio.

A most remarkable result in support of the atmospheric neutrino deficit,

$$\frac{R'_{\text{exp}}}{R_{\text{cal}}} = 0.59 \pm 0.08\,, \tag{11.4}$$

was reported by the Kamiokande Collaboration [273] from the analysis of events with the mean energy of $\langle E_\nu \rangle = 6$ GeV all of which reached the sensitive volume of the detector. This result fairly well describes ν_e-fluxes and suggests a small deficit of ν_μ-fluxes which conforms to that predicted from the $\nu_\mu \leftrightarrow \nu_\tau$ hypothesis.

Figure 6 shows the real distribution of events over the zenith angle, based on the results of the Kamiokande experiment. If the oscillation length amounts to several thousand kilometers, the zenith angle must change for upcoming neutrinos which pass through the Earth but remain unaltered for downgoing neutrinos.

Another interesting explanation for the deficit of atmospheric ν_μ-neutrinos relates to the MSW effect and is considered in [274]. Were the matter effect a reality, resonance on the Sun and Earth would take place for neutrinos with energies $E_\nu = 1-15$ MeV and $E_\nu = 10-1500$ MeV respectively, the density of the Earth being 10–100 times lower than in the center of the Sun. It is this energy region that is characteristic of atmospheric neutrinos.

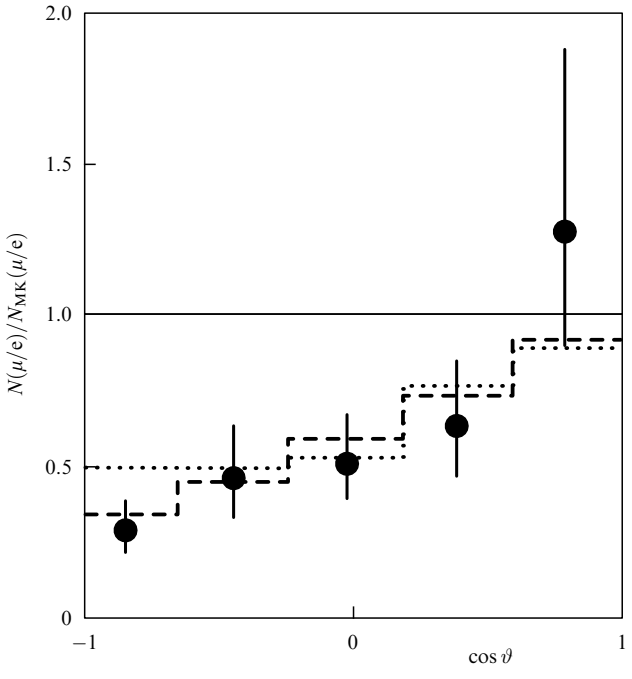

Figure 6. Distribution of events over the zenith angle (Kamiokande experiments). The results of Monte Carlo calculations of $\Delta m^2 = 1.8 \times 10^{-2}$ eV^2 and $\sin^2(2\theta) = 1.0$ for $\nu_\mu \leftrightarrow \nu_e$ oscillations (dashed line) and $\Delta m^2 = 1.6 \times 10^{-2}$ eV^2 and $\sin^2(2\theta) = 1.0$ for oscillations (dotted line).

Neutrino oscillations can be induced by a gravitational MSW effect [275, 276]. This exotic effect is to be examined in future experiments.

The interpretation of the atmospheric neutrino deficit as a sequel to oscillations is not the only one. The discrepancy between experimental and theoretical data may be due to the incorrect use of the Fermi-gas model for computation; it can probably be realized more successfully [277].

It has been shown in [278] that there is no deficit of atmospheric neutrinos if the ratio of π^+ to π^--mesons created in interactions of protons with the Earth's atmosphere is higher than it is usually assumed to be for the purpose of computation. Studies on the probability of a systematic error in calculations of the $R(\nu_\mu)/R(\nu_e)$ ratio due to the additional effect of cosmic ray neutrinos and their decays in the atmosphere or to the proton decay $p \to e\nu\nu$ are underway [279, 280].

The problem of atmospheric neutrinos can not be successfully approached without the calibration of the existing and new detectors. The first results of calibration of Kamiokande in the electron/muon beam from KEK have demonstrated that the detector effectively separates electron and muon-containing events. In addition to the calibration of detectors, it is necessary to evaluate intensity of muon fluxes at altitudes 10–20 km above the Earth's surface where atmospheric neutrinos are created. In a way, such measurements would be analogous to those in a near detector in experiments with long-baseline neutrinos from accelerators. The available data on muon fluxes in the atmosphere [280] agree with the normalization used in calculations.

Collectively, the results of current experiments are in line with the $\nu_\mu \leftrightarrow \nu_\tau$-interpretation of atmospheric neutrinos, but more reliable information is expected to come from experiments to be performed in the near future using the Superkamiokande and ICARUS-Superkamiokande facilities able to detect 3×10^3 events containing atmospheric neutrinos per year. The ICARUS experiment will annually detect around 1.2×10^3 events containing atmospheric neutrinos in each 5×10^3 ton module with high resolution and effective separation of electrons and muons. The matter effect will be studied, taking advantage of the possibility to differentiate between neutrino and antineutrino interactions in the CC-channel [36].

12. Conclusion

The primary objective of the present review was to consider the theoretical ideas which have given incentive to the progress in neutrino physics over the last 20 years. Secondly, we wished to demonstrate the physical motivation of certain models of neutrino mass generation and, hence, the possibility of observing neutrino oscillations. The third and last purpose was to illustrate a great variety of experimental approaches to better understanding the fundamental properties of neutrinos.

Renormalization has long remained an indispensable attribute of any basic field theory. Therefore, the neutrino was regarded as massless in the framework of the standard $SU(2) \otimes U(1)$ model which contains no electroweak neutrino singlets. It was generally accepted that there are no fundamental reasons for the neutrino to have a mass. The progress in the development of Grand Unification Theories required

Table 8. Neutrino masses and the possibility of explaining the hidden mass problem and the deficit of solar and atmospheric neutrinos in different theoretical models.

Model, references	Predictable mass		Does the model explain:		
	m_{ν_μ}, eV	m_{ν_τ}, eV	dark matter deficit	solar neutrino deficit	atmospheric neutrino deficit
Standard Model	0	0	no	no	no
Akhmedov E [282]	10^{-1}	10	yes	no	yes
Hall L [283]	10^{-3}	10	yes	yes	no
GINO [284]	0	0	no	yes	yes
Cadwell D [285]	3	3	yes	yes	yes
Wolfenstein L	3×10^{-4}	3×10^{-3}	no	yes	no
Maximum mixing	0.085	$< 3 \times 10^{-6}$	no	yes	no
Heavy ν_τ, Dodelson S [286]	—	10^6	no	yes	yes
Pakvasa S [287]	10^{-3}	10^{-1}	no	yes	yes

the prevailing view of quantum field theory to be revised. Extension of the standard model by including Higgs and lepton sectors and the possibility of generating neutrino masses from invariant operators of higher dimensions suppressed at the scale of the Unification Theory $\simeq 1/M_{\rm GUT}$ has led to the appearance of a neutrino mass, if a very small one. Leaving the necessity of renormalization at quantum gravitation scales for future superstring theories, it should be emphasized that small neutrino masses with a stable hierarchy $m_{\nu_{e,\mu,\tau}} \simeq (m_{u,c,t})^2/M_{\rm GUT}$ arise naturally from the 'see-saw' mechanism in the SO(10)-based GUT. This mechanism ensures that the heaviest ν_τ-neutrino has a mass of about 5–30 eV.

At present, there are three independent indications that the neutrino must have a mass restricted to this range. The first is related to the problem of dark matter in the Universe. A massive neutrino is predicted by contemporary cosmological models compatible with the observation of quadrupole mode of relic radiation in the COBE satellite experiment. Specifically, the Mixed Dark Matter model considers massive neutrinos (mass $\simeq$ 20 eV) as the most probable candidates of hot dark matter responsible for almost 30% of the total density of the Universe. Neutrinos with a mass of about 30 eV equally well describe the formation of the large-scale structure of the Universe.

The second and third indications come from observations of the solar neutrino deficit in many experiments. The most elegant explanation of this paradox would be the effect of neutrino oscillations in the matter traversed on their way to a detector.

There are a large number of theoretical models which interpret the dark mass problem and the deficit of solar and atmospheric neutrinos [281]. The values predicted by some of them are presented in Table 8.

If the real world is organized in such a way as to contain massive neutrinos, they, in conjunction with lepton number conservation, must create conditions for the existence of oscillations. Moreover, if the neutrino mass is of the order of several electronvolts, oscillations with the presumed parameter ranges shown in Fig. 2 will soon be detected in further experiments [288]. The authors set a major hope on accelerator-based long-baseline experiments with two precise detectors.

Anyway, our understanding of the Grand Unification Theory is sure to change as basic aspects of the neutrino and dark matter problem are highlighted in forthcoming experiments.

References

1. Pauli V *An unpublished letter to the Physical Society of Tubingen*. Reprinted in,: Brown L M *Physics Today* No 9 23 (1930)
2. Fermi E *ZS. Phys.* **88** 161 (1934)
3. Weinberg S, in *Proc. of the XXVI Int. Conf. on HEP* (New York, 1993) p. 346
4. Pontecorvo B Preprint PD-205 (Chalk River, 1946)
5. Reines F, Cowen C L *Phys. Rev. Lett.* **92** 8304 (1953)
6. Lee T D, Yang C N *Phys. Rev.* **104** 254 (1956); Landau L *Nucl. Phys.* **3** 127 (1957)
7. Garwin R, Lederman L, Weinrich M *Phys Rev.* **105** 1415 (1957)
8. Pontecorvo B M *Zh. Eksp. Teor. Fiz.* **37** 1751 (1959) [*Sov. Phys. JETP* **37** 1236 (1960)]
9. Danby G et al. *Phys. Rev Lett.* **9** 36 (1962)
10. Lederman L M *Usp. Fiz. Nauk* **160** 299 (1990) [*Sov. Phys. Usp.* **33** 199 (1990)]
11. Glashow S L *Nucl. Phys.* **22** 579 (1961)
12. Weinberg S *Phys. Rev. Lett.* **19** 1264 (1967)
13. Salam A, in *Elementary Particle Theory, Relativistic Group and Analyticity, Lerum, Sweden, 19–25 May 1968* (London: Wiley, 1968) p. 367
14. Hasert F J et al. *Phys. Lett. B* **46** 138 (1973)
15. Hasert F J et al. *Phys. Lett. B* **46** 121 (1973)
16. Glashow S L , Iliopoulos J, Maiani L *Phys. Rev. D* **2** 1285 (1970)
17. Benvenuti A et al. *Phys. Rev. Lett.* **34** 419 (1975)
18. Perl M L et al. *Phys. Rev. Lett.* **35** 1489 (1975)
19. Herb S W et al. *Phys. Rev. Lett.* **39** 252 (1977)
20. Arnison G et al. *Phys. Lett. B* **122** 103 (1983)
21. Pontecorvo B M *Zh. Eksp. Teor. Fiz.* **33** 49 (1957) [*Sov. Phys. JETP* **6** 429 (1958)]
22. Pontecorvo B M *Zh. Eksp. Teor. Fiz.* **34** 247 (1958) [*Sov. Phys. JETP* **34** 172 (1958)]
23. Maki Z, Nakagawa M, Sakata S *Prog. Theor. Phys.* **28** 870 (1962)
24. Pontecorvo B M *Zh. Eksp. Teor. Fiz.* **28** 493 (1967) [*Sov. Phys. JETP* **26** 984 (1968)]
25. Gribov V, Pontecorvo B *Phys. Lett. B* **28** 493 (1969)
26. Pontecorvo B M *Zh. Eksp. Teor. Fiz.* **141** 675 (1983) [*Sov. Phys. Usp.* **26** 575 (1983)]
27. Bilen'ky C M *Fiz. Elem. Chastits At. Yadra* **18** 449 (1987) [*Sov. J. Part. Nuclei* **18** 188 (1987)]
28. Gell-Mann M, Ramond P, Slansky R, in *Proc. of the Supergravity Work-shop at Stony Brook* (Amsterdam: North-Holland, 1979) p. 315
29. Belesev A I et al. *Phys. Lett. B* **350** 263 (1995)
30. Lobashev V, in *Proc. of 27th Int. Conf. on HEP* (Glasgow, Scotland, 1994)
31. Assamagan K et al. *Phys. Lett. B* **335** 231 (1994)
32. ALEPH Collaboration Preprint CERN-PPE/94-107 (Geneve, 1994)
33. Berezinsky V Preprint INFN 93-85 (Gran Sasso, 1993)
34. Mikheev S P, Smirnov A Yu *Usp. Fiz. Nauk* **153** 3 (1987) [*Sov. Phys. Usp.* **30** 3 (1987)]
35. Rubbia C Preprint CERN-PPE/93-08 (Geneve, 1993)
36. Revol J P Preprint CERN-PPE/93-84 (Geneve, 1993)
37. Abreu P et al. *Nucl. Phys. Ser. B* **418** 403 (1994)
38. Acciarri M, Adam A, Adriani O *Z. Phys.* **62** 551 (1994)
39. Akers R et al. *Z. Phys.* **61** 19 (1994)
40. Buskulic D, Casper D, De Bonis I *Z. Phys.* **62** 539 (1994)

41. LEP Electroweak Working Group, Preprint LEPEWWG/94-01 (1994)
42. Bilenky S M, Pontecorvo B M *Phys. Lett. B* **95** 233 (1980)
43. Kobzarev I Yu et al. *Yad. Fiz.* **32** 1590 (1980) [*Sov. J. Nucl. Phys.*]
44. Barger V et al. *Phys. Rev. Lett.* **45** 692 (1980)
45. Barger V et al. *Z. Phys. C* **8** 63 (1981)
46. Kobayashi M, Maskawa T *Progr. Theoret. Phys.* **49** 652 (1973)
47. Georgi H, Glashow S L *Phys. Rev. Lett.* **28** 1494 (1972)
48. Gelmini G B, Roncadelli M *Phys. Lett. B* **99** 411 (1981)
49. Georgi H, Glashow S L, Nussinov S *Nucl. Phys. B* **193** 297 (1981)
50. Shchepkin M G *Usp. Fiz. Nauk* **143** 513 (1984) [*Sov. Phys. Usp.* **27** 413 (1984)]
51. Barber D P et al. *Phys. Rev. Lett.* **43** 830 (1979)
52. Chikashige Y, Mohapatra R N, Peccei R D *Phys. Lett. B* **98** 265 (1981)
53. Hayashi T, Karino T, Yanagida T *Progr. Theor. Phys.* **60** 1066 (1978)
54. Georgi H, Glashow S L *Phys. Rev. Lett.* **32** 438 (1974)
55. Higgs P W *Phys. Lett.* **12** 132 (1964)
56. Higgs P W *Phys. Rev.* **145** 1156 (1966)
57. Georgi H, Nanopoulos D V *Phys. Lett. B* **82** 392 (1979)
58. Georgi H, Nanopoulos D V *Nucl. Phys. B* **155** 52 (1979)
59. Georgi H, Nanopoulos D V *Nucl. Phys. B* **159** 16 (1979)
60. Bludman S A , Kennedy C, Langacker P G *Phys. Rev. D* **45** 1810 (1992)
61. Dimopoulos S, Hall L, Raby S *Phys. Rev. Lett.* **68** 1984 (1992)
62. Dimopoulos S, Hall L, Raby S *Phys. Rev. D* **45** 4192 (1992)
63. Ellis J, Fogli G L, Lisi E *Phys. Lett. B* **274** 456 (1992)
64. Ellis J, Lopez J L, Nanopoulos D V *Phys. Lett. B* **292** 189 (1992)
65. Antoniadis I et al. *Phys. Lett. B* **194** 231 (1987)
66. Barr S M *Phys. Rev. D* **40** 2457 (1989)
67. Leontaris G, Nanopoulos D V *Phys. Lett. B* **212** 327 (1988)
68. Abel S *Phys. Lett. B* **234** 113 (1990)
69. Leontaris G, Vergados J D *Phys. Lett. B* **305** 242 (1993)
70. Kalara S, Lopez J L, Nanopoulos D V *Phys. Lett. B* **245** 421 (1990)
71. Kalara S, Lopez J L, Nanopoulos D V *Nucl. Phys. B* **353** 650 (1991)
72. Lopez J L, Nanopoulos D V *Phys. Lett. B* **251** 73 (1990)
73. Zel'dovich Ya B, Novikov I D *Stroenie i Evolyutsiya Vselennoiÿ* (Structure and Evolution of the Universe) (Moscow: Nauka, 1975)
74. Faber S M, Gallagher J J *Ann. Rev. Astron. Astrophys.* **17** 135 (1979)
75. Fabricant D, Gorenstein P *Astrophys. J.* **267** 535 (1983)
76. Mushotzky R, in *Proc. Relativistic Astrophysics and Particle Cosmology. Texas. 1992* (Ann. New York Acad. Sci., 1993) Vol. 688, p. 1984
77. Walker T P et al. *Astrophys. J.* **376** 51 (1991)
78. Heggi D J, Olive K A *Astrophys. J.* **303** 56 (1986)
79. Zel'dovich Ya B *Usp. Fiz. Nauk* **89** 647 (1966) [*Sov. Phys. Usp.* **9** 547 (1966)]
80. Gershteĭn S S, Zel'dovich Ya B *Pis'ma v Zh. Eksp. Teor. Fiz.* **4** 174 (1966) [*JETP Lett.* **4** 120 (1966)]
81. Cowsik R, McClelland J *Phys. Rev. Lett.* **29** 669 (1972)
82. Szalay A S, Marx G *Astron. Astrophys.* **49** 437 (1976)
83. Landau L D, Lifshitz E M *Statisticheskaya Fizika* Ch 1 (Statistical Physics Part 1) (Moscow: Nauka, 1990)
84. Mather J C et al. *Astrophys. J.* **420** 439 (1994)
85. Schramm D N *Ann. Rev. Astron. Astrophys.* **12** 383 (1974)
86. Steigman G, Schramm D N, Gunn J E *Phys. Lett. B* **66** 202 (1977)
87. Doroshkevich A G et al. *Pis'ma Astron. Zh.* **6** 457 (1980) [*Sov. Astron. Lett.*]
88. Dolgov A D, Zel'dovich Ya B *Usp. Fiz. Nauk* **130** 559 (1980) [*Sov. Phys. Usp.* **23** 459 (1980)]
89. Zel'dovich Ya B, Khlopov M Yu *Usp. Fiz. Nauk* **135** 45 (1981) [*Sov. Phys. Usp.* **24** 40 (1981)]
90. Peebles P J E *Astrophys. J.* **258** 415 (1982)
91. Shandarin S F, Doroshkevich A G, Zel'dovich Ya B *Usp. Fiz. Nauk* **139** 83 (1983) [*Sov. Phys. Usp.* **26** 63 (1983)]
92. Guth A H *Phys Rev. D* **23** 347 (1981)
93. Linde A D *Phys. Lett. B* **108** 389 (1982)
94. Albrecht A, Steinhardt P J *Phys. Rev. Lett.* **48** 1220 (1982)
95. Linde A D *Usp. Fiz. Nauk* **144** 177 (1984) [*Sov. Phys. Usp.* **27** 150 (1984)]
96. Zel'dovich Ya B *Astrofizika* **6** 319 (1970)
97. Zel'dovich Ya B, Shandarin S F *Pis'ma Astron. Zh.* **8** 259 (1982) [*Sov. Astron. Lett.*]
98. Zel'dovich Ya B *Pis'ma Astron. Zh.* **8** 195 (1982) [*Sov. Astron. Lett.*]
99. Smoot G F et al. *Astrophys. J.* **396** L1 (1992)
100. Berezinsky V, Masiero A, Valle J *Phys. Lett. B* **266** 382 (1991)
101. Harari H *Phys. Lett. B* **216** 413 (1989)
102. Dodelson S et al. *Preprint Fermilab-Pub-94/026-A* (1994)
103. Dobyns Y *Astrophys. J. Lett.* **329** 5 (1988)
104. Albrecht A, Stebbins A *Phys. Rev. Lett.* **69** 2615 (1992)
105. Fisher K B et al. *Astrophys. J.* **402** 42 (1993)
106. Taylor A N, Rowan-Robinson M *Nature* (London) **359** 396 (1992)
107. Ostriker J B *Ann. Rev. Astron. Astrophys.* **31** 689 (1993)
108. Bergkvist K-E *Nucl. Phys. B* **39** 317 (1972)
109. Lubimov V A et al. *Phys. Lett. B* **94** 266 (1980)
110. Boris S et al. *Phys. Lett. B* **159** 217 (1985)
111. Fritschi M et al. *Phys. Lett. B* **173** 485 (1986)
112. Kawakami H et al. *Phys. Lett. B* **256** 105 (1991)
113. Holzsehuh E, Fritschi M, Kundig W *Phys. Lett. B* **287** 381 (1992)
114. Robertson R G H et al. *Phys. Rev. Lett.* **67** 957 (1991)
115. Winheimer Ch et al. *Phys. Lett. B* **300** 210 (1993)
116. Albrecht H et al. *Phys. Lett. B* **292** 221 (1992)
117. Cinabro D, Henderson S, Kinoshita K *Phys. Rev. Lett.* **70** 3700 (1993)
118. Vergados J D *Nucl. Phys. B* **218** 109 (1983)
119. Vergados J D *Phys. Rep.* **133** 1 (1986)
120. Wolfenstein L *Phys. Lett. B* **107** 77 (1981)
121. Hennecke E W, Manuel O K, Sabu D D *Phys. Rev. C* **11** 1378 (1975)
122. Alston-Garnjost M et al. *Phys. Rev. Lett.* **71** 831 (1993)
123. Vuilleumier J -C et al. *Phys. Rev. D* **48** 1009 (1993)
124. Balysh A et al. *Phys. Lett. B* **283** 32 (1992)
125. Zuber K et al., in *Proc. 27 Int. Conf. on HEP* (Glasgow, Scotland: 1994)
126. Bolton R D et al. *Phys. Rev. D* **38** 2077 (1988)
127. Arisaka K et al. *Phys. Rev. Lett.* **70** 1049 (1993)
128. Shrock R E *Phys. Rev. D* **24** 1232 (1981)
129. Shrock R E *Nucl. Phys. B* **206** 359 (1982)
130. Berezhiani Z G, Vysotsky M I *Phys. Lett. B* **199** 281 (1987)
131. Wietfeldt F E, Norman E B *Phys. Rep.* **273** 151 (1996)
132. Bergsma F et al. *Phys. Lett. B* **128** 361 (1983)
133. De Leener-Rosier N et al. *Phys. Lett. B* **177** 228 (1986)
134. Britton D I et al. *Phys. Rev. D* **49** 28 (1994)
135. Dorenbosch J et al. *Phys. Lett. B* **166** 473 (1986)
136. Bernardi G et al. *Phys. Lett. B* **203** 332 (1988)
137. Konoplich R V, Khlopov M Yu *Yad. Fiz.* **57** 452 (1994)
138. Zatsepin G T *Pis'ma Zh. Eksp. Teor. Fiz.* **8** 333 (1968) [*JETP Lett.* **8** 205 (1968)]
139. Imshennik V S, Nadezhin D K *Usp. Fiz. Nauk* **156** 561 (1988) [*Phys. Usp.* **31** 461 (1988)]
140. Bowers R, Wilson J R *Astrophys. J.* **263** 366 (1982)
141. Woosley S E et al. *Astrophys. J.* **318** 664 (1987)
142. Morrison D R *Usp. Fiz. Nauk* **156** 461 (1988) [*Sov. Phys. Usp.* **31** 361 (1988)]
143. Hirata K J et al. *Phys. Rev. Lett.* **58** 1490 (1987)
144. Hirata K J et al. *Phys. Rev. D* **38** 448 (1988)
145. Hirata K J et al. *Phys. Rev. Lett.* **61** 2653 (1988)
146. Nakahata M et al. *Phys. Rev. Lett.* **55** 3786 (1986)
147. Bionta R M et al. *Phys. Rev. Lett.* **51** 27 (1983)
148. Haines T J et al. *Phys. Rev. Lett.* **57** 1986 (1986)
149. Bionta R M et al. *Phys. Rev. Lett.* **58** 1494 (1987)
150. Becker-Szen dy R et al. Preprint VINER-92-6 (Boston: Boston University, 1992)
151. Aglietta M et al. *Nuovo Cimento C* **9** 185 (1986)
152. Dadykin V L et al. *Pis'ma v Zh. Eksp. Teor. Fiz.* **45** 464 (1987) [*JETP Lett.* **45** 593 (1987)]
153. Aglietta M et al. *Europhys. Lett.* **3** 1315 (1987)
154. Alekseev E N et al. *Pis'ma v Zh. Eksp. Teor. Fiz.* **45** 461 (1987) [*JETP Lett.* **45** 589 (1987)]
155. Alexeyev E N et al. *Phys. Lett. B* **205** 209 (1988)
156. Dadykin V L, Zatsepin G T, Ryazhskaya O *Usp. Fiz. Nauk* **158** 139 (1989) [*Sov. Phys. Usp.* **32** 100 (1989)]
157. Bahcall J *Neutrinos Astrophysics* (Cambridge: Cambr. Univ. Press, 1989) [Translated into Russian (Moscow: Mir, 1993)]
158. Bahcall J N, Glashow S L *Nature* (London) **326** 476 (1987)
159. Kolb E W, Stebbins A J, Turner M S *Phys. Rev. D* **35** 3598 (1987)
160. Spergel D N, Bahcall J N *Phys. Lett. B* **200** 366 (1988)
161. Spergel D N, Weinberg D H, Gott J R *Phys. Rev. D* **38** 2014 (1988)
162. Abbott L F, de Rujula A, Walker T P *Nucl. Phys. B* **299** 734 (1988)
163. Avignone F T, Collar J I *Phys. Rev. D* **41** 682 (1990)
164. Wolfenstein L *Phys. Rev. D* **17** 2369 (1978)
165. Wolfenstein L *Phys. Lett. B* **107** 77 (1981)
166. Lewis R R *Phys. Rev. D* **21** 663 (1980)
167. Langacker P, Leveille J P, Sheiman J *Phys. Rev. D* **27** 1228 (1983)
168. Mikheev S P, Smirnov A Yu *Yad. Fiz.* **42** 1441(1985) [*Sov. J Nucl. Phys.* **42** 913 (1985)]

169. Ermilova V K, Tsarev V A, Chechin V A *Pis'ma v Zh. Eksp. Teor. Fiz.* **43** 353 (1986) [*JETP Lett.* **43** 453 (1986)]
170. Zharkov V N *Vnutrennee Stroenie Zemli i Planet* (Internal Structure of Earth and Planets) (Moscow: Nauka, 1983)
171. Vasil'ev P S et al. *Yad. Fiz.* **58** 2210 (1995)
172. Kajita T, in *Proc. Workshop on Long Baseline Neutrino Oscillation* (Ed. M Goodman) (FNAL, Illinois, USA, 1992) p. 145
173. Boehm F, Vogel P *Physics of Massive Neutrinos* (Cambridge: Cambr. Univ. Press, 1987) [Translated into Russian (Moscow: Mir, 1990)]
174. Borovoĭ A A, Khakimov S Kh *Neiÿtrinnye Eksperimenty na Yadernykh Reaktorakh* (Neutrino Experiments Using Nuclear Reactors) (Moscow: Energoatomizdat, 1990)
175. Boehm F et al. *Phys. Lett. B* **97** 310 (1980)
176. Kwon H et al. *Phys. Rev. D* **24** 1097 (1981)
177. Gabathuler K et al. *Phys. Lett. B* **138** 449 (1984)
178. Zacek G et al. *Phys. Rev. D* **34** 2621 (1986)
179. Cavaignac J F et al. *Phys. Lett. B* **148** 387 (1984)
180. Afonin A I et al. *Zh. Eksp. Teor. Fiz.* **94** (2) 1 (1988) [*Sov. Phys. JETP* **67** 213 (1988)]
181. Vidyakin G S et al. *Zh. Eksp. Teor. Fiz.* **98** 764 (1990) [*Sov. Phys. JETP* **71** 424 (1990)]
182. Reines F *Nucl. Phys. A* **396** 469 (1983)
183. Boehm F, Vogel P *Ann. Rev. Nucl. Part. Sci.* **34** 125 (1984)
184. Vogel P *Nucl. Phys. B* (Proc. Suppl.) 38 204 (1995)
185. Krastev P I, Petrov S T *Phys. Lett. B* **229** 99 (1993)
186. Krauss L M, Gates E, White M *Phys. Lett. B* **298** 94 (1993)
187. Krauss L M, Gates E, White M *Phys. Rev. Lett.* **70** 375 (1993)
188. Bergsma F et al. *Z. Phys. C* **40** 171 (1988)
189. Dydak F et al. *Phys. Lett. B* **134** 281 (1984)
190. Stockdale I E et al. *Phys. Rev. Lett.* **52** 1384 (1984)
191. Angelini C et al. *Phys. Lett. B* **179** 307 (1986)
192. Ahrens L A et al. *Phys. Rev. D* **31** 2732 (1985)
193. Astier P et al. *Phys. Lett. B* **220** 646 (1989)
194. Brucker E B et al. *Phys. Rev. D* **34** 2183 (1986)
195. Ammosov V et al. *Z. Phys. C* **40** 487 (1988)
196. Erriquez O et al. *Phys. Lett. B* **102** 73 (1981)
197. Baker N J et al. *Phys. Rev. Lett.* **47** 1576 (1981)
198. Ushida N et al. *Phys. Rev. Lett.* **57** 2897 (1986)
199. Batusov Y A et al. *Z. Phys. C* **48** 209 (1990)
200. Gruwe M et al. *Phys. Lett. B* **309** 463 (1993)
201. Armenise N et al. Preprint CERN-PPE/93-131 (Geneve, 1993)
202. Winter K Preprint CERN-PPE/95-165 (Geneve, 1995)
203. Asakawa T et al. *Nucl. Instr. Meth. A* **340** 458 (1994)
204. Aoki S et al. *Nucl. Instr. Meth. A* **344** 143 (1994)
205. Buontempo S et al. *Nucl. Instr. Meth. A* **344** 85 (1994)
206. Astier P et al. Preprint CERN-SPSLC/91-48 (Geneve, 1991)
207. Eggert E et al. *Nucl. Phys. B* (Proc. Suppl.) **38** 40 (1995)
208. Otten E *Nucl. Phys. B* (Proc. Suppl.) **38** 26 (1995)
209. Carrigan R A *Preprint Fermilab-Pab-95/365* (*1995*)
210. Bulgakov M K et al. Preprint IFVE 95-18 (Protvino, 1995)
211. Dar A, Eilam G, Gronau M *Nucl. Phys. B* (Proc. Suppl.) **38** 56 (1995)
212. Goodman M *Nucl. Phys. B* (Proc. Suppl.) **38** 337 (1995)
213. Ball A et al. Preprint CERN-SL/92-75 (Geneve, 1992)
214. Cennini P et al. *Nucl. Instr. Meth. A* **345** 230 (1994)
215. ICARUS collaboration Preprint LNGS-94/99-II (May, 1994)
216. Benetti P et al. Preprint LNGS -95/59 (September, 1995)
217. Bari G et al. *Nucl. Instr. Meth. A* **277** 11 (1989)
218. Cecchini S et al. *Nucl. Instr. Meth. A* **264** 18 (1988)
219. Ambrosio M et al. *Nucl. Instr. Meth. A* **363** 604 (1995)
220. Cavanna F Preprint CERN -PPE/95-133 (Geneve, 1995)
221. Alner G J et al. LNGS-GENIUS Proposal (May, 1994)
222. Resvanis L K et al. *Nucl. Phys. B* **35** 294 (1994)
223. Totsuka Y ICRR Report 227-90-20 (1990)
224. Nakamura K ICRR Report 309-94-4 (1994)
225. Nishikama T, in *Proc. in the Workshop on Long Baseline Neutrino Oscillation* (Fermilab., November 17–20, 1991) p. 171
226. E-889 Collaboration *Long Baseline Neutrino Oscillation Experiment* (BNL Design Report 52459. April, 1995)
227. Thron J L *Nucl. Instr. Meth. A* **283** 642 (1989)
228. Ables E et al. (P-875) *A Long Baseline Neutrino Oscillation Experiment at Fermilab* (February, 1995)
229. Berezinsky V S, Zatsepin G T *Usp. Fiz. Nauk* **122** 3 (1977) [*Sov. Phys. Usp.* **30** 3 (1977)]
230. *A Neutrino Beam from MI FNAL to DUMAND* (Fermilab Letter of Intend P-824) (October, 1990)
231. Adams A et al. Preprint GRANDE facility SSC-90/07 (1990)
232. Isaev P S, Tsarev V A *Fiz. Elem. Chastits At. Yadra* **21** 5 (1990)
233. *Materialy Rabochego Soveshchaniya 'UNK-600'. Protvino, 23-24 noyabrya 1993* (Abstracts of UNK-600 Workshop) (Protvino: Izd IFVE, 1994)
234. Aref'ev A S et al. Preprint IFVE 94-36 (Protvino: Izd. IFVE, 1994)
235. Fedotov Yu et al. Preprint IHEP 94-34 (1994)
236. Belolaptikov J A et al. *Nucl. Phys. B* **19** 338 (1991)
237. Belolaptikov J A et al., in *Proc. of the 23rd Int. Cosmic Ray Conf., Calgary, 1993* (University of Calgary, 1993) Vol. 4, p. 573
238. Bahcall J N et al. *Rev. Mod. Phys.* **54** 767 (1982)
239. Bahcall J N, Ulrich R K *Rev. Mod. Phys.* **60** 297 (1988)
240. Bahcall J N, Pinsonneault M N *Rev. Mod. Phys.* **64** 885 (1992)
241. Davis R *Phys. Rev. Lett.* **12** 303 (1964)
242. Bahcall J N, Davis R *Science* **191** 264 (1976)
243. Davis R, Mann A K, Wolfenstein L *Ann. Rev. Nucl. Part. Sci.* **39** 467 (1989)
244. Davis R, in *Proc. of 21 Intern. Cosmic Ray Conf.* (Ed. R J Protheroe) (Adelaide: University of Adelaide Press, 1990) p. 143
245. Anselmann P et al. *Phys. Lett. B* **314** 445 (1993)
246. Anselmann P et al. *Phys. Lett. B* **342** 440 (1995)
247. Pomansky A A *Nucl. Instr. Meth. A* **271** 254 (1988)
248. Abazov A I et al. *Phys. Rev. Lett.* **67** 3332 (1991)
249. Hirata K S et al. *Phys. Rev. D* **44** 2241 (1991)
250. Hirata K S et al. *Phys. Lett. B* **280** 146 (1992)
251. Kennedy D, Langasker P *Nucl. Phys. B* **374** 373 (1992)
252. Anselmann P et al. *Phys. Lett. B* **285** 390 (1992)
253. Krastev P I, Petcov S T *Phys. Lett. B* **299** 99 (1992)
254. Voloshin M B, Visotsky M I, Okun' L B *Zh. Eksp Teor. Fiz.* **91** 754 (1986) [*Sov. Phys. JETP* **64** 446 (1986)]
255. Akhmedov E Kh *Yad. Fiz.* **48** 475 (1988)
256. Lim C-S, Marciano W J *Phys. Rev. D* **37** 1368 (1988)
257. Frieman J, Haber H E, Freese K *Phys. Lett. B* **200** 115 (1988)
258. Gvozdev A A, Mikheev N V, Vasilevskaya L A *Phys. Lett. B* **289** 103 (1992)
259. Vasilevskaya L A, Gvozdev A A, Mikheev N B *Yad. Fiz.* **57** 124 (1994)
260. Krastev P I, Petcov S T *Phys. Lett. B* **285** 85 (1992)
261. Press W H, Spergel D N, in *Dark Matter in the Universe* (Eds J N Bahcall et al.) (Singapore: World Sci., 1988) p. 206
262. Krauss L M, Gates E, White M *Phys. Lett. B* **298 94 (1993)**
263. Parke S *Phys. Rev. Lett.* **74** 839 (1995)
264. Ewan G T *Nucl. Instr. Meth. A* **314** 373 (1992)
265. Campanella M, in *Proc. of the 3-rd Intern. Workshop on Neutrino Telescopes, 1991, Venezia(Venice), Italy* (Ed. M Baldo-Geolin) (Inst. Nazionale D.: Fizika Nucleare, 1991) p. 73
266. De Rujula A, Glashow S L Preprint CERN-TH6665/92 (Geneve, 1992)
267. Laurenti G et al. Preprint CERN-LAA-PC/93-10 (Geneve, Feb. 1993)
268. Becker-Szendy R. et al. *Phys. Rev. D* **46** 378 (1992)
269. Hirata K S et al. *Phys. Lett. B* **280** 146 (1992)
270. Berger et al. *Phys. Lett. Ser. B* **245** 305 (1990)
271. Goodman M C, in *Proc. of 23 Intern. Cosmic Ray Conf.* (Calgary, 1993) Vol. 4, p. 446
272. Aglietta M et al. *Europhys. Lett.* **8** 611 (1989)
273. Fukuda J et al. *Phys. Lett. B* **335** 205 (1994)
274. Akhmedov E, Lipari P, Lisignoli C *Phys. Lett. B* **300** 128 (1993)
275. Gasperini M *Phys. Rev. D* **39** 3606 (1989)
276. Halprin A, Leung C N *Nucl. Phys. B* **28** 139 (1992)
277. Engel J et al. *Phys. Rev. D* **48** 3048 (1993)
278. Volkova L V *Phys. Lett. B* **316** 178 (1993)
279. Mann W A, Kafka T, Leeson W *Phys. Lett. B* **291** 200 (1992)
280. Perkins D H *Astroparticle Phys.* **2** 249 (1994)
281. Valle J W F *Nucl. Phys.* **26** 91 (1991)
282. Akhmedov E et al. *Phys. Lett. B* **69** 3013 (1992)
283. Dimopoulos S, Hall L J, Raby S *Phys. Rev. D* **47** R3697 (1993)
284. Pantaleone J, Halprin A, Leung C *Phys. Rev. D* **47** R4199 (1993)
285. Caldwell D, Mohapatra R *Phys. Rev. D* **50** 3477 (1994)
286. Dodelson S, Gyuk G, Turner M *Phys. Rev. Lett.* **72** 3754 (1994)
287. Learned J, Pakvasa S, Weiler T J *Phys. Lett. B* **207** 79 (1988)
288. Gonzalez-Garcia M C, Preprint CERN-TH/95-285 (1995)